ISSN 1512-1127

საქართველოს გეოფიზიკური საზოგადოების ჟურნალი

სერია ა. დედამიწის ფიზიკა

JOURNAL OF THE GEORGIAN GEOPHYSICAL SOCIETY

Issue A. Physics of Solid Earth

ტომი 18ა 2015

vol. 18A 2015

ISSN 1512-1127

საქართველოს გეოფიზიკური საზოგადოების ჟურნალი

სერია ა. დედამიწის ფიზიკა

JOURNAL OF THE GEORGIAN GEOPHYSICAL SOCIETY

Issue A. Physics of Solid Earth

ტომი 18ა 2015

vol. 18A 2015

საქართველოს გეოფიზიკური საზოგადოების ჟურნალი

მთავარი რედაქტორი: თ. ჭელიძე

სერია ა. დედამიწის ფიზიკა

სერიის შინაარსი:

ჟურნალი (ა) მოიცავს მყარი დედამიწის ფიზიკის ყველა მიმართულებას. გამოქვეყნებულ იქნება: კვლევითი წერილები, მიმოხილვები, მოკლე ინფორმაციები, დისკუსიები, წიგნების მიმოხილვები, განცხადებები.

ЖУРНАЛ ГРУЗИНСКОГО ГЕОФИЗИЧЕСКОГО ОБЩЕСТВА

Главный редактор: Т. Челидзе

Серия А. Физика Твердой Земли

Содержание журнала:

Журнал (А) Грузинского геофизического общества охватывает все направления физики твердой Земли. В журнале будут опубликованы научные статьи, обозрения, краткие информации, дискуссии, обозрения книг, объявления.

JOURNAL OF THE GEORGIAN GEOPHYSICAL SOCIETY

Editor-in-Chief: T. Chelidze

Issue A. Physics of Solid Earth

Scope of the Journal:

The Journal (A) is devoted to all branches of the Physics of Solid Earth. Types of contributions are: research papers, reviews, short communications, discussions, book reviews, and announcements.

მისამართი:

საქართველო, 0160, თბილისი, ალექსიძის ქ. 1, მ. ნოდიას გეოფიზიკის ინსტიტუტი

ტელ.: 233-28-67; Fax; (995 32 2332867); e-mail: tamaz.chelidze@gmail.com; akordzadze@yahoo.com; anzor_gvelesiani@yahoo.com; avtandilamiranashvili@gmail.com

გამოქვეყნების განრიგი და ხელმოწერა

სერია (ა) გამოიცემა წელიწადში ერთხელ. ხელმოწერის ფასია (უცხოელი ხელმომწერისათვის) 30 დოლარი, საქართველოში – 10 ლარი, ხელმოწერის მოთხოვნა უნდა გაიგზავნოს რედაქციის მისამართით. შესაძლებელია ონლაინ წვდომა: http://openjournals.gela.org.ge/index.php/GGS/index

Адрес:

Грузия, 0160, Тбилиси, ул. Алексидзе, 1. Институт геофизики им. М. З. Нодиа

Тел: 33-28-67; 94-35-91; Fax: (99532) 332867; e-mail: tamaz.chelidze@gmail.com; akordzadze@yahoo.com; anzor_gvelesiani@yahoo.com; avtandilamiranashvili@gmail.com

Порядок издания и условия подписи:

Том серии (А) издается по одному номеру в год. Подписная цена 30 долларов США, включая стоимость пересылки. Заявка о подписке высылается в адрес редакции. Возможен онлайн доступ http://openjournals.gela.org.ge/index.php/GGS/index

Address:

M. Nodia Institute of Geophysics, 1 Alexidze Str., 0160 Tbilisi, Georgia

Tel.: 233-28-67; Fax: (99532) 332867; e-mail: tamaz.chelidze@gmail.com; akordzadze@yahoo.com; anzor_gvelesiani@yahoo.com; avtandilamiranashvili@gmail.com

Publication schedule and subscription information:

One volume of issue (A) per year is scheduled to be published. The subscription price is 30 $, including postage.

Subscription orders should be sent to editor's address. Online access is possible: http://openjournals.gela.org.ge/index.php/GGS/index

Journal of Georgian Geophysical Society,
Issue (A), Physics of Solid Earth, v.18a, 2015, pp.3-18

Search of Attractors in seismic time series of Caucasus

Tamaz Chelidze, Natalia. Zhukova, Teimuraz Matcharashvili, Ekaterine Mepharidze
M. Nodia Institute of Geophysics, 1, Alexidze str. 0160, Tbilisi, Georgia,
e-mail: tamaz.chelidze@gmail.com

Abstract

Last years appear controversial publications both on revealing attractors in seismic time series (which means that they can be represented by deterministic chaos model) as well as on theabsence of such ordered structures. So, it seems interesting to study, what methodology should be applied to earthquake time series (ETS) in order to reveal possible attractor structures. There are two main approaches to the problem: i. events in ETSare considered individually; ii. the number of events in ETS in some time window (a seismic rate) is calculated, which is widely used as a proxy of the strain rate in the Earth crust.

The study considers how the spatio-temporal parameters of seismic rate calculations affects the nonlinear structures (phase space plots) in low seismicity areas (Batumi region) as well as before, during main event aftershocks and after strongest Caucasian earthquakes Spitak (1988) and (Racha, 1991).The seismic phase portraits and recurrence plots are constructed for several time windows, different epicentral distances and different magnitude thresholds. The nonlinear structure of laboratory natural and synchronized stick-slip sequences are also considered. The phase space plots' analysis can reveal some fine details of seismic process dynamics.

Introduction

Earthquake time series (ETS) documented as seismic catalogs are objects of detailed statistical analysis, which show that catalogs contain both independent and correlated events (clusters), which means that mentioned data represent complex time series. In some earlier works (Goltz, 1997;Matcharashvili et al., 2000) it is shown that at least one component of catalogs considered as a point process, namely, interevent or waiting time series has a low fractal dimension, which means that catalogs contain some hidden nonlinear structures, which however cannot be considered as attractorsand are more similar to a pink noise pattern.

Last yearsappear publications on revealing attractors in seismic time series, which means that they can be represented by deterministic chaos model (Sobolev, 2011; Srivastava et al., 1996) as well as on absence of such ordered structures (Beltrami and Mareschal, 1993). So, it seems interesting to study, what methodology should be applied to earthquake time series (ETS) in order to reveal possible attractor structures. There are two main approaches to the problem: i. events in ETSare considered individually; ii. the number of events in ETS in some time window or a seismic rate (SR) is calculated, which is widely used as a proxy of the strain rate.

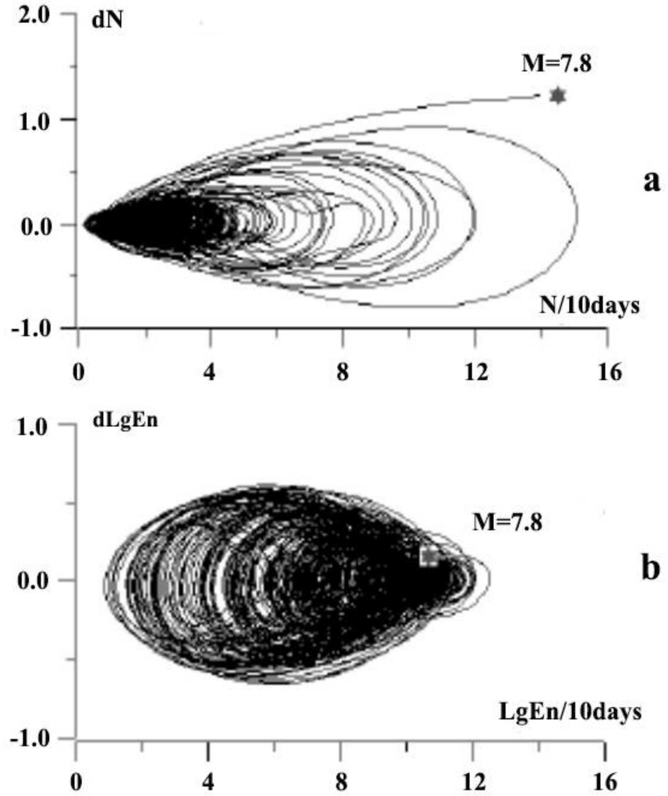

Fig.1. Phase portrait of seismicity within a radius of 100 km from the epicenter of the Kronotskoe earthquake for a 35-year period(1 January 1962–5 December 1997). The smoothed number N of earthquakes (a)or energy LgEn, Joules (b)for 10 consecutive days is marked on the X axis. Rates at which these parameters change (dN or $dLgEn$), i.e. the difference between the following and the preceding values are shown on the Y axis. The clockwise movement along the curve corresponds to an increase in time. The star marks the position of the main shock(Sobolev, 2011).

Recently many new methods of complex time series analysis, mainly due to intensive progress in nonlinear dynamics (complexity) theory (Abarbaneland Tsimring,1993;Anishchenko, 1995;Eckmann,1987;Goltz, 1997). The new tools developed in complexity theory reveal a lot of important information, contained in seismic catalogs, considered as discrete earthquake (EQ) time series (Chelidze and Matcharashvili, 2015). Methods, developed in complexity theory allow visualization and quantification of seismic rate patterns and their variation in time, what enriches significantly traditional statistical approach, presented in Marsan and Wyss (2011).

Data andMethods of ETS analysis

The statistical approach to seismic rate (SR) provides mainly tools for statistically reliable assessment of rate change using long enough earthquake (EQ) time series, e.g. for comparison of SR before and after strong earthquake (Marsan and Wyss, 2011). The same methods are applied to nonstationary time series (ETAS, Z-statistics). These methods are too crude to reveal fine anomalies in ETS, due, for example hidden non-linear structures.Presently for visualization and quantitative analysis of hidden non-linear structures are widely used such methods as phase space plots (PSP), Recurrence Plots (RP), Recurrence Quantification Analysis (RQA), see for example WebberandMarwan (2015). PSP and RP are two interconnected ways to reveal the recurrence in time series: for example, diagonal lines in PR appear when segments in PSP trajectory (attractor) run on close paralleltrajectories.The advantage of RP is that it enables qualitative visualization of highdimensional dynamics, while PSP is convenient for lowdimensional processes, where trajectories in the attractor run on close to parallel trajectories.

We analyze mainly seismic rates, which according to general statistics terminology correspond to a conditional rate (conditional intensity) models in point process theory. We used the rates, obtained either by simple averaging (Sobolev,2011) or by Savitsky-Golay (S-G)-filtering. Savitzky-Golay filter helps to resolve smoothing problem in the time domain. It approximates the data locally (corresponding to some user-chosen window) with an n^{th} degree polynomial preserving up to the n^{th} moments of the data. Hence it has the advantage over, for instance, moving average filter as the magnitude of the variations in the data, i.e., the value of the local extremes, is preserved to a large extent.The optimal lag for PSP reconstruction from daily series of EQ occurrences by Mutual Information (MI) test is close to 50 days.

The averaging/smoothing is widely used in the processing of real data though there are fierce opponents, who call down curses on the heads of "datasmoothers" such as: "Do not smooth times series, you hockey puck!" (http://wmbriggs.com/blog/?p=195). Still we consider the smoothing procedure is a quite lawful procedure (Simonoff,1998; Einicke, 2012), accepted in many signal processing packages (MATLAB, Matematica, etc). It isa very useful tool: the operation of smoothingperforms actually a low-pass filtering of the sequence, which in turn allow revealing long-range correlations in the data (here -in ETS).

For nonlinear analysis the seismic catalogue of Caucasus (1960-2011) has been used; the representative magnitude for the period is M2 (Fig.2). The following parameters of ETSwere varied: i. the area, where ETS were obtained; ii. the length of time window for rate counting; iii. the years span (periods in catalog); iv. periods before and after strong events.

The PSP plots are compiled by two methods: i. The whole EQ data sets from the catalog were declusteredusing Reasenberg algorithm (Matthews and Riesenberg, 1988)and smoothed in the following way:on the X axis are plotted the mean values of number N of EQs per n days(n = 10,20,50) or N/n and on the Y axis is plotted just differential of X, i.e $(N_{i+1} - N_i)/n = dN$.This approach was used by Sobolev (2011).

ii. The whole EQ data sets from the catalog were declustered and smoothed by Savitzky-Golay (S-G) filter. Then on the X axis is plotted the smoothed by S-G filter value of number N of EQs for a given day N/day and on the Y axis - smoothed by S-G filter N value with some days delay $(N + lag)$, we plot smoothed by S-G filter lagged by 10,20, 50 days daily valuesof $(N + lag)$ versus daily value N/day.

iii. Combined approach: PSP is compiled for one day step (like in Sobolev approach) as dN versus N/day for the data declustered and smoothed by S-G filter (in contrast to Sobolev approach, where just the mean value of N in the sliding window are used).

The trajectories on PSP plots are obtained by connecting the consecutive phase states. The consecutive phase spacepoints are plotted in clockwise direction, which corresponds to increase in time.For plotting phase plots were used either standard MATLAB scripts -seism_port and phase_portrait (in following - standard) or Sobolev (2011) approach (in following - Sobolev).

Both approaches sometimes produce negative values of phase states, which means that the smoothed lagged values are smaller than previous ones.As an example of processing, on the Fig.2are presented phase space plots of daily EQ occurrence sequence of EQs compiled for original non-smoothed data (a) and for the same data, smoothed by Savitzky-Golay filter (b). It is evident that the former is less informative and the latter one reveals some interesting structure in the phase space.

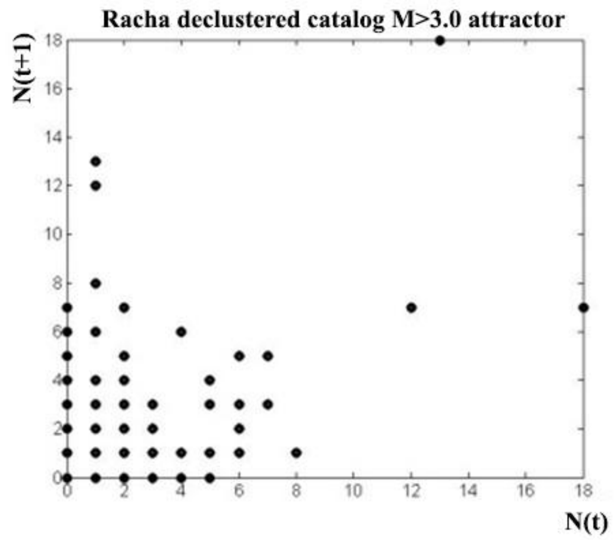

a.

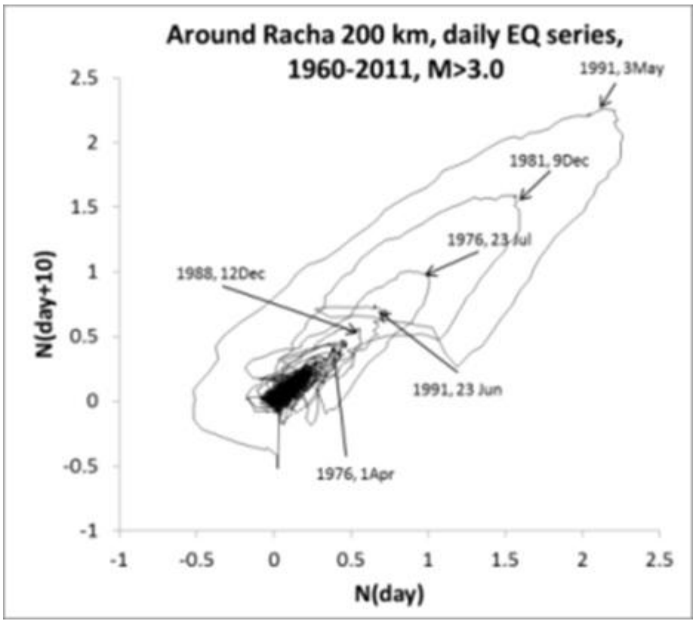

b.

Fig. 2. Phase space plots of daily EQ occurrence sequence in Caucasian earthquake catalog(1961-1991) for the area in the radius 200 km around Racha EQ compiled by above mentioned standard scripts for original non-smoothed data (a) and for the same data, smoothed by Savitzky-Golay filter (b).

Results and Discussion

Nonlinear analysis of data sets obtained from the seismic catalogue of Caucasus for the period 1960-2011 has been performed; the representative magnitude for the period is M2.In the analyzed period 1960-2011 two largest Caucasian Spitak and Racha (M6.9-7) earthquakes (EQs) stroke the region in 1988 and 1991 correspondingly. Thus, three areas were selected: i. Batumi(in order to show the pattern of ETS in relatively quiet region; ii. Spitak and iii.Racha(Fig.3). We analyzed both original and declustered by Matthews and Riesenberg(1988) approach catalogs.

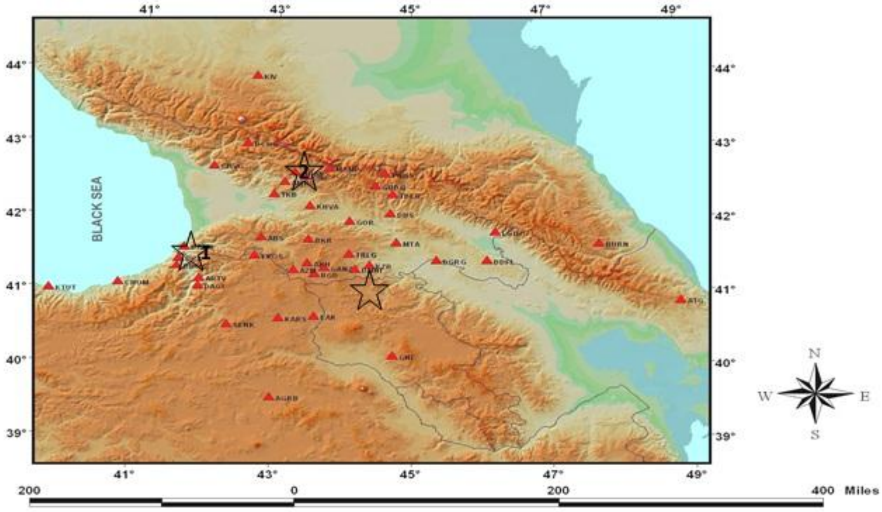

Fig.3. Areas in Caucasus where the analysis of seismic data sets was carried out for revealing possible attractors. Blue stars are centers of test areas: 1 – Batumi; 2 – Racha and 3 – Spitak. Triangles show seismic stations' locations.

Batumi area

Batumi area (Fig.2) was chosen as a (relatively) seismically quiet area:though there were nostrong EQs on the distance 100 km from Batumi, two EQs of M6.4-6.9 occur on the distance of the order 200 km in the considered period (Chkhalta, 16.07.1963 and Erzurum, 30.10.1983).Fig. 4presents original and Savitzky-Golay filtered daily series of EQ occurrences in Batumi area (R=200 km) in 1960-1986 declustered by Reasenberg algorithm. Fig. 5 a, b, c showsstandard phase space portraits of declustered daily series of EQ occurrences in Batumi area smoothed by the S-G filter for various Lags. On the *X*-axis is plotted the S-G filtered daily number of EQs and on the*Y*-axis the same value for *Lag*10, 20 and 50 days.These PSP plots demonstrate two main details: a highly populated area between 0 and 1, which can be considered as a relatively stable domain (or a source area) due to a background seismic activity(this area is shown by arrows for two successive enlargement scales) and strongly deviated trajectories (Fig. 5 a, b, c). These latter orbit-like figures, should reflect deviations from the background activity due to some extremes - swarms, foreshocks and aftershocks. This is a bit strange, as the declustering procedure should eliminate such effects. Still it seems that Reasenberg procedure does not eliminate all correlated events as it is shown in (Matcharashvili et al., 2015) and these orbits can be related to correlated events left after declustering.

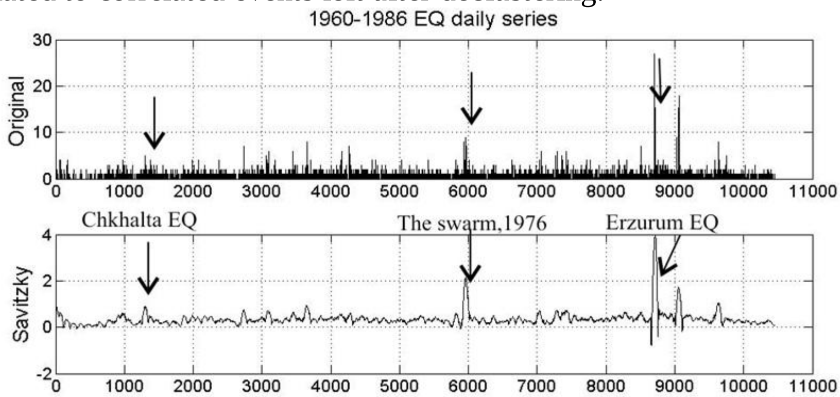

a.

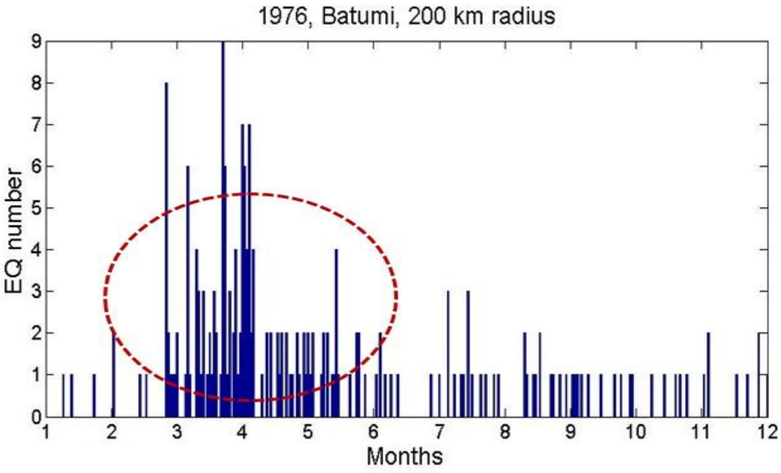

b.

Fig. 4. a) Daily series of EQ occurrences in Batumi area (R=200 km) in 1960-1986declustered by Reasenberg algorithm: original (upper) and (lower); b) the swarm in 1976.

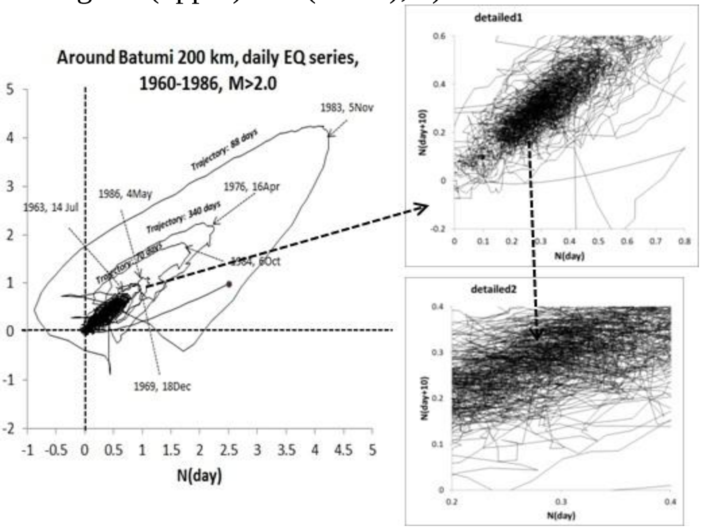

a.

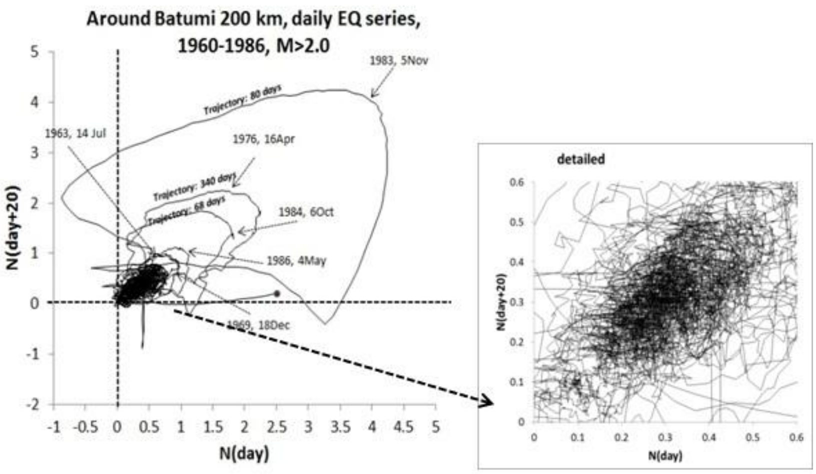

b.

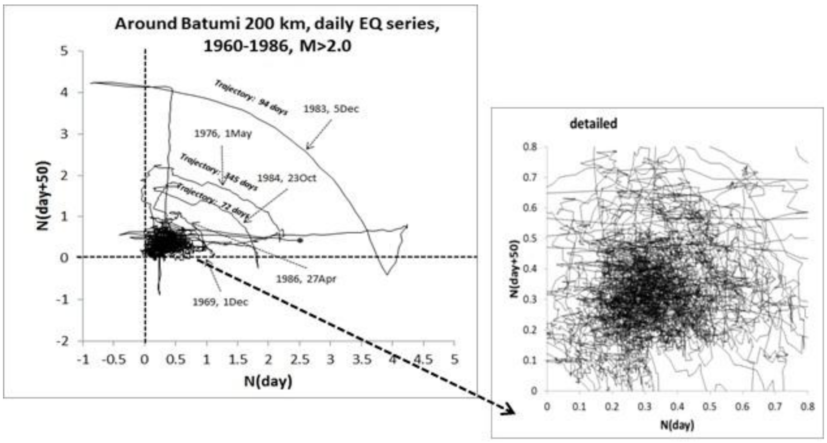

c.

Fig.5. a, b, c) Phase space portraits PSP (standard) of daily series of EQ occurrences in Batumi area for R=200 km, declustered and smoothed by the S-G filtered data sets from catalogs (data of Fig.4). PSPs of EQ occurrences daily value *N* (day) with: (a) *N* in 10; (b) *N* in 20 and (c) *N* in 50 days versus corresponding the lagged values ($N + lag$), where the *Lag* is 10, 20 and 50 days.

Some of extended (anomalous) orbits seem to be related to: i - in1968 - possibly to a swarm; ii - in 1983 - to Erzerum EQ 30.10.1983 Ms 6.9;iii. - 1984 - probably extended aftershocks of Erzerum EQ. Note – for the R=100 km around Batumi the Erzerum EQ 30.10.1983 Ms6.9 response (length of obit) is less significant than that of the 1968 swarm in contrast to data for R=200 km, due to lesser number of ErzerumEQ aftershocks in a more distant from the epicenter area (at R=100 km).The length of the whole trajectory (loop) corresponds to the summary period of foreshocks and aftershocks (Table 1).

Table 1. Duration of the most outlying trajectories on Fig. 5 a,b.

Trajectories on Fig. 5 a, b,c.	Duration of full trajectory, days	Half trajectory duration
Most outlying (1983)	80-94	40
Second distant (1976)	340-345	210
Third distant (1984)	68-72	40

Surprisingly, the strong 1963 ChkhaltaEQ (M6.4, distance from Batumi 175 km) caused relatively small deviations from the source area - see trajectories for Chkhalta in Fig. 5 a, b

.

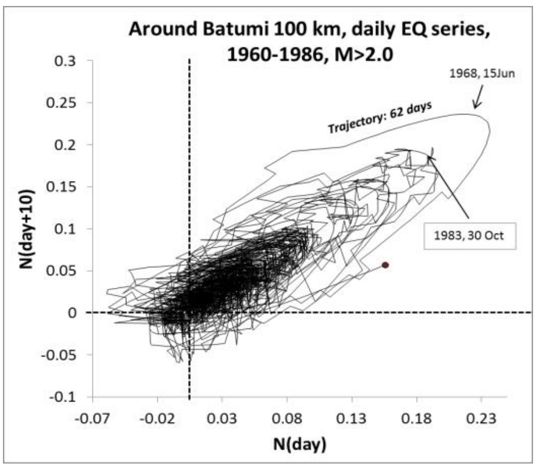

a.

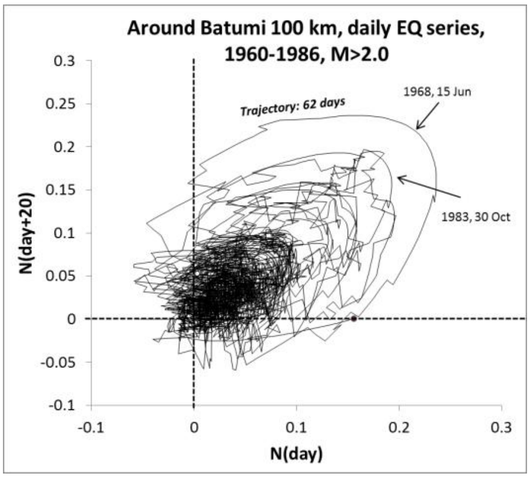

b.

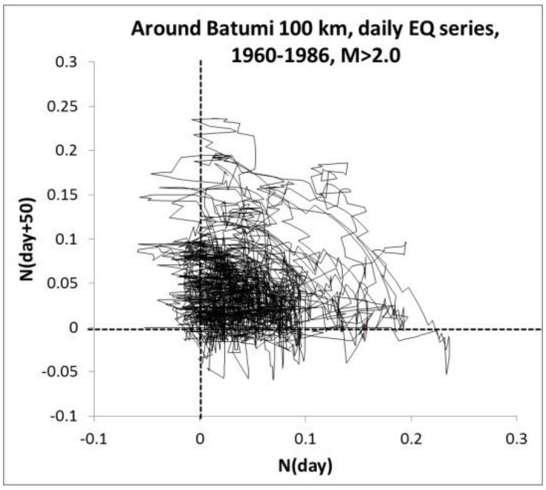

c.

Fig. 6. a) Phase space portraits (standard) of daily series of EQ occurrences in Batumi area for R=100 km, declustered and smoothed by the S-G filtered data sets from catalogs (data of Fig.4). PSPs of EQ occurrences daily value *N* (day) with: (a) *N* in 10; (b) *N* in 20 and (c) *N* in 50 days versus corresponding the lagged values ($N + lag$), where the *Lag* is 10, 20 and 50 days.

The PSPs of trajectories for R=100 km distance form Batumi (Fig. 6) differs from the PSPs for R= 200 km. Extended (anomalous) orbits are possibly related: i. - 1968 - to a swarm in 1968.The length of this most outlying trajectory for 1968 event is 62 days; ii. - 1983 - to Erzerum EQ 30.10.1983 Ms 6.9. Note – for the R=100 km around Batumi the Erzerum EQ 30.10.1983 Ms 6.9 the corresponding orbit is less significant than that for the local swarm in contrast to data for R=200 km, due to smaller number of aftershocks farther from the Erzerum epicenter area. According to the Table 1, the duration of the trajectory till Erzerum EQ is approximately 40 days - this can be considered as a precursory sign.

Finally, Fig. 7 illustrates the impact of processing methodology of EQ time series on the structure of PSP. Note that trajectories of orbits in PSPs plotted using differential of current and previous *N* (differential $N_{i+1} - N_i / n$) not versus smoothed *N*/10 days (Fig.7) are much more smooth and ordered compared to results obtained with larger stepsFigs. 4, 5)as the successive *N*/10 days input data sets plotted with 1 day step differ insignificantly, only by 2 days data; the rest of data in the sets are the same. In contrast, the data sets in Figs. 4 and 5 do not contain identical data (the successivedata sets are not overlapping), which results in more jogged trajectory. It is evident that for strongly overlapping data sets the PSP structure is close to that of attractor - we can see almost ordered orbits in the expanded source area (Fig.7 b)

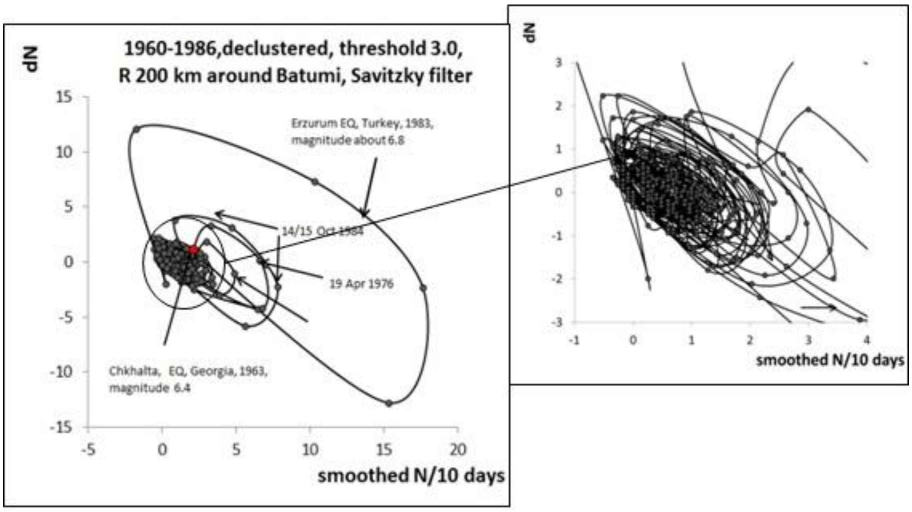

a. b.

Fig.7.a) PSP of *dN* versus declustered and S-Gsmoothed for *N*/10 days data (catalog 1960-1986) in Batumi area (here we apply S-G smoothing and 1 day *Lag* in contrast to Figs 5, 6, i.e. we combine standard and Sobolev approaches), R=200 km; b) expanded view of the source area, limited by a circle in Fig. 7a.

In order to test whether the methodology used to obtain Fig.7 is really informativewe apply this procedure to the random sequence of numbers (Fig.8). It is evident that combination of smoothing with small successive steps (*Lags*) lead to appearance of smooth orbit-like trajectories even for random number sequences, so the similar ordered trajectories in EQ rate time series (Fig.7) appear just as result of a definite smoothing procedure and are not related to fundamental properties of the seismic rate dynamics. At the same time significant deviations from the source area in PSPs of earthquake time series, due to swarms and strong events are clearly revealed by both (standard and Sobolev) approaches - compare Fig.5 and 7.

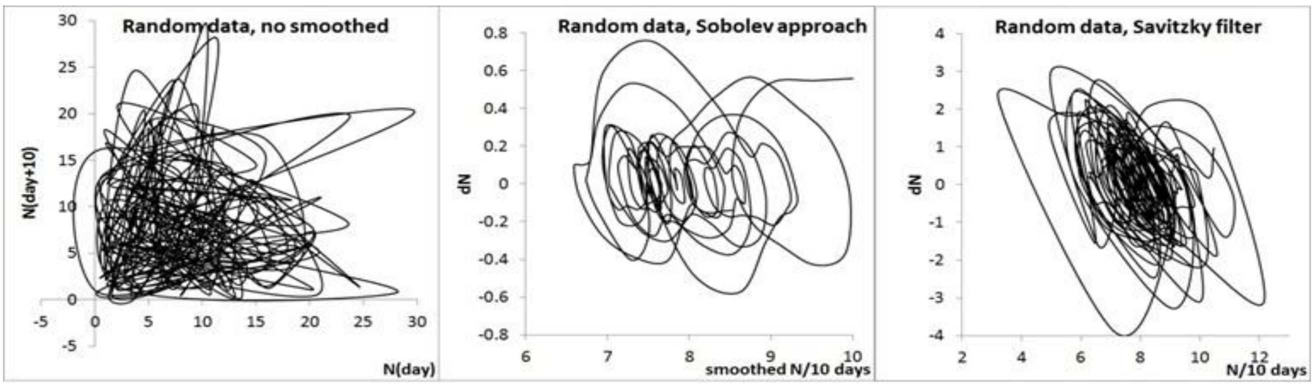

a. **b.** **c.**

Fig.8. PSP compiled for a "rate" of random sequence of numbers considered as a proxy to number of EQ occurrences in 10 days; a) standard attractor, no smoothing applied; b) plot of *dN* versus *N/10* "days" for original (non-smoothed) data; c) plot of *dN* versus *N/10* "days" for S-G smoothed data; standard plot

Spitak earthquake area

Spitak earthquake (Fig.2) occurred in Armenia, December 7, 1988. The earthquake measured 6.9 on the surface wave magnitude scale. In following we calculated PSPs of EQ time series in Spitak EQ area– data for area of radius 100 km around Spitak EQ epicenter (catalogs1960-1988 and 1960-2011); both original and declustered ETS were analyzed. Fig. 9

shows the daily occurrence of EQs in Spitak EQ epicenter area for R= 100 km.According to PSP in Fig. 10e, the deviating orbits are visible for 1967, 1971, 1978, 1986 and 1988. The last orbit is definitely related to Spitak EQ foreshock/aftershock activity. Note big difference in the structure of PSP for analyzed two catalogs, which can be explained by the strong influence of seismicity, caused by foreshocks/aftershocks activity of Spitak EQ included in the plots 10 d, e, f. It seems informative to divide the most outlying orbit in Figs. 10 d, e, f into pre- and post-Spitak parts in order to assess the "precursory" part of the trajectory. The full duration of the orbits is in Figs. 10 d, e, f is approximately 120-200 days and the duration of the "precursory" part is 30-50 days for various lags . Thus, a strong deviation of the orbit from the source area can be considered as the precursor of the strong event, due probably to foreshock activity (not excluded fully by Reasenberg declustering).

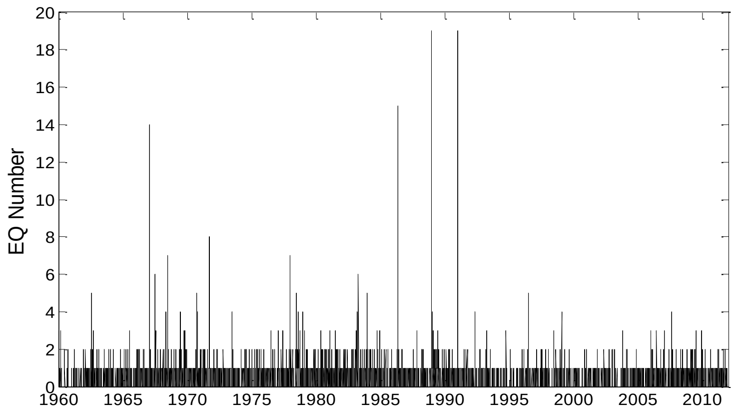

Fig.9. Daily occurrence of EQ in Spitak area in 1960-2011for R= 100 km; two largest spikes are related to 1988 Spitak and 1991 Racha EQs.

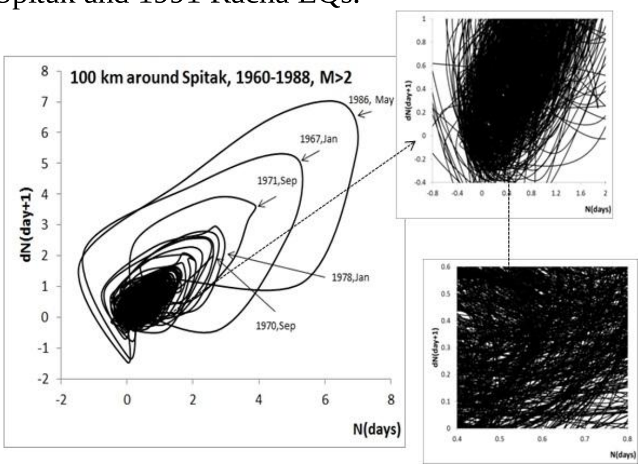

a.

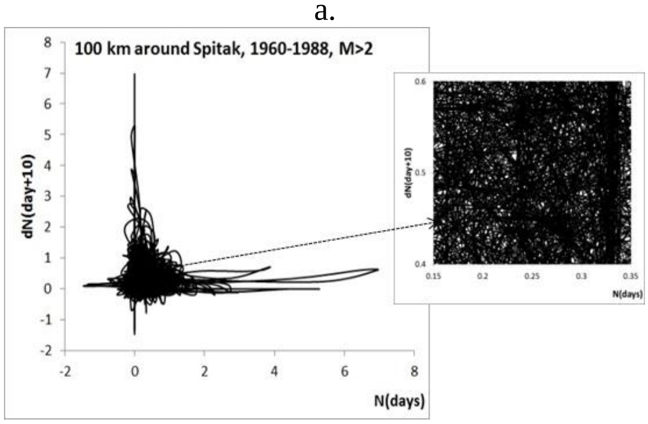

b.

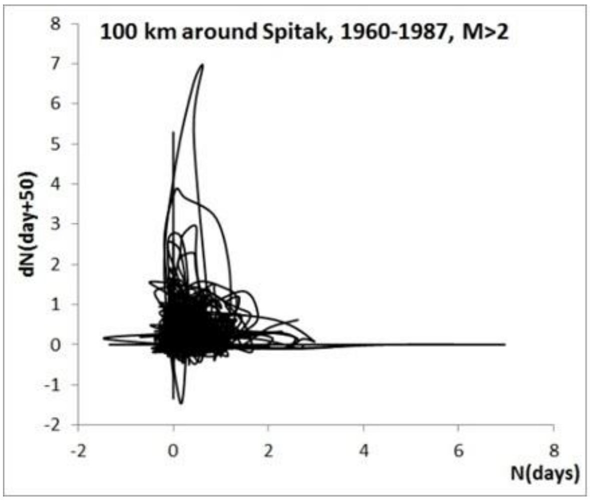

c.

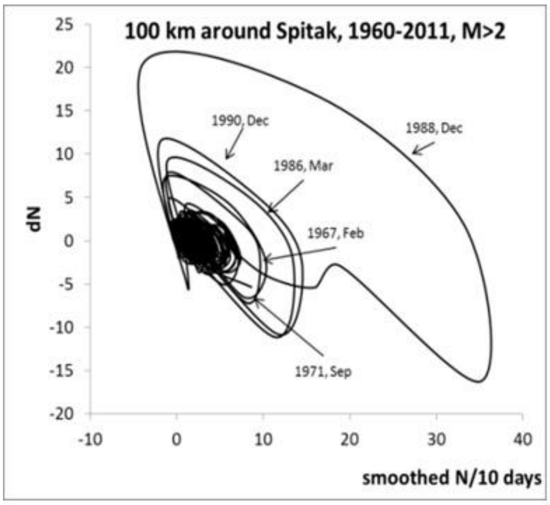

d.

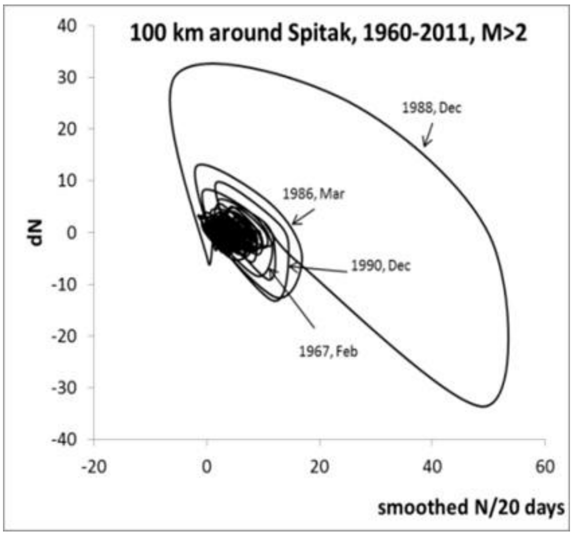

e.

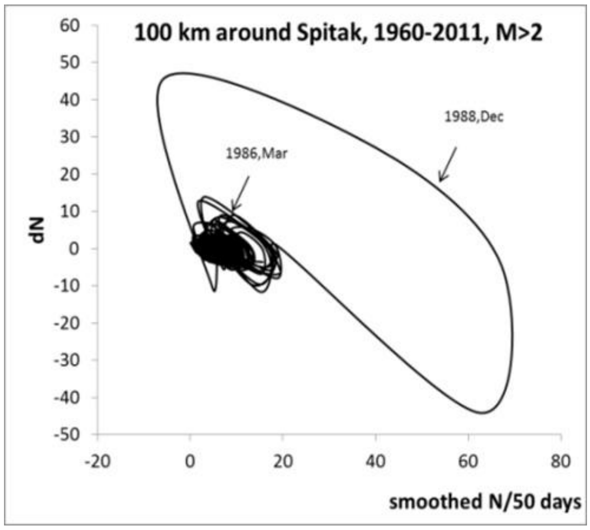

f.

Fig. 10. Phase space portraits of daily series of EQ occurrences in Spitak area for R=100 km, declustered and smoothed by the S-G filtered data sets from catalogs; a, b, c - PSPs (standard) for catalog 1960-1988, of smoothed by S-G filter lagged value (*N+lag*) where the *Lag* is 1, 10, 20 and 50 daysversus daily value *N*(day) with *N* 10; 20 50 days not including Spitak EQ; d, e, f - PSPs of *dN* versus declustered and smoothed for *N*/10 days data in the same area for catalog 1960-2011, R=100 km. Note a big difference in the structure of PSP for two catalogs caused by inclusion of foreshocks/aftershocks activity of Spitak EQ in the plots 10 d, e, f.

Racha EQ area

The Racha earthquake occurred in the Racha province of Georgia at 9:12 UTC on 29 April 1991 on the southern foothills of the Greater Caucasus mountains. It had a magnitude of 7.0 and was the most powerful earthquake recorded in the Caucasus.

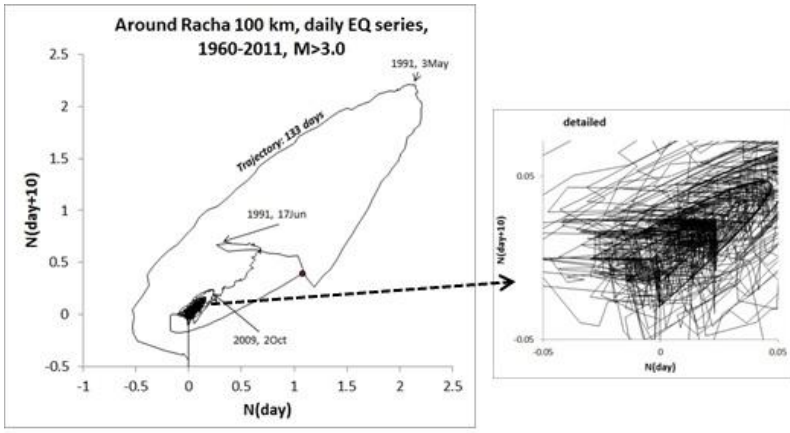

a.

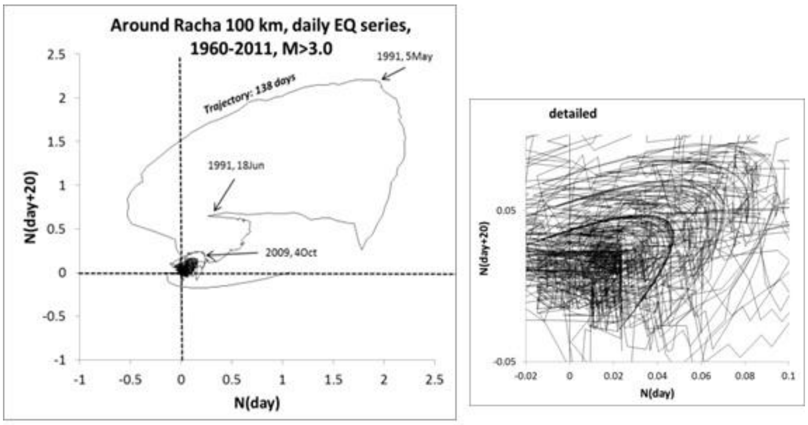

b.

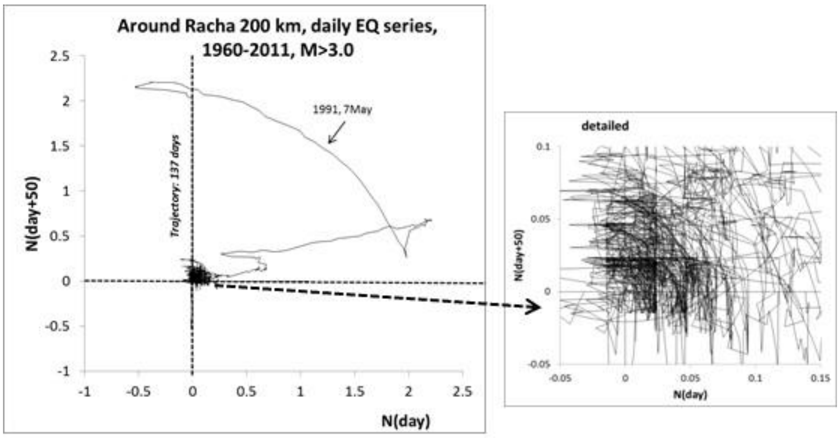

c.

Fig.11. a, b, c. Phase space portraits of data set for Racha test area for declustered S-G filtered catalog 1960-2011 (R= 100 km), for lags 10,20,50 days; note ordered structures in the source area.

Table 2. Duration of the most outlying trajectories on Fig. 11 a, b,c.

Trajectories on Fig. 11 a, b,c.	Duration of a full trajectory, days	Trajectory duration till Racha EQ, days
Most outlying (1991)	133-138	64

The most extended orbits reach the following maximal deviations at lags 10 and 20: i. the point on the orbit for 1991, 3 May is close to the mainshock moment of Racha EQ, which occur

29 April; ii. - the point 1991, June corresponds to Java strong aftershock of Racha EQ, 15 June, 1991, M6.2; iii. - 2009, Oct is related to Racha EQ, 8 Sep 2009, M6.

The length of the most extended trajectory with a label 1991, 3 May is 133 days (beginning from the central cluster). If we assume that the time to a label 1991, 3 May is a half of the full duration (133 days) than the significant deviation from the background seismicity (central cluster) begin before the Racha mainshock. Possibly, this time, needed for forming the half-orbit - approximately 60 days (Table 2) - can be considered as a precursor of the mainshock.

The phase space portraits of Fig.11a,b seems to be the most interesting ones: here in the radius R=100 km in the detailed (expanded) plots of the central cluster of trajectories some clear recurrent orbits are visible with strange configurations – parabolas, right angles. We cannot see such recurrent configurations at PSP for the larger test area, namely, for R=200 km.

PSP of waiting time series

Besides seismic rates the phase space plots of EQ waiting times were investigated (Fig. 11); earlier studies reveal low values of correlation dimension of EQ time series (Matcharashvili et al., 2000). The results do not confirm existence of any clear ordered structure in PSPs of EQ waiting time series.

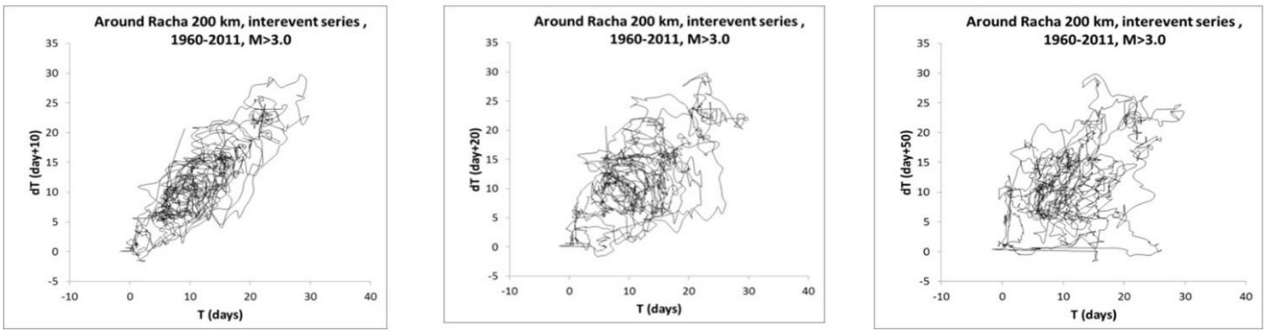

Fig. 12. PSPs of waiting time series were obtained from declustered 1960-2011 catalogs of Racha EQ area (R=200 km) using standard approach.

Recurrence Quantification Analysis of EQ time series

Last years for visualization and quantitative analysis of hidden non-linear structures are widely used Recurrence Plots (RP) and Recurrence Quantification Analysis (RQA) - see for example (Webber and Marwan, 2015). As mentioned earlier, PSP and RP are two interconnected ways to reveal the recurrence in time series. RQA is preferable at quantitative assessment of high-dimensional dynamics. In Chelidze and Matcharashvili (2015) RQA method is usedfor investigation of earthquakes catalogues' complexity. Exactly, earthquakes' daily and monthly occurrences data sets have been derived both from the original as well as from the declustered (according to Matthews and Reasenberg, 1988) catalogues with a magnitude threshold $M \geq 3.0$.

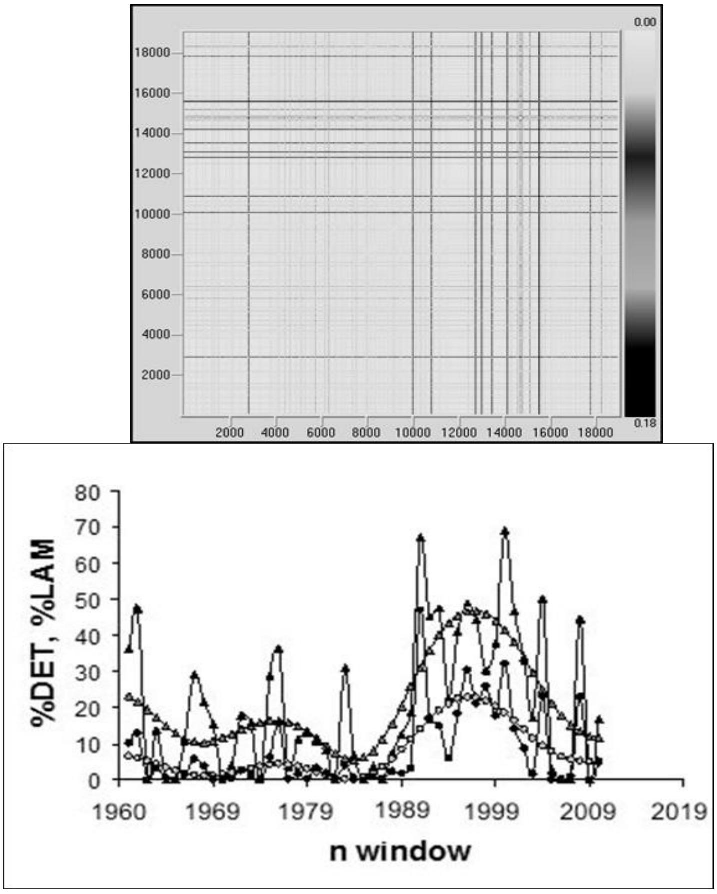

a b.

Fig. 13.a) RP and b) RQA %DET (black circles) and %LAM (triangles) of daily frequency of earthquake occurrence time series, 365 days length sliding window and 365 days step. Grey circles - Savitzky-Golay smoothing(Chelidze and Matcharashvili, 2015).

In Fig. 12 results of RP and RQA calculations for consecutive one year length daily frequency of earthquake occurrencesets at one year step are shown. Because of essential variation of RQA measures calculated for short (365 data) segments, results for data smoothed according to Savitzky-Golay filtering method are also presented (filled triangles and circles). Indeed we see that the EQ timeseries contain component with significant % of determinism (%DET) and laminarity (%LAM), which varies in time: large values of %DET and %LAM are fixed approximately from 1990 to 2005.

Thus, it is evident that Recurrence Quantification Analysis is more effective in revealing hidden nonlinear structures in the EQ timeseries than PSP or RPapproach.

Conclusions

1. The structures in phase pace portraits of 10 days smoothed earthquake rate time series at volcanic area (Kronotskoe EQ) obtained by Sobolev seem to be very similar to attractors: this can be related to the processing methodology (using 1 day step and overlapping 10 days windows) as well as to a specific seismic regime in such areas. Investigations in volcano seismology show that seismic events near volcanic centers reveal some regularities due to weak external periodic forcings (e.g.tides), which is explained by high sensitivity of such areas to small perturbations.
2. The possibility of existence of seismic attractors and correspondingly, of deterministic chaos regime in non-volcanic areas, which are less sensitive to weak forcings remain obscure: analysis of nonlinear dynamics of earthquake time series (namely, Recurrence

Quantitative Analysis) shows that there are nonlinear structures of relatively low fractal dimension, especially intime and space domains; at the same time trajectories in the phase space are not very regular.

3. Phase Space Portraits (PSP) and Recurrence Plots can be considered as interesting visualization tools for analysis of seismicity dynamics. On phase space plots of smoothed (for 10,20,50 days) seismic rate sequences in Racha area there are some attractor-like clusters generated by background seismicity. It seems that before/after strong earthquake there are some anomalies in PSPs even using declustered (by Riesenberg approach) catalogs, presumably well expressed in case of significant foreshock/aftershock activity or presence of clusters. In principle this can be used in strong earthquake precursors' search.
4. More detail studies in various tectonic regions should be performed in order to make definite conclusions on the dynamic structure of seismic rate time series and on potential of the used methods (PSP, RQA) for analysis of seismic process.

Acknowledgments

The authors express their gratitude to the Rustaveli National Science Foundation of Georgia (Project FR/567/9-140/12) for financial support.

References

[1] Abarbanel, H. and Tsimring, L. S. 1993.The Analysis of Observed Chaotic data in Physical Systems, Rev. Mod.Phys, 65, 1331-1392.
[2] Anishchenko, V. S. 1995.Dynamical Chaos—Models and Experiments, World Scientific Series on Nonlinear Science—Series A, Singapore.
[3] Beltrami, H.,Mareschal, J.-C.1993. Strange seismic attractors?Pure and Applied Geophysics, 141, 71-81
[4] Chelidze, T.,Matcharashvili, T. 2015. Dynamical Patterns in Seismology. In: Recurrence Quantification Analysis: Theory and best practices. (Eds. C.Webber and N.Marwan). Springer Cham Heidelberg, pp. 291-335.
[5] Eckmann, J-P., Kamphorst, S., Ruelle, D. 1987. Recurrence plots of dynamical systems. Europhysics Letters. 4, 973-977.
[6] Einicke, G. A. 2012. Smoothing, Filtering and Prediction: Estimating the Past, Present and Future. Intech.
[7] Goltz, C.1997. Fractal and chaotic properties ofearthquakes.Springer, Berlin.
[8] Marsan, D., and Wyss, M. 2011. Seismicity rate changes. Community Online Resource for Statistical Seismicity Analysis; doi:10.5078/corssa-25837590.
[9] Matcharashvili, T., Chelidze, T., Javakhishvili, Z. 2000. Nonlinear analysis of magnitude and interevent time interval sequences for earthquakes of the Caucasian region. Nonlinear Processes in Geophysics, 7, 9 – 19.
[10] Matcharashvili, T., Chelidze, T., Zhukova, N. 2015. Assessment of a ratio of the correlated and uncorrelated waiting times in the Southern California earthquake catalogue. Physica A 433, 291-303.
[11] Matthews, M. and Reasenberg, P.1988.Statistical methods for investigating quiescence and other temporal seismicity patterns.Pure Appl. Geophys. 126, 357-372.
[12] Simonoff, J. S. 1998. Smoothing Methods in Statistics, 2nd edition.Springer.
[13] Sobolev, G. 2011. Seismicity dynamics and earthquake predictability. Nat. Hazards Earth Syst. Sci., 11, 445–458.
[14] Srivastava, H. N., Bhattacharya, S. N. and Sinha Ray, K. C. 1996. Geophys. Res. Lett.,23, 3519–3522.
[15] Webber, C., Marwan, N. (Eds). 2015. Recurrence Quantification Analysis. Theory and Best Practices. Springer Cham Heidelberg

ატრაქტორების ძიება კავკასიის სეისმურ დროით სერიებში

თამაზ ჭელიძე, ნატალია ჟუკოვა, თეიმურაზ მაჭარაშვილი, ეკატერინე მეფარიძე

რეზიუმე

ბოლო წლებში, გამოჩნდა სადავო პუბლიკაციები სეისმურ დროით სერიებში ატრაქტორების როგორც არსებობის (რაც ნიშნავს, რომ შეიძლება წარმოადგენდეს დეტერმინირებული ქაოსის მოდელს), ასევე ასეთი მოწესრიგებული სტრუქტურების არარსებობის შესახებ. აქედან გამომდინარე საინტერესოა მეთოლოგიის შესწავლა, რომელიც შეიძლება გამოყენებულ იქნას მიწისძვრის დროით სერიების (ETS) დამუშავებისას შესაძლო ატრაქტორების გამოსავლენად. ასეთი პრობლემის გადასაწყვეტად შემუშავდა 2 მიდგომა: 1. მოვლენები ETS განიხილებიან ინდივიდუალურად; 2. მოვლენების რაოდენობა ETS- ში გამოითვლება რამდენიმე დროის ფანჯარაში (სეისმურობის დონე). ეს უკანასკნელი სიდიდე ფართოდ გამოიყენება მიწის ქერქის დეფორმაციის სიჩქარის დასახასიაღთებლად.

კვლევები გვიჩვენებენ თუ რა გავლენას ახდენს სეისმურობის სივრცული-დროითი პარამეტრები არაწრფივ სტრუქტურებზე (ე.წ. ფაზურ სივრცულ პორტრეტებზე) როგორც დაბალი სეისმურობის რეგიონებში (ზათუმის რეგიონი), ასევე კავკასიის ძირითადი ძლიერი მიწისძვრების (სპიტაკი, 1988 და რაჭა, 1991) წინ, მიწისძვრების დროს და მიწისძვრების შემდეგ. რამდენიმე დროითი ფანჯრისათვის, სხვადასხვა ეპიცენტრული მანძილებისა და მაგნიტუდის მნიშვნელობებისათვის აგებული იქნა სეისმურობის ფაზური და რეკურენტული გამოსახულება. ასევე განვიხილეთ ნატურალური და სინქრონიზირებული სტიქ-სლიპის არაწრფივი სტრუქტურები. ფაზური სივრცის სტრუქტურის ანალიზი ავლენს ახალ მნიშვნელოვან დეტალებს სეისმური პროცესის დინამიკაში.

Journal of Georgian Geophysical Society,
Issue (A), Physics of Solid Earth, 2015, pp.19-25

Mass-movement and seismic processes study using Burridge-Knopoff laboratory and mathematical models

Nodar Varamashvili, Tamaz Chelidze, Marina Devidze, Zurab Chelidze, Victor Chikhladze, Alexander Surmava, Khatuna Chargazia, Dimitri Tefnadze

Abstract

Simple models of mass movement and seismic processes are important for understanding the mechanisms for their observed behavior. In the present paper, we analyze the dynamics of a single-block and Burridge-Knopoff model on horizontal and inclined slope with Dieterich–Ruina and Carlson friction laws. In our experiments, the slip events are distinguished by acoustic emission bursts, which are generated by slider displacement. Also acceleration was recorded on each sliding plate using attached accelerometer. In the case of the inclined slope experimental model a seismic vibrator, which produces low periodic impact (forcing) was attached to the sliding plate. This was a numerical simulation of dynamic processes occurring at one- and four-plate Burridge-Knopoff system.

Introduction

The aim of the study was the selection of optimum methods to monitor landslides and develop practical methods of reducing the risk of landslides. For many countries around the world landslides are one the most severe of all natural disasters, with large humanitarian and economic losses. The earth surface is not static, but dynamic system and landforms change over time as a result of weathering and surface processes (i.e., erosion, sediment transport and deposition). The fast mass-movement has a potential to cause significant harm to population and civil engineering projects. Large-scale experiments and field observations show that the landslide may reveal stick-slip motion [Helmstetter et al., 2004, Fabio Vittorio De Blasio, 2011]. When the friction between two solids shows velocity weakening behavior, stationary motion becomes unstable and stick-slip motion appears [Nasuno et al., 1998], which repeats stopping and fast moving states. Analysis of the experimental data, obtained by investigating of spring-slider system motion has lead to empirical law, named rate- and state-dependent friction law [Dieterich 1979, Ruina 1983]. The rate and state dependent friction can be quantified as follows [Dieterich 1979, Ruina 1983]:

$$\tau = \sigma_0\left(\mu_0 + a\ln\left(\frac{V}{V_0}\right) + b\ln\left(\frac{V_0\theta}{D_0}\right)\right), \quad (1)$$

where μ_0 is the initial coefficient of friction, V is the new sliding velocity, V_0 is the initial sliding velocity, θ is the state variable and D_0 is the critical slip distance, a and b are two experimentally determined constants.

The state variable varies according to:

$$\frac{d\theta}{dt} = 1 - \frac{V\theta}{D_0} \quad (2)$$

To study the stick-slip process a mathematical model proposed by Burridge-Knopoff is also used [Burridge R. and Knopoff L. 1967, Erickson et al.,2010, Matsukawa, H., Saito, T., 2007] (Fig.1). Plates are arranged on a massive platform and pulled by the upper platform. The upper plate moves with a constant loading velocity *v*. The blocks of mass *m* are connected to the upper plate by linear springs with spring constant k_p. The blocks are also connected to each other by linear springs with springs of natural length *a* and the constant k_c,. Frictional force acts between the lower plate and each block.

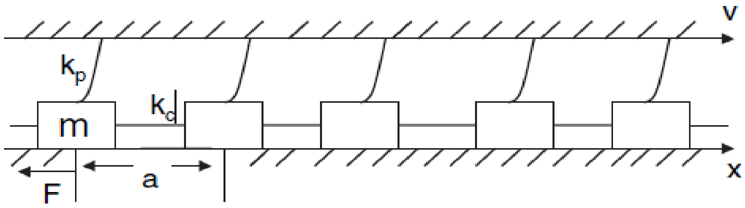

Fig.1. The schematic presentation of Burridge-Knopoff model

The Burridge-Knopoff model is convenient as it allows us to simulate many scenarios of rupture without being too expensive in regard to computing time. Thus we have the ability to explore the parameter space of the system more broadly and observe the emergent dynamics introduced by the friction law.

Experimental setup

Experiments were conducted on a Burridge-Knopoff laboratory device for the models consisting of one and three basalt plates (Fig.2). Registration was made with the help of accelerometers and piezo sensors. On one plate model three accelerometers were attached on the plate, which recorded x, y and z components. Plates were pulled via the upper platform at a speed of 1 mm/s. The experiments were also conducted for the model of the three plates. Each plate was attached on one accelerometer, which measures the x component of the acceleration. Accelerations and acoustic emissions recording are presented in Figure 3. In experiments Tri-axis accelerometer MXR9500G/M and piezo sensors were used. Mass of the each sliding plate $\approx 335\ g$, spring constants $k_c \approx 360\frac{N}{m}$ and $k_p \approx 155\frac{N}{m}$. Dragging velocity was $v \approx 1\frac{mm}{s}$.

Fig.2. The Burridge-Knopoff one- and three plate experiments

a) b)

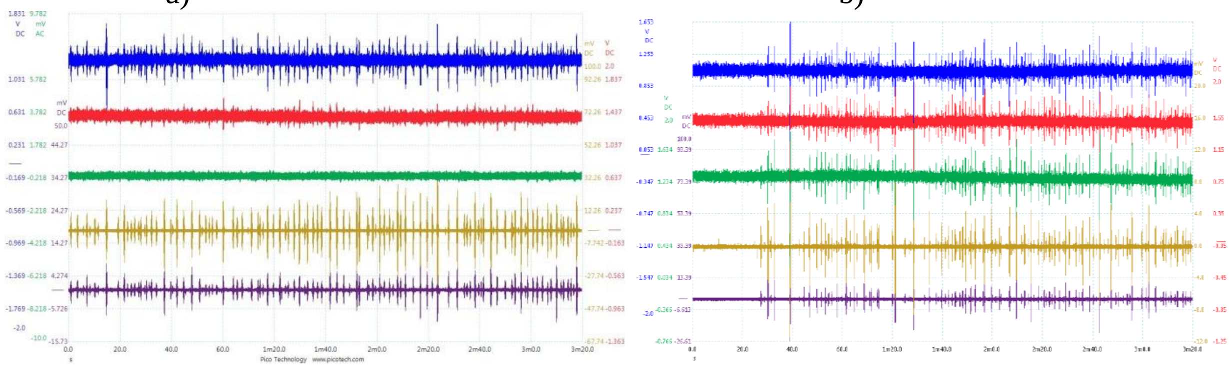

Fig.3. The Burridge-Knopoff system experiments accelerometers and acoustic emission data recordings: a)one plate and b)three plate experiments.

Burridge-Knopoff stick-slip experiments were conducted for the horizontal position of fixed and sliding plates with clean surfaces and with a layer of sand between the sliding plates (Figure 4).

Fig.4. The Burridge-Knopoff experiments with clean surfaces plates and with a layer of sand between the plates

In experiments the upper platform moved at a speed of 1 mm/sec. To the each sliding plate was attached an accelerometer, which measures the acceleration of the plate. Also was recorded acoustic emission using piezo sensor. The information was recorded on a 8-channel PicoScope 4824. These records are shown in Figure 5.

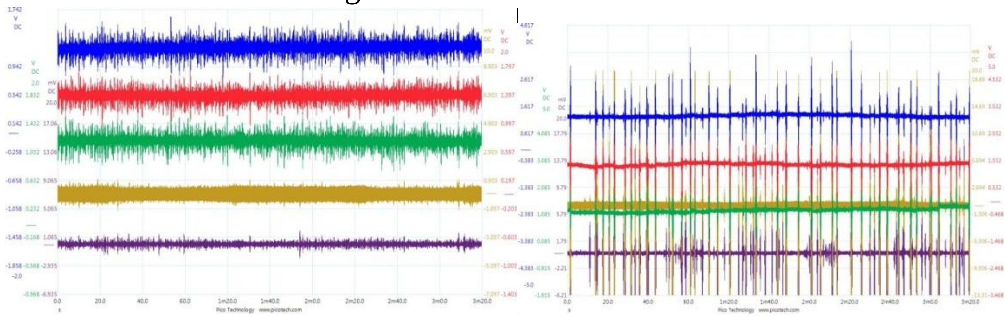

Fig. 5. Records of accelerations and acoustic emissions arising during the Burridge-Knopoff experiments with clean surfaces plates (a) and with a layer of sand between the plates (b). Blue, red and green channels, show respectively accelerometer records attached to the first, second and third sliding plate. Yellow and purple channels present the piezo sensors records.

To study the phenomena of stick-slip and triggering of Burridge-Knopoff model under the influence of gravitational forces we accembled laboratory equipment with an inclined plane (Fig. 6). These settings may help to learn the process of landslide stick-slip motion triggering under different conditions on the sliding surface between basalt plates and under the influence of gravitational forces. The acoustic emission arising during sliding of upper plate was recorded. To this goal piezo sensors were attached to the upper and lower corners of the large (fixed) plate. At the critical angle of inclination of the system triggering forcing was applied by a seismic vibrator attached to the sliding plate. The information was recorded on a 8-channel PicoScope. In experiments the inclination slope of boards was measured.

Fig. 6. Laboratory model for series of Burridge-Knopoff experiments, under the influence of gravitational forces. Middle figure shows the seismic vibrator attached to sliding plate.

Experimental results for one- and three plate models under the influence of gravitational force are presented in Fig.7. The critical angle of slip is different for one- and three plate models. Triggering of sliding close to the critical slope but still stable occurs by a seismic vibrator. Namely, the system was left close to the critical angle for 45 minutes. Then, on the attached seismic vibrator a forcing of 20 Hz frequency and 1.6 V intensity was applied. The information was recorded on a 8-channel PicoScope. As can be seen from Fig.7 during the experiment several intermediate slips took place. The beginning of sliding of system of plates was caused by influence of the seismic vibrator. The seismic vibrator played the role of a trigger in slip.

a) b)

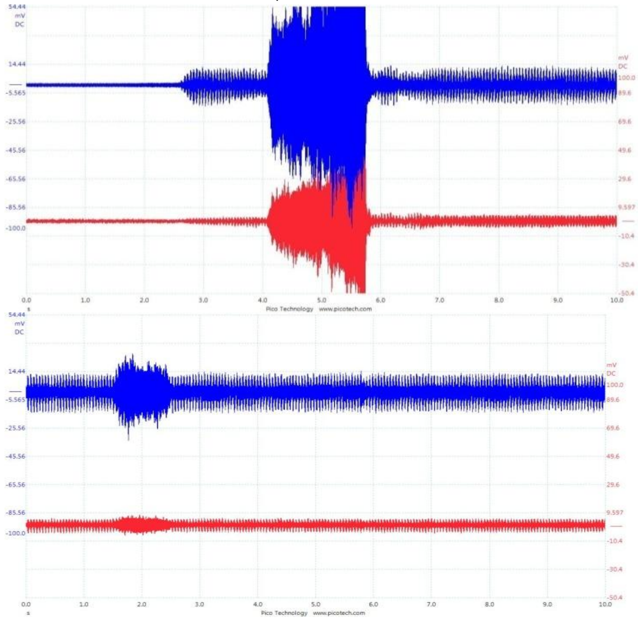

c) d)

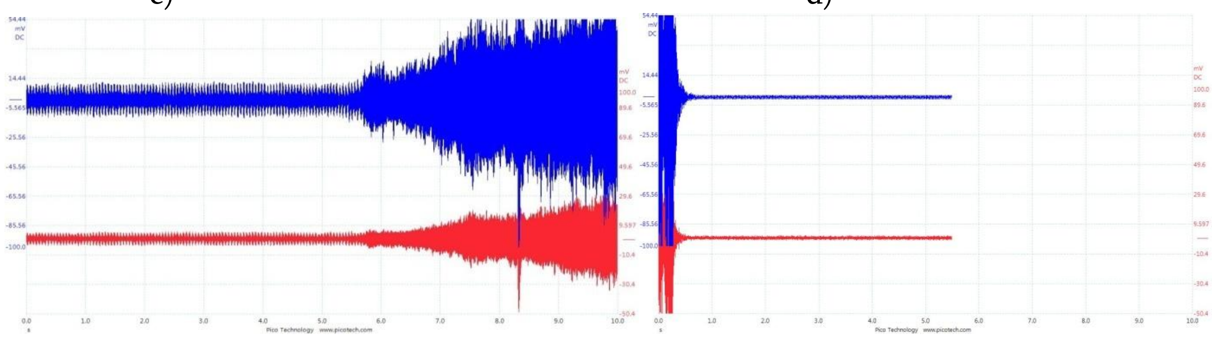

Fig.7. a) The record the acoustic emission occurred on one-plate model, b), c), d) record the acoustic emission when sliding occurred on three-plate model.

Numerical modeling

Because of the nonlinearity imposed into equation by the logarithmic term in the Dietrich-Ruina friction law, analytic integration cannot be done even in the simplest case of a single block. For this reason we proceed by implementing a numerical method as a system of 3 first order ODEs [Erickson et al., 2010]:

$$\dot{u}_j = v_j \tag{3}$$

$$\dot{v}_j = \gamma^2 (u_{j-1} - 2u_j + u_{j+1}) - \tilde{\gamma}^2 u_j - \left(\frac{\gamma^2}{\xi}\right)\left(\theta_j + \ln\left(v_j + 1\right)\right) \tag{4}$$

$$\dot{\theta}_j = -(v_j + 1)\left(\theta_j + (1 + \epsilon) \ln\left(v_j + 1\right)\right) \tag{5}$$

Where u_j is the non-dimensional slip, $\gamma = \sqrt{\left(\frac{\mu}{m}\right)\left(\frac{D_0}{V_0}\right)}$ and $\tilde{\gamma} = \sqrt{\left(\frac{\lambda}{m}\right)\left(\frac{D_0}{V_0}\right)}$ are the dimensionless frequencies, $\xi = \frac{\mu_0 D_0}{a}$ is the dimensionless spring constant, $\epsilon = \frac{b - a}{a}$.

Numerical experiments have been conducted in the case of three blocks. At the initial time zero displacements from equilibrium were assigned to blocks and the maximum deviation of the central block - on the Gaussian distribution. Revealed the originality of the sliding of the central block. At certain intervals of instability amplified and enhanced non-linearity the central unit is experiencing periodic motion.

N=3;
γ =0.5;
$\tilde{\gamma}$=0.5;
ξ =0.5;
ϵ =0.5;
sigma=1;

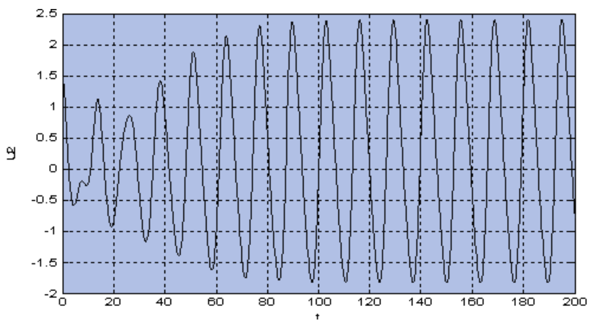

Fig.8. Numerical experiments for three-block Burridge-Knopoff model

Burridge-Knopoff model (Fig. 1) can be also described in terms of the normalized equation[Matsukawa, Saito, 2007]:
The normalized equation of motion of the model (Fig. 1) is expressed as:

$$\ddot{x}_i = (vt - x_i) + l^2(x_{i+1} + x_{i-1} - 2x_i) - \phi(\dot{x}_i), \tag{6}$$

here $l = \sqrt{\frac{k_c}{k_p}},$ is the dimensionless stiffness parameter; $x_i,$ $t,$ v and $\phi(\dot{x}_i)$ are normalized dimensionless parameters. In order for the model to exhibit a dynamical instability, it is essential that the friction force exhibits a frictional weakening property, i.e., the friction should become weaker as the block slides. As the simplest form of the friction force, we assume here the form used by Carlson:

$$\phi(\dot{x}_i) = \frac{1 - \sigma}{1 + \frac{2\alpha \dot{x}_i}{1 - \sigma}}, \tag{8}$$

Numerical experiments were conducted for one- and four plates for $l = \sqrt{60},$ a=1, $\sigma = 0.01$ and $\alpha = 4$ numeric values. The results are presented in Fig. 9.

a) b)

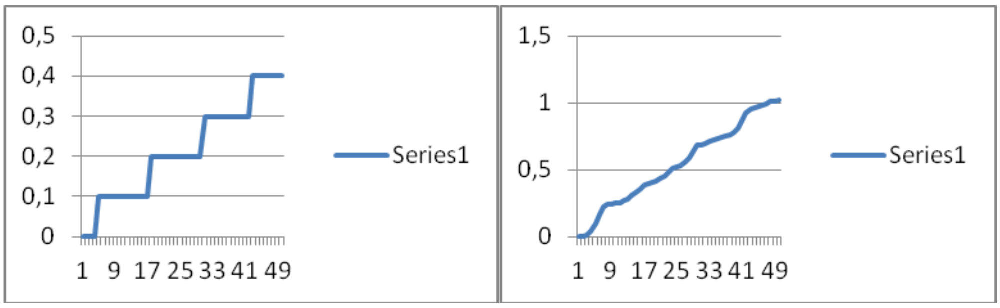

Fig. 9. a) Numerical simulation of displacement (ordinate) versus time (abscissa) for one block, b) the same calculations carried out for moving the center of gravity of the system in conditional units the Burridge-Knopoff model of four plates. (abscissa - time, ordinate - displacement).

For each experiment we have files of large volume with records of accelerations and acoustic issues. Data recording in a digital form was made at the sampling rate 2 kHz. Each experiment proceeded about 10 minutes. Gravitational experiments taking into account a parking phase (prior to influence by the seismic vibrator) proceeded about 50 minutes. At this stage our task is to transfer these accelerations to movements to compare data of experiment with data of mathematical modeling.

References

[1] Boettcher, M. S., and C. Marone, Effects of normal stress variation on the strength and stability of creeping faults,. J. Geophys. Res., 109, B03406, doi:10.1029/2003JB002824, 2004

[2] Fabio Vittorio De Blasio, Introduction to the Physics of Landslides, Springer, 2011

[3] A.Helmstetter, D. Sornette, J.-R. Grasso, J. V. Andersen, S. Gluzman, and V. Pisarenko, Slider block friction model for landslides: Application to Vaiont and La Clapie`re landslides, Journal of Geophysical Research, 109, 2004

[4] Dieterich, J.H. (1979), Modeling of rock friction 1. Experimental results and constitutive equations. Journal of Geophysical Research, **84, B5,** 2161-2168.

[5] Burridge R. and Knopoff L. 1967. Model and theoretical seismicity. Bulletin of the Seismological Society of America, 57(3): 341-371,

[6] Ruina A. 1983. Slip instability and state variable friction laws. Journal of Geophysical Research, 88, 10359-10370

[7] Chelidze T., N. Varamashvili, M. Devidze, Z. Chelidze, V. Chikhladze and T. Matcharashvili (2002), Laboratory study of electromagnetic initiation of slip. Annals of Geophysics, **45,** 587-599

[8] Chelidze T., Gvelesiani A., Varamashvili N., Devidze M., Chikchladze V., Chelidze Z., and Elashvili M. 2004. Electrmagnetic initiation of slip: laboratory model. Acta Geophysica Polonica, 52, 49-62

[9] Chelidze T., Matcharashvili T., Gogiashvili J., Lursmanashvili O., and Devidze M. 2005. Phase synchronization of slip in laboratory slider system. Nonlinear Processes in Geophysics, 12, 163 – 170.

[10] Chelidze T., Lursmanashvili O. Matcharashvili T. Devidze M. 2006. Triggering and synchronization of stick slip: waiting times and frequency-energy distribution. Tectonophysics, 424, 139-155

[11] Nasuno S., Kudrolli A., Bak A., and Gollub J. P. 1998, Time-resolved studies of stick-slip friction in sheared granular layers. Phys. Rev. E 58, 2161–2171

[12] Matsukawa, H., Saito, T., Friction, Stick-Slip Motion and Earthquake, Lect. Notes Phys. 705, 169–189, 2007.

[13] Erickson B., Birnir B., Lavallee D., Periodicity, Chaos and Localization in a Burridge-Knopoff Model of an Earthquake with Dieterich-Ruina Friction, Center for Complex and Nonlinear Science, UC Santa Barbara, 2010, http://escholarship.org/uc/item/3r5811tp

ბურიჯ-კნოპოვის ლაბორატორიული და მათემატიკური მოდელის გამოყენებით მასების მოძრაობის და სეისმური პროცესის შესწავლა

ნოდარ ვარამაშვილი, თამაზ ჭელიძე, მარინა დევიძე, ზურაბ ჭელიძე, ვიქტორ ჩიხლაძე, ალექსანდრე სურმავა, ხათუნა ჩარგაზია, დიმიტრი ტეფნაძე

რეზიუმე

მასების მოძრაობის და სეისმური პროცესების მარტივი მოდელები მნიშვნელოვან როლს თამაშობენ მათი მექანიზმების შესასწავლად. წარმოდგენილ სტატიაში ჩვენ ვაანალიზებთ, ჰორიზონტალურ და დახრილ სიბრტყეზე დიტრიხ-რუინას და კარლსონის ხახუნის კანონების გამოყენებით, ზამბარა-ბლოკის და ბურიჯ-კნოპოვის მოდელის დინამიკას. ჩვენს ექსპერიმენტებში, დასრიალების გამორჩევა ხდება დასრიალების პროცესში გენერირებული აკუსტიკური ემისიის საშუალებით. ასევე ხდებოდა თითოეული მოსრიალე ბლოკის აჩქარების ჩაწერა. დახრილი მოდელის შემთხვევაში ერთ-ერთ მოსრიალე ფილაზე მიმაგრებული იყო სეისმური ვიბრატორი, რომლის საშუალებითაც ხორციელდებოდა სისტემაზე მცირე გარეშე ზემოქმედების მოდება. განხორციელდა ერთ და ოთხ ბლოკიანი ბურიჯ-კნოპოვის სისტემაში მიმდინარე დინამიკური პროცესების რიცხვითი მოდელირება.

8Journal of Georgian Geophysical Society,
Issue (A), Physics of Solid Earth, 2015, pp.26-39

Georadiolocation physical modeling for disk-shaped voids

D. Odilavadze, T. Chelidze, G. Tskhvediashvili

Abstract

Georadiolocation\5,6,9,10,11\, one of modern and rapidly developing branches of Geophysics, according to its activity spheres, requires maximally increased resolution of textures of certain objects located near the surface. For discovering and verification of the textures of such targets the field of Georadiolocation uses the direct and inverse tasks \7,8.\, widely used in electrodynamics, by means of mathematical modeling. In electrodynamics for mathematical tasks some initial and boundary conditions are introduced. For them Maxwell's electrodynamics equations are solved, according to the solution results the correspondence of the model to its physical reality is determined and the physical essence of the phenomenon is revealed.

Introduction

The theoretical basis of physical modeling \4,5,6,7,11\ of electro dynamical processes is the similarity theory based on the isomorphism of the reality and equations. The prerequisite for the study of a phenomenon by means of modeling equipments is geometrical similarity of the real structure and its model and also fulfillment of the similarity law of varying electromagnetic fields /1,2/. Hereby, we introduce similarity criteria for similarity numerical coefficients /1,8/ by the similarity principles of georadiolocation frequency fields, which may be used in physical modeling:

$$\phi_\nu^2 \cdot \varepsilon_\nu \cdot \lambda_\nu^2 = \phi_\mu^2 \cdot \varepsilon_\mu \cdot \lambda_\mu^2 \qquad (1),$$

where ϕ_ν is the central frequency of georadar impulse electromagnetic waves used in the field, λ_ν - geometric size of the real, i.e. georadiolocation object-for-study placed in the field, ε_ν- relative dielectric conductivity of the georadiolocation layer measured in the field, ϕ_μ- modeling frequency, i.e., the central frequency of georadar impulse electromagnetic waves used for the modeling equipment, λ_μ- modeling geometric size, i.e., the geometric size of the georadiolocation object-for-study placed in the modeling equipment, ε_μ- correlative dielectric conductivity of the georadiolocation layer measured in the modeling equipment.

Let us admit that $\varepsilon_\mu = \varepsilon_\nu$, which is quite acceptable in the most cases of modeling and geological mediums. For (1) we receive the simplification:

$$\phi_\nu^2 \cdot \lambda_\nu^2 = \phi_\mu^2 \cdot \lambda_\mu^2 \qquad (2),$$

or $\phi_\nu \ \lambda_\nu = \phi_\mu \lambda_\mu$ (3) ,

In this case for similarity coefficients we will receive:

$$K_\phi = \frac{\phi_\mu}{\phi_\nu} \qquad \frac{1}{K_\lambda} = \frac{\lambda_\nu}{\lambda_\mu} \qquad (4).$$

Thus, in Georadiolocation it is possible to use the GEORADAR Zond-12 2 GHz and sometimes 500 MHz \3\.(according to the equipment modeling space measure in regard to the given physical modeling task) screened antennas for laboratory modeling for real (natural, field) phenomena. Low MHz frequency antennas (38 MHz, 75 MHz, 150 MHz, 300 MHz) are also used in natural, i.e. field conditions. Besides, interpretation results for frequency diapasons taking into account the measures, geometry of the object and correlative dielectric conductivity, will be preserved.

On the basis of the similarity theory let us introduce the georadiolocation comparison principle, according to which we determine frequency similarity coefficients for central frequencies and the characteristic length, in which the sizes of the laboratory model for the real object are measured and which is considered as 1m model measurement unit for the length measurement of the real, i.e. natural object.

Let us see, for example, determination of frequency-length coefficients for the sizes of modeling and natural discs.

$\phi_\mu = 2$ GHz for the central frequency, to which in natural situation we conform $\phi_\nu = 38$ MHz the central frequency of the antenna, for which we receive frequency similarity coefficient $K_\nu = 52,63$, which is equal to $\frac{1}{K_\lambda}$, for the length similarity modeling 1 m we receive $\lambda_\nu = \lambda_\mu \cdot \frac{1}{K_\lambda} = 1\text{m} \cdot 52,63 = 52,63\text{m}$, i.e., 0.37m size model expresses $0.37 \cdot 52.63 = 19.47$ m natural size object.

Thus, for transformation of the modeling characteristic length into natural characteristic length it is necessary to multiply the frequency similarity coefficient, which is equal to the inverse length similarity coefficient, by the characteristic natural length similarity coefficient. The natural sizes for the given disk model will be counted in the same way by 2 GHz modeling frequency for the rest natural central frequencies (500, 300, 150, 75, 38 MHz) of the georadiolocation antenna.

In the case of the different dielectric conductivity the similarity correlation written in $K_\varepsilon = \frac{\epsilon_\mu}{\epsilon_\nu}$ similarity coefficients receives the following form:

$$K_\phi^2 \cdot K_\lambda^2 \cdot K_\varepsilon = 1, \qquad (5).$$

For characteristic natural size we will receive:

$$\lambda_\nu = \frac{1}{K_\lambda} \cdot \lambda_\mu = K_\phi \cdot \sqrt{K_\varepsilon} \cdot \lambda_\mu \qquad (6).$$

The peculiarities in the direct task model, which appear on the radiogram (the first inverse task) must also appear and correspondingly be interpreted on the field (the second inverse task) radiogram, which will make it easy to identify the object with the corresponding natural peculiarities.

An article in Georadiolocation on the solution of direct and inverse tasks, including modeling and numerical scaling, was published in 2013 in Geophysical Journal V.35, №4, 2013 (Odilavadze, Chelidze, ...).

Experimental setup

Experimental setup consisted of a tank of dimensions 1.2x1.2x2.4 cub.m filled up with quartz ("Sachkhere") sand at room humidity. For a modeling equipment georadiolocation set Zond-12 with its 2 MHz component antennas, ultrahigh frequency and 500 MHz screened antennas was used.

As a georadiolocation target-object, an air-containing thin (2-3 mm thick) organic glass disc was chosen with its measures and given placement coordinates (direct task). For determining the form of the disk (the first inverse task) we used georadiolocation physical modeling equipment.

For the equipment we selected a modeling space maximally free from external field influence.

In order to receive radiograms we passed the 2 GHz GEORADAR antenna over the profiles of the target-object (disc) diameter and chords located at different depths.

We had to determine the minimal reflection area by passing over the disc by means of georadiolocation physical modeling, i.e., Fresnel area value for modeling and natural sizes.

For calculation of the Fresnel reflection area we used /6./ formula:

$$r = \frac{l}{4} + \frac{H}{\sqrt{\varepsilon - 1}},$$

where r is an approximate radius of the reflection area, l −central frequency wave length, H −reflection area depth, ε -average correlative dielectric conductivity according to H depth.

By this formula we calculated the reflection areas with minimal resolution at correspondent depths - when $l = c/v$. $v = 2$ GHz, $H =$ 0.05 m, $\varepsilon = 5$ than $r = 0.06$ m and the reflection area $S = 0.01$ sq. m=100 sq. m.

The areas for the rest of the depths are calculated in the same way.

For example, the modeling frequency 500 MHz reflection area for 0.5 m depth is: $S = 0.5$ sq. m = 500 sq. m.

Results and discussion

We constructed parallel profiles for investigation of the modeling background tank (without the disc model) image. We will consider just one among them, namely the radiogram received at central profile 4. As seen from the image the modeling space is rather homogeneous that enables sharply distinguishing of the modeling object (disc).

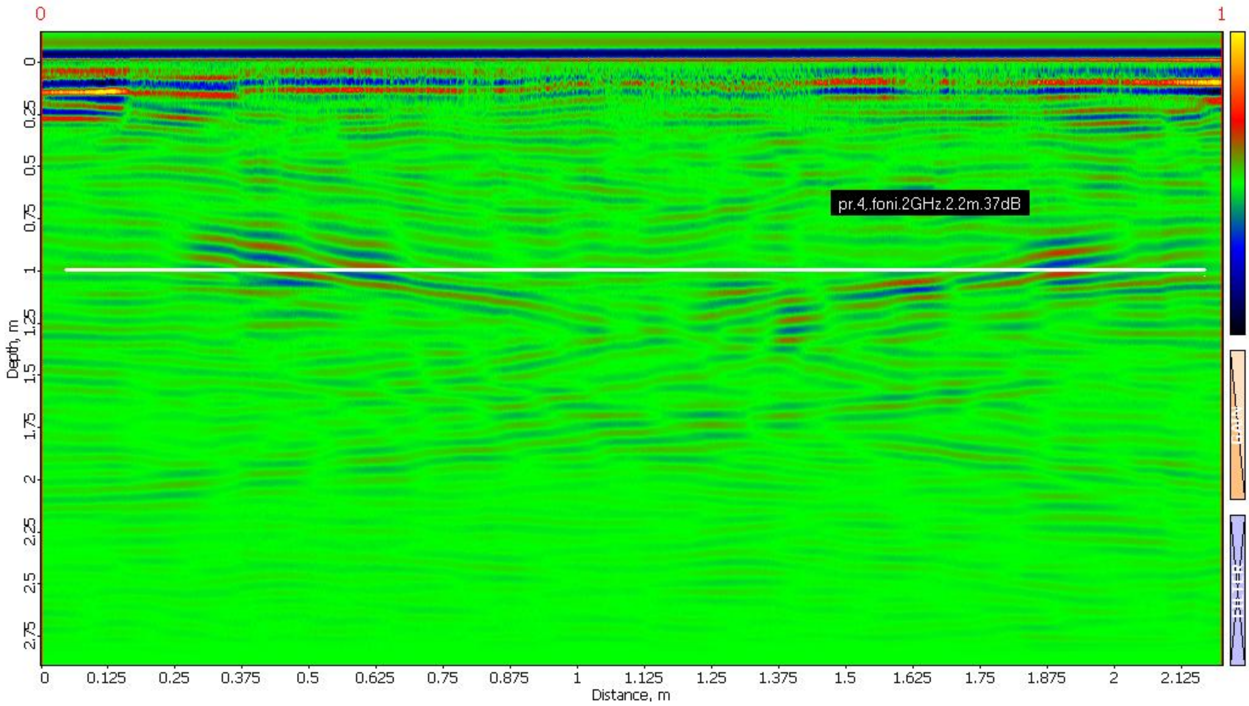

Figure 1. The background value of the field corresponding to the central profile (profile 4) of the modeling space surface without void disk. Profile length 2.2 m. 2 GHz antenna.

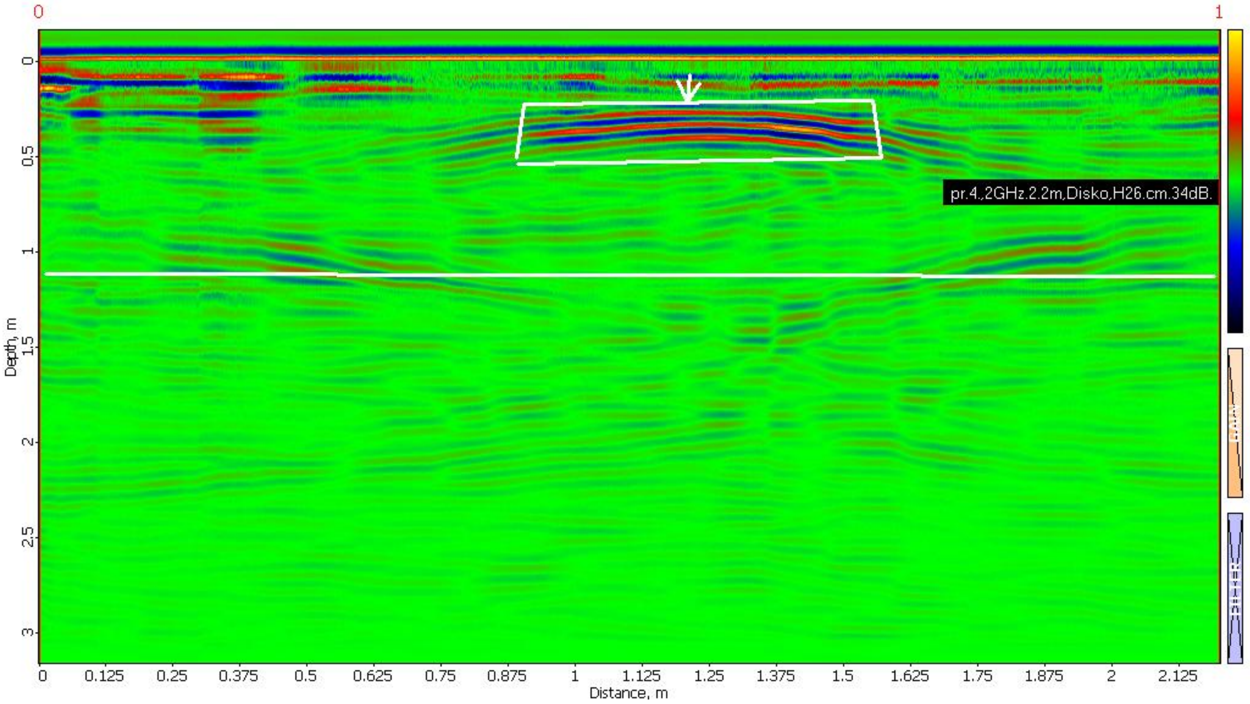

Figure 2. The model profile with void disc is given on the radiogram with wave amplitude density image. The maximum, minimum and zero values of which correspond to the colours in the scale. The depth of the model placement is H =25 cm. Central profile 4 passing over the disc diameter. 2 GHz central frequency GEORADAR antenna is used.

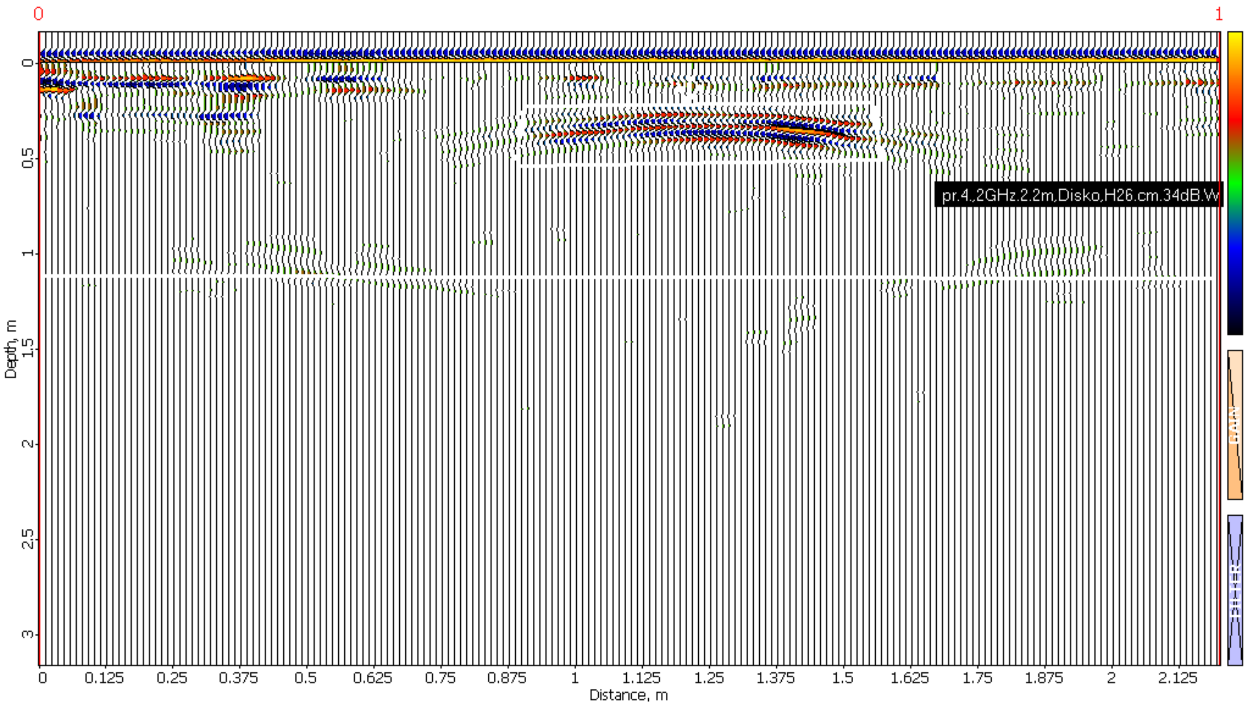

Figure 3. Central diameter profile 4 with a disc model, H = 25 cm.. This radiogram shows the wave image of the profile. The maximum, minimum and zero of the amplitude correspond to the scale colours.

Figures 2 and 3 show the existence of the void (air) of the disc (reverberation). They also show less sharp forms of the parabola of the electromagnetic wave phase synchronism axes created by the influence of the external surface of the disc. The superposition of the forms makes the texture of the object. The interpretation of the disc texture revealed the distance between the sharply expressed upper and lower electromagnetic wave phase synchronism axes is 0.08 m, which coincides with the real thickness of the disc. In the void filled with air, due to multiple internal dispersions of the electromagnetic waves a sharply expressed interference image has been created.

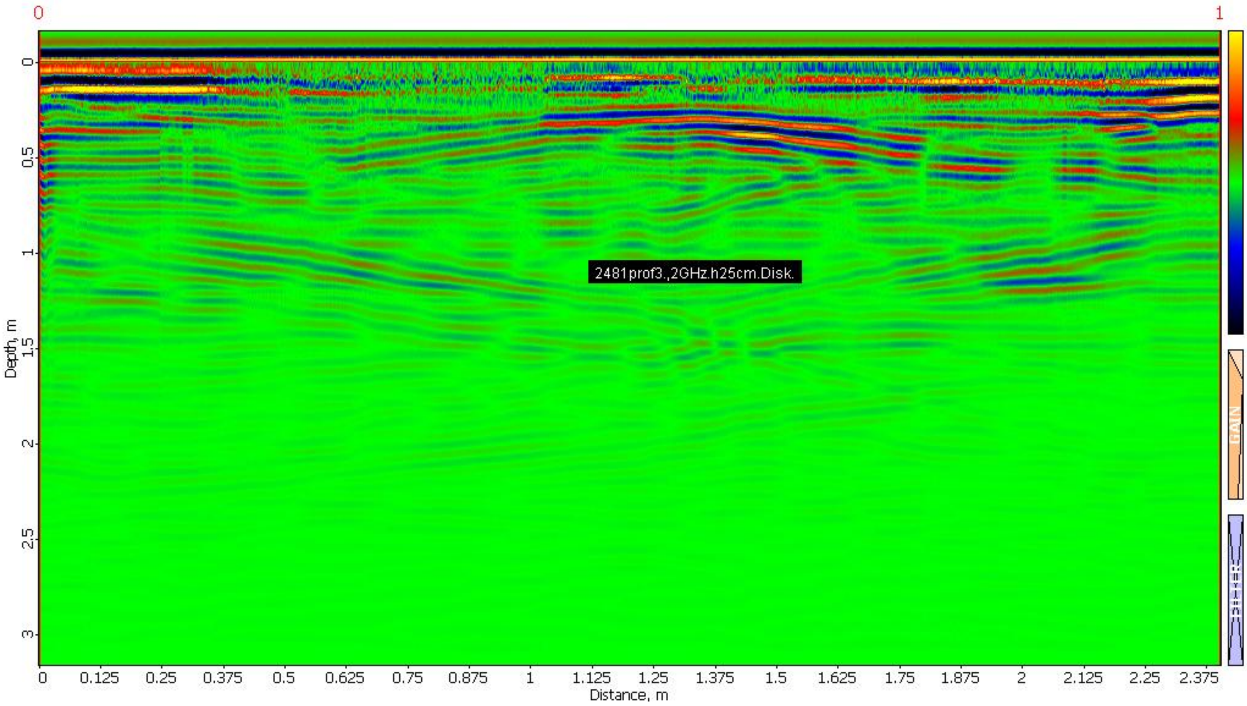

Figure 4. The disc model. The depth of the model placement surface H = 25 cm. Profile 3 passing over the disc diameter, parallel to profile 4. The distance between the parallel profiles is 0.13 cm. Profile 3 crosses the minimized part of the disc surface. 2 GHz central frequency GEORADAR antenna is used for modeling.

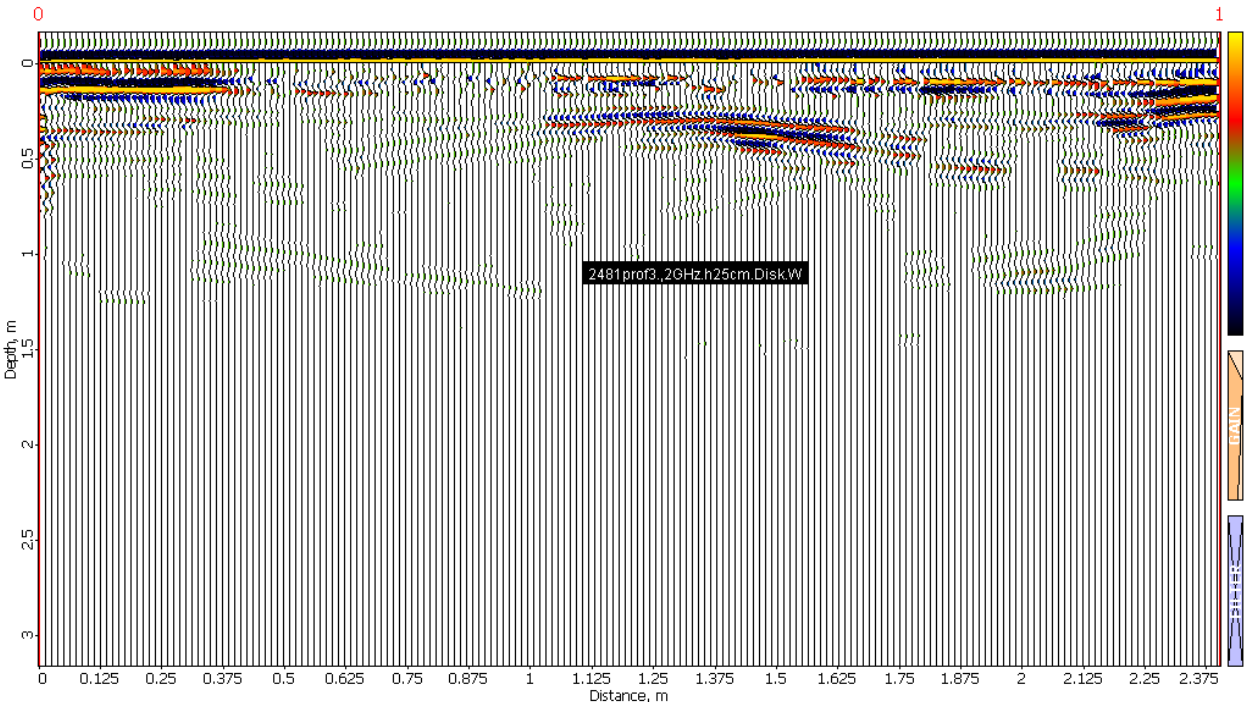

Figure 5. The disc model, H = 25 cm. The wave image of the parallel profile (№3).

Figures 4 and *3* show the existence of the void (air) of the disc. The upper parabola (the upper facet of the disc) corresponds to the air dielectric conductivity 1, the lower one (the lower facet of the disc) corresponds to the medium (sand) conductivity 5. The distance between the sharply expressed upper and lower electromagnetic wave phase synchronism axes is 0.08 m, which coincides with the real thickness of the disc. Besides, the profile cuts a part of the reflection surface of the disc, due to which the texture has changed its measures as reverberation image is recorded not for the whole void, but for its part, which is more clearly seen on the given profile wave image.

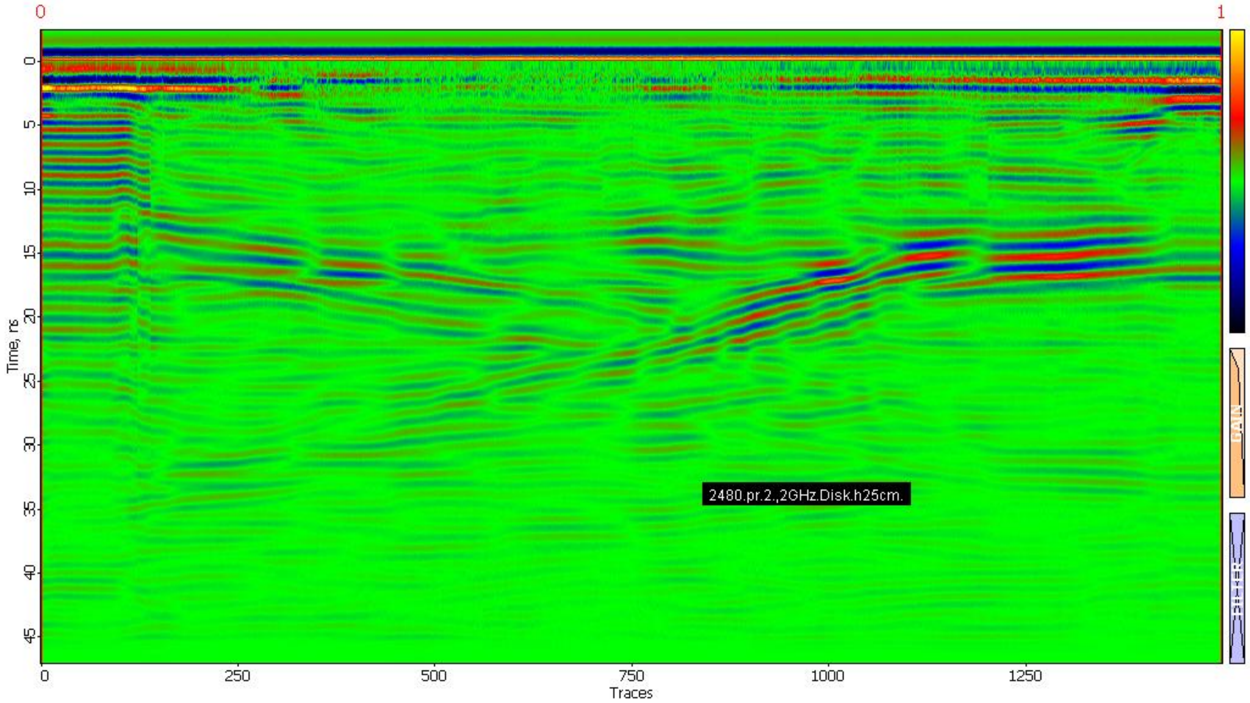

Figure 6. The disc model. The depth of the model placement surface is H = 25 cm. Profile 2 passing over the disc diameter, parallel to profile 4. The distance between the parallel profiles is 0.28 cm. Profile 2 crosses a minor part of the disc surface. 2 GHz central frequency GEORADAR antenna is used for modeling.

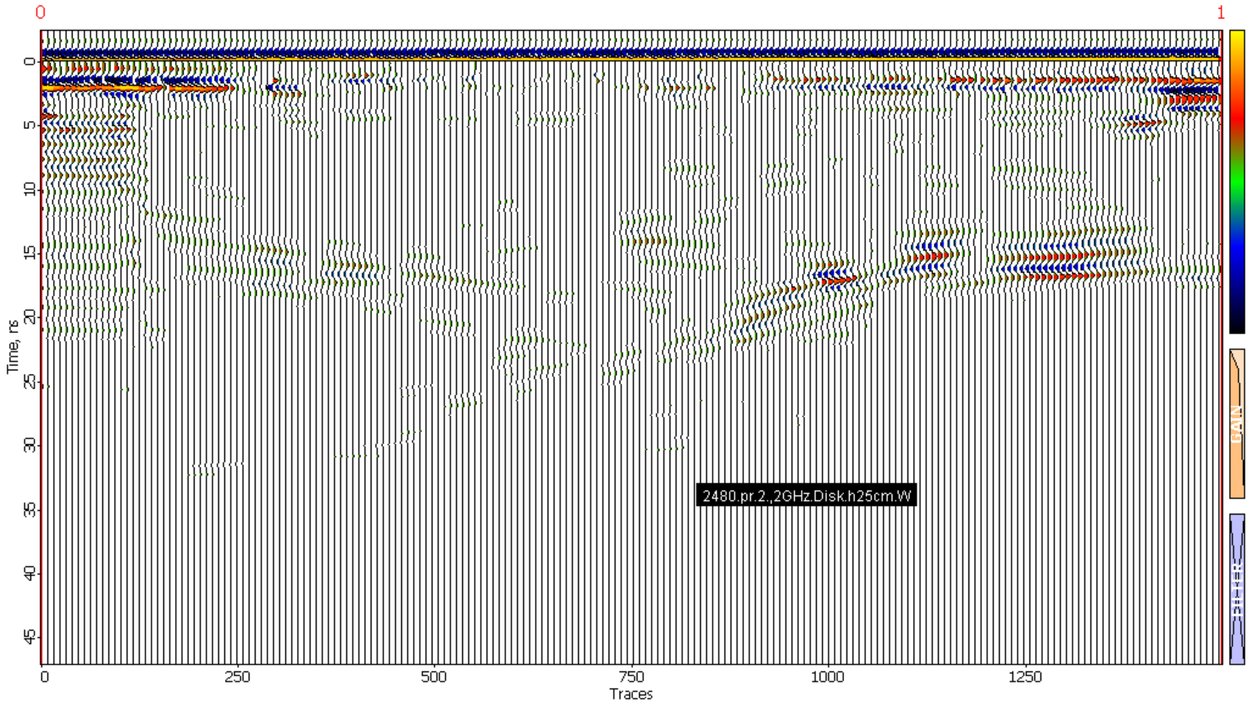

Figure 7. The disc model on the radiogram, H = 25 cm. Profile 2, parallel to profile 4, is presented. A wave image.

There is no existence of disc texture on the radiograms shown in *Figures 6 and 7*. That is caused by the decrease of the Fresnel zone area. The phase synchronism axes of these reflected electromagnetic waves do not appear in the profile, which is located from the disc center at the distance almost equal to the radius. Thus, the size of the disc containing air and located in the 0.25 m depth is now outlined according to depth, length, width and thickness. The increased sharpness of the phase synchronism axes existed at the edge must be caused not by horizontal placement of the disc but by the edge surface effect.

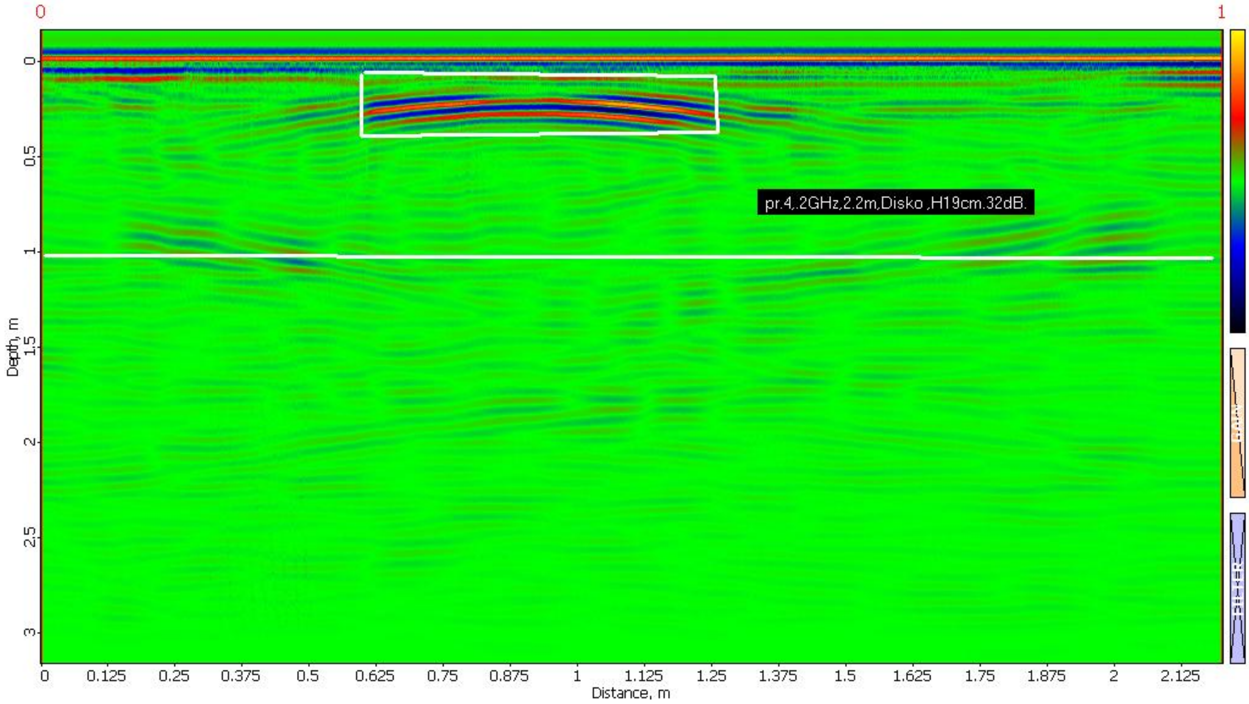

Figure 8. The disc model, H = 19 cm. The central frequency - 2 GHz. Profile 4 passing over the diameter.

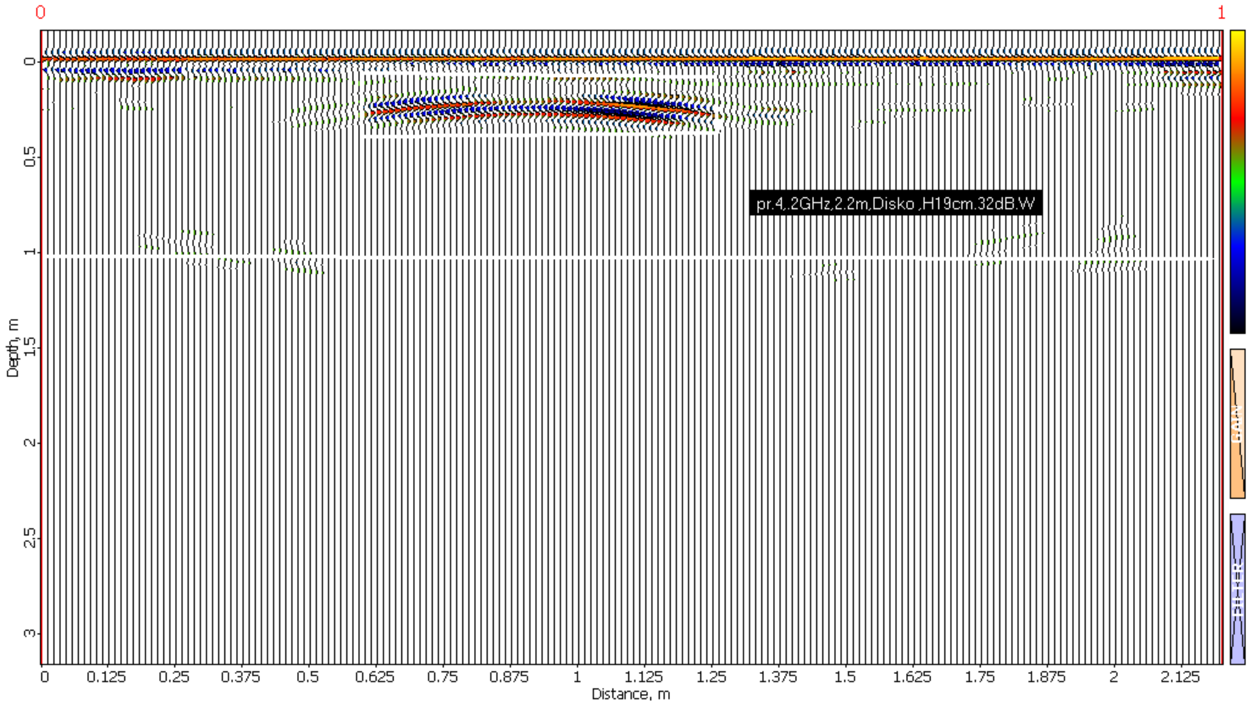

Figure 9. The disc model, H = 19 cm. The central frequency - 2 GHz. The diameter profile 4 (the profile is presented in a wave form on the radiogram).

Figures 8 and *9* clearly show the texture of the air containing disc, which definitely outlines the length measures and placement depth of the disc. Besides, the texture is changed, namely, the fixation of the upper part of the maximum of the phase synchronism axes is changed, the upper parabola has lost its sharpness, i.e., there are no radio-waves reflected from the surface. This must be caused by the effect of the electromagnetic wave dispersing by surface inhomogeneity (the received signal becomes immeasurable) when the antenna is moved off. On the radiogram the surface inhomogeneity of the cavity (diameter – 0.13 m, depth – 2 cm) in the disc form corresponds to the 0.13 m diameter phase synchronism axes cut at the upper part. Thus, now the measures of the disc have been outlined and the inhomogeneity of its surface and its sizes in length and depths has been defined.

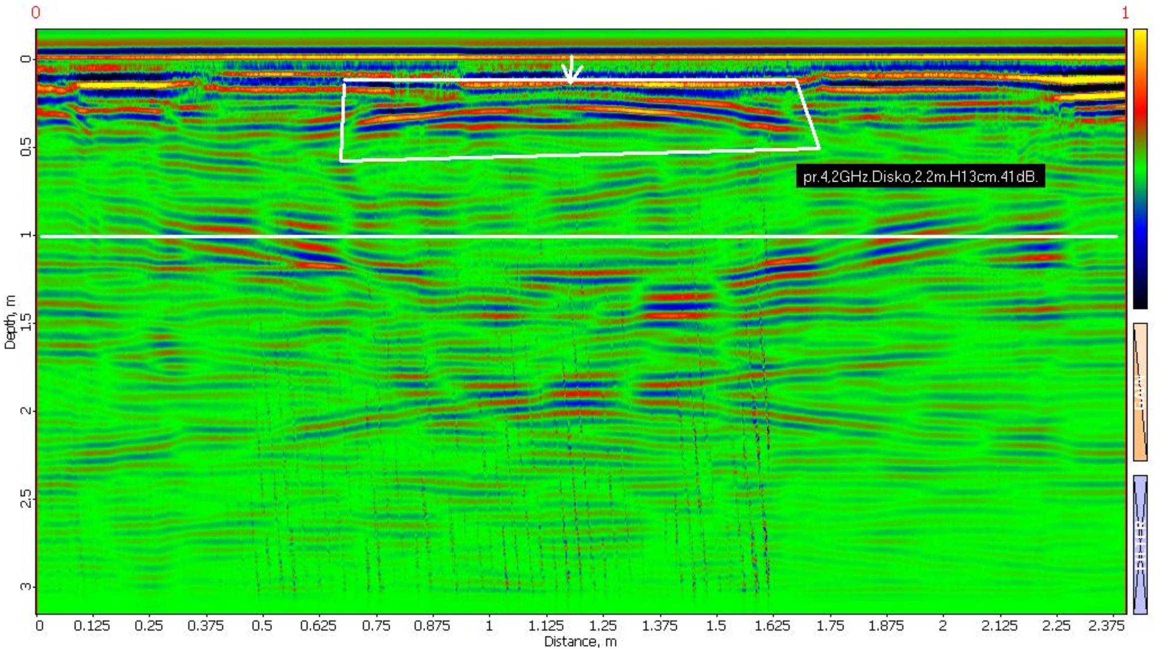

Figure 10. The disc model on the radiogram, H = 13 cm. The central diameter profile was constructed according to a density image.

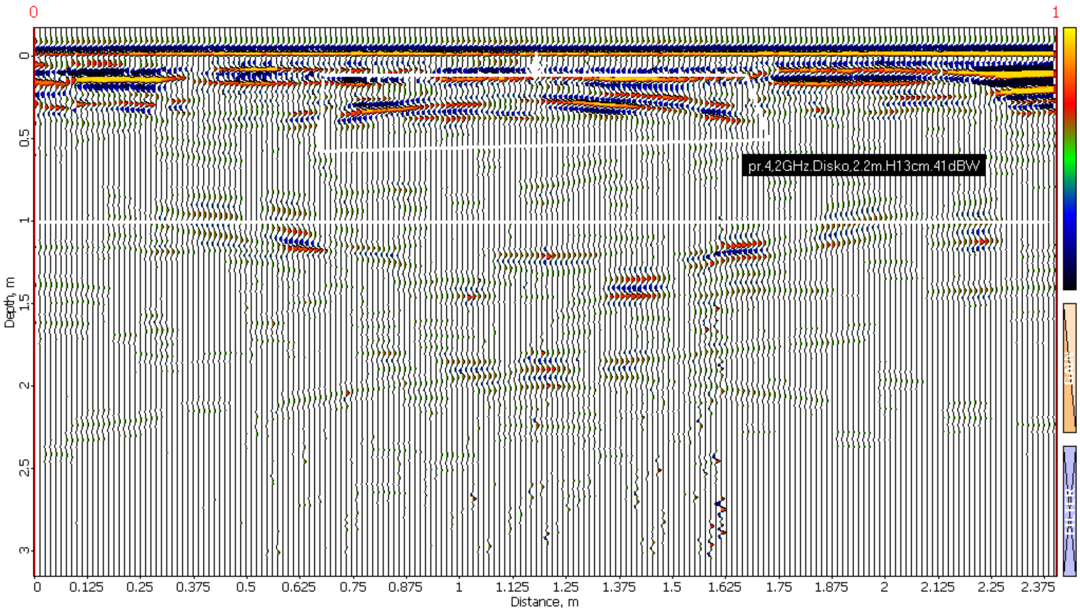

Figure 11. The disc model on the radiogram, H = 13 cm. The central diameter profile was constructed according to a wave image.

Figures 10 and *11*clearly show the texture of the air containing disc, which outlines the length measures and placement depth of the disc. Besides, the texture is changed, namely, the fixation of the upper part of the maximum of the phase synchronism axes is changed, the upper parabola is less sharp than at the 0.19 m depth, i.e., there are no radio-waves reflected from the surface. This must be caused by the effect of the electromagnetic wave dispersing by surface inhomogeneity (0.13 m diameter and 2 cm depth cavity in the disc form) when the antenna is moved off and approaching of the disc surface cavity to the mean wave zone of the antenna (which causes entering into the "shade zone" of the antenna). On the radiogram the disc corresponds to the increased incompatible peculiarity of the diameter at the parabola vertex. Thus, when approaching to the mean zone the disc measures were outlined and the inhomogeneity of its surface was determined. Approaching of the target-object to the mean zone of the antenna appeared to be a factor preventing from determining the disc surface inhomogeneity.

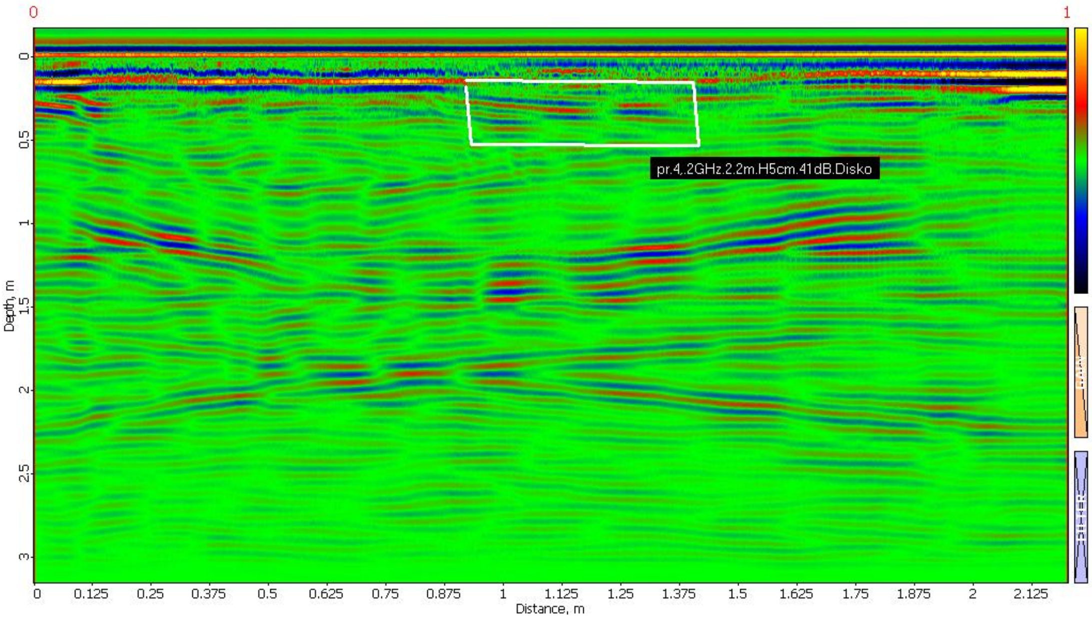

Figure 12. The disc model, H = 5 cm. The central diameter profile.

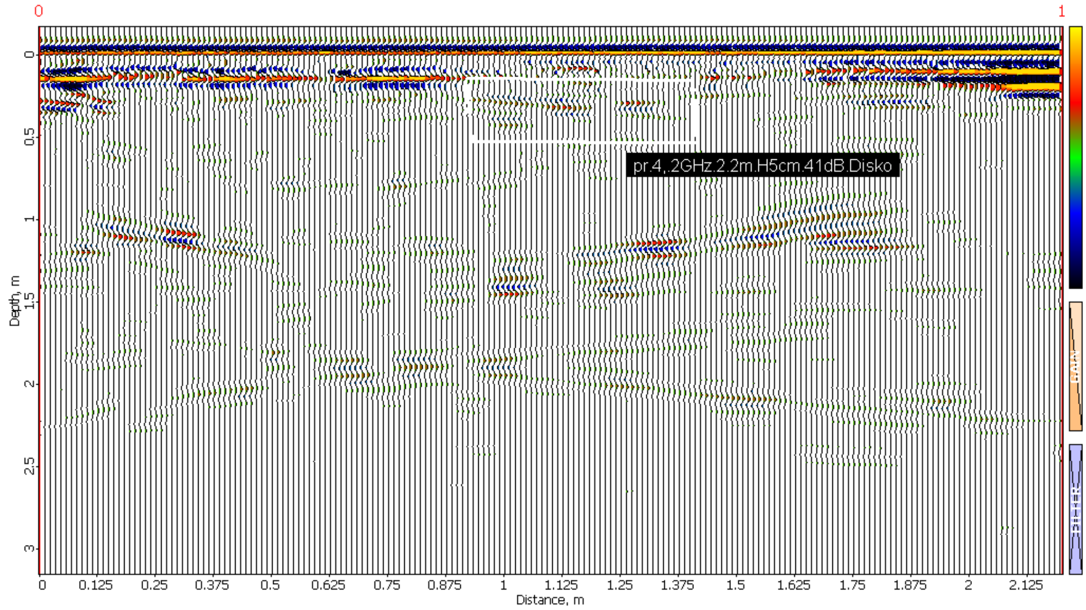

Figure 13. The disc model on the radiogram, H =5 cm. It was constructed by placing at the depth, according to a wave image of the central diameter profile.

Figures 12 and *13* indistinctly show the texture of the air containing disc, which indefinitely outlines the length measures and placement depth of the disc. The texture is changed, namely, the fixation of the phase synchronism axes is changed, it has lost its sharpness at depth up to 0.05 m, i.e., there are no radio-waves reflected from the surface. This must be caused by approaching to the antenna zone. However, the existence of air cavity is partially proved by its light reverberation image. Approaching of the target-object to the mean zone of the antenna appeared to be a factor preventing from determining the disc surface inhomogeneity.

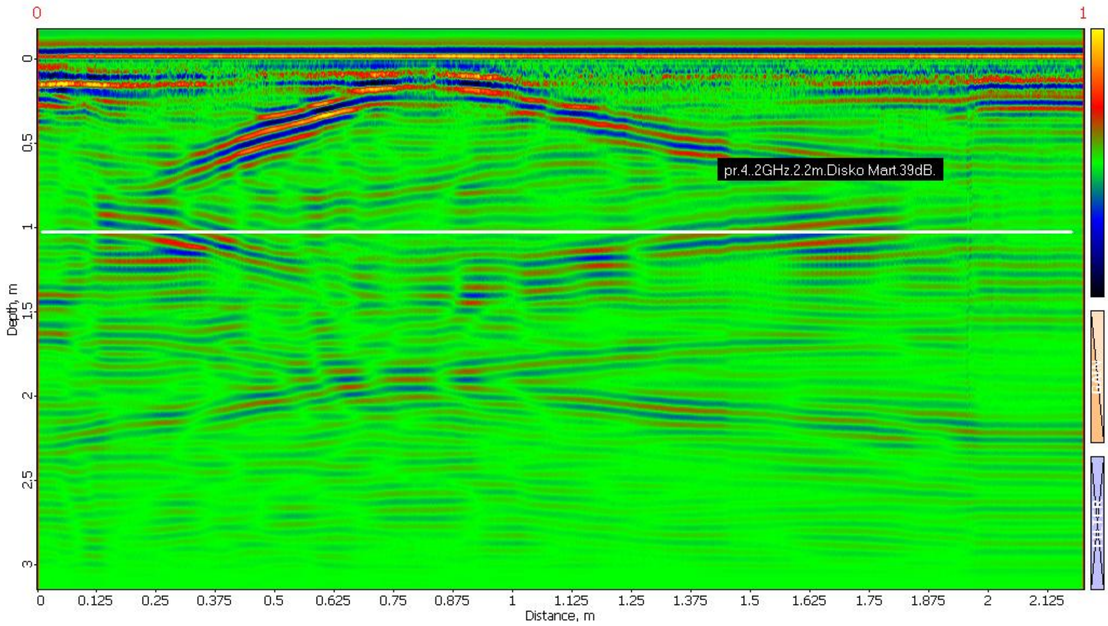

Figure 14. The disc model placed vertically, H = 7 cm. The central frequency – 2 GHz. Central profile 4.

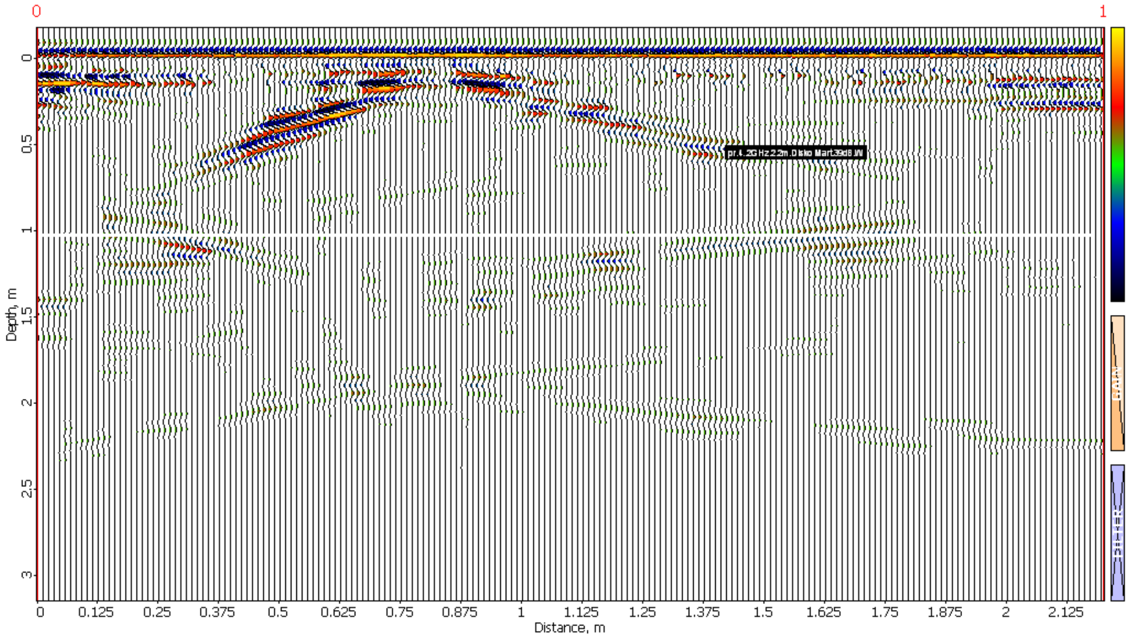

Figure 15. The disc model placed vertically, H = 7 cm. The central frequency – 2 GHz. (A radiogram according to the electromagnetic wave amplitude image).

Figures 14 and *15* indistinctly show radiograms for the same object (disc) placed in 0.07 m depth; namely, the disc is placed vertically in the perpendicular plane of the central profile, the texture of the object in the profile 4 clearly show the length measures and placement depth of the object. However, the texture of the vertical disc at the used frequencies does not appear. The air object is seen as a separate texture of an object with two parabolic symmetric phase synchronism axes. This must be caused by partially entering of the upper part of the object to the middle zone of the antenna and dispersing of wave by the side surface (0.08 m width) of the disc.

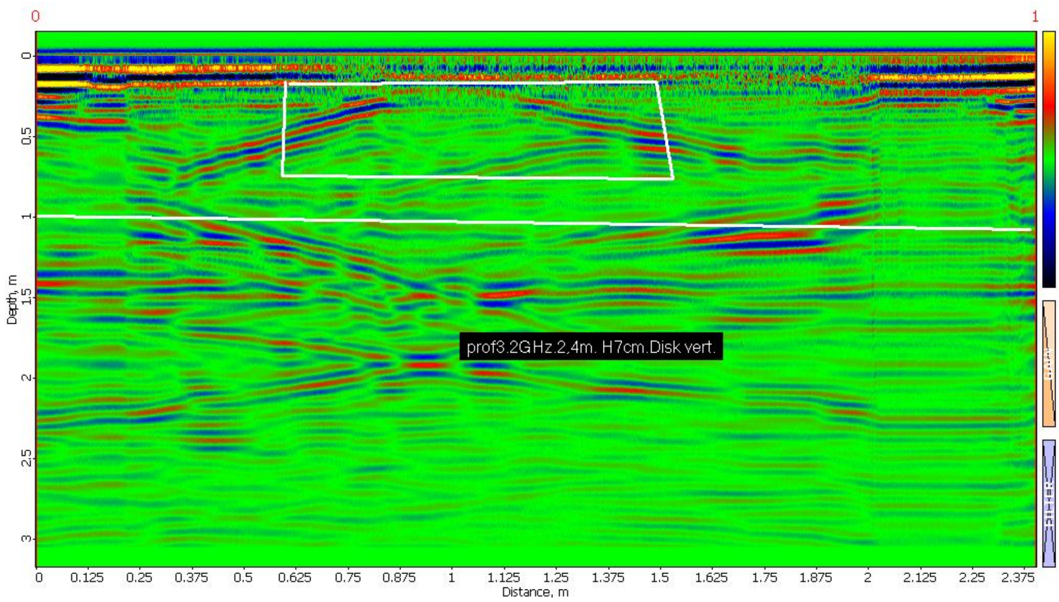

Figure 16. The disc model, H =11 cm. Profile 3 parallel to the central diameter profile.

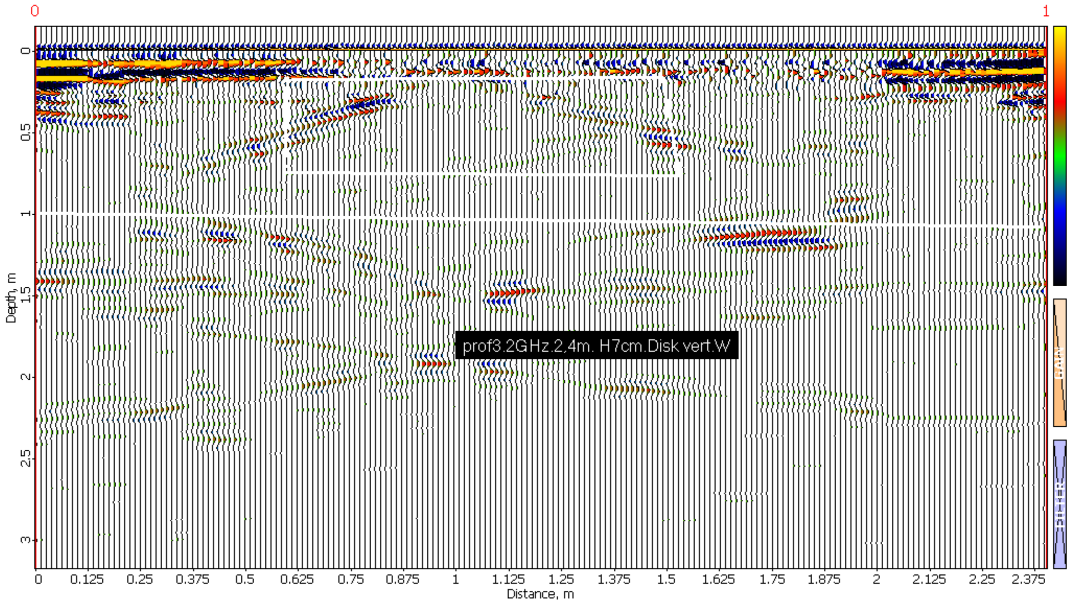

Figure 17. The disc model, H =11 cm. Profile 3 parallel to the central diameter profile (according to the wave image).

Figures 16 and *17* show a radiogram of the same object ("vertical" disc) placed at 0.11 m depth. The texture of the "vertical" disc in profile 3 proves the existence of the vertical plane of the object. However, the reverberation effect is not seen in the air containing space at the used frequencies. The object appears as two planes reflecting vertical placement. This is caused by placement of the upper part of the object in the middle zone of the antenna and dispersion of the side reflected waves from the uneven surface, which are not received by the antenna.

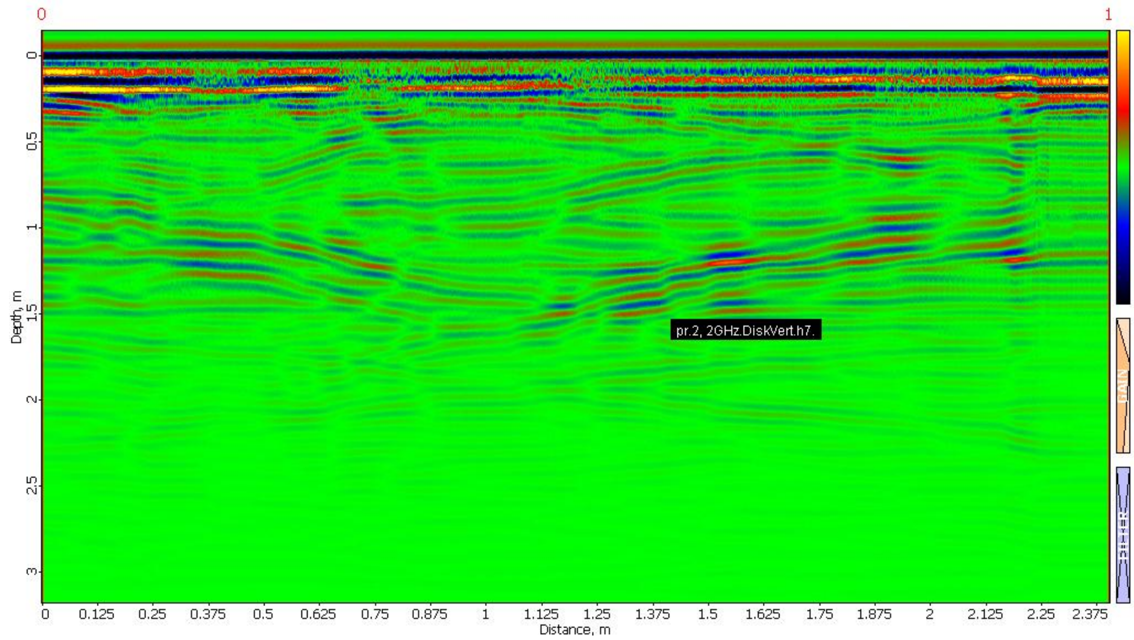

Figure 18. The disc model. Profile 2 parallel to the central diameter profile.

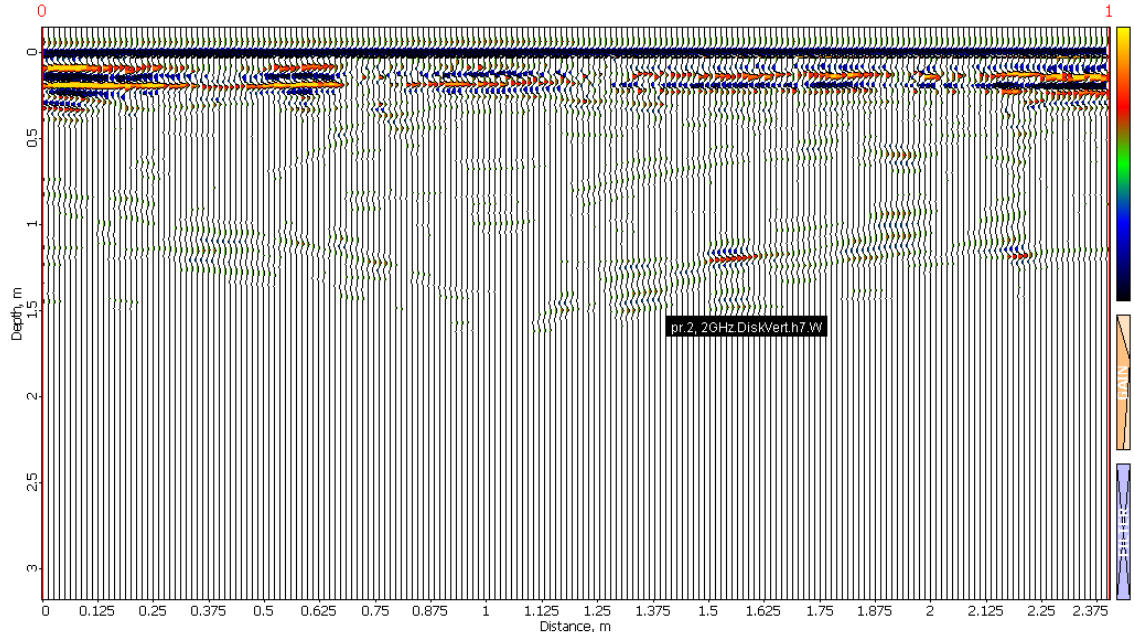

Figure 19. The disc model. Profile 2 parallel to the central diameter profile (wave image).

According to the analysis of *Figures 19* and *20* we can say that the object texture does not at all appear in profile 2 located at a distance equal to the disc radius as a result of dispersion of the reflected waves due to the significantly decreased received signal (impact).

Conclusion:

1. On the basis of physical modeling of electrodynamic processes, according to the comparison principles of the given georadiolocation frequencies, georadiolocation physical modeling was conducted for an empty object in a disc form by means of a physical modeling equipment.

2. The texture of the target-object (empty disc) was discovered and studied for different placement depths and orientation (placement of the disc axis in parallel and perpendicular directions to the day surface) of the object.

3. The electro dynamical effects influencing on the variation of the disc-shape object texture in the profiles at the disc center and far from it have been revealed.

4. For determining a texture of an object in field conditions a georadar frequency comparison method is suggested, according to which physical modeling, taking into account similarity coefficients, is used as an additional means of interpretation of radiolocation results.

References:

[1] Berdichevskiyi M.N., Moroz I.P., Kobzova V. M., Bilinskiyi A.I., Physical modeling in geoelectrics. Kiev. Nauk. Dumka, 1987. p. 140 *(in Russian)*.
[2] Bursian V.R. The theory of electromagnetic fields used in electrical prospecting. Leningrad, Nedra, 1972, p. 368 *(in Russian)*.
[3] Prizm 2.5, a software for georadar Zond-12 E. 2011*(in Russian)*.

[4] Czaja K. Application of modeling of electromagnetic field and GPR measurements in investigations of antique tenement. Geophys. Res. Abstr. 2012.
[5] Gurel L., Oğuz U. Three-Dimensional electromagnetic modeling of various GPR problems // Geophys. Res. Abstr. 2012. 14.
[6] Neal A. Ground-penetrating radar and its use in sedimentology: principles, problems and progress Earth-Sci. Rev. 2004. 66, 261—330.
[7] Negi J. G., Gupta C. P. Models in applied geoelectromagnetics // Earth Sci. Rev. — 1968. — 4. — P. 219—241.
[8] D.T. Odilavadze, T.L. Chelidze. *Физическое моделирование георадиолокационного поля в прямой и обратной задачах электродинамики © Д. Т. Одилавадзе, Т. Л. Челидзе,* Geophysical Journal V.35, №4, 2013 *(in Russian).*
[9] Sena D'Anna A. R. Modeling and imaging of ground penetrating radar data. — Texas: The University of exas at Austin, 2004. 251 p. (repositories. Lib.Utexas. edu).
[10] Sharma P.V. Environmental and engineering geophysics. Cambridge: Cambridge University Press, 1997.
[11] Sena D'Anna A. R. Modeling and imaging of ground penetrating radar data. — Texas: The University of exas at Austin, 2004. 251 p. (repositories. Lib.Utexas. edu).

გეორადიოლოკაციური ფიზიკური მოდელირება დისკოსებური ფორმის სიღრუვისათვის

დ. ოდილავაძე, თ. ჭელიძე, გ. ცხვედიაშვილი

რეზიუმე

1. ელექტროდინამიკური პროცესების ფიზიკური მოდელირების საფუძველზე შემოტანილი გეორადიოლოკაციური სიხშირეების შედარებითობის პრინციპის თანახმად მყარ გარემოში ფიზიკური მოდელირების დანადგარზე ჩატარდა გეორადიოლკაციური ფიზიკური მოდელირება დისკოსებრი ცარიელი ობიექტისათვის.
2. დაფიქსირებულ და გამოკვლეულ იქნა სამიზნე –ობიექტის (ცარიელი დისკო) რადიოსახე ობიექტის განთავსების სხვადასხვა სიღრმეებისა და ორიენტაციისათვის (დისკოს განთავსება დღიური ზედაპირის პარალელურად და მართობულად).
3. გამორკვეულ იქნა ელექტროდინამიკური ეფექტები რომლებიც გავლენას ახდენენ დისკოსებრი ობიექტის რადიოსახის ცვლილებაზე.
4. საველე პირობებში დაფიქსირებული ობიექტის რადიოსახის გარკვევისათვის, შემოთავაზებულია გეორადარული სიხშირული შედარებითობის პრინციპი რომლის თანახმად გამოიყენება ფიზიკური მოდელირება მსგავსობის კოეფიციენტების გათვალისწინებით, როგორც რადიოლოკაციური შედეგების ინტერპრეტაციის დამატებითი საშუალება (ხერხი) .

Journal of Georgian Geophysical Society,
Issue (A), Physics of Solid Earth, v.18a, 2015, pp. 40-48

3D non-stationary Thermo-geodynamics of the Caucasus and the Black and the Caspian seas water areas

Gugunava G.E. , Kiria J.K. , Kiria T.V., Z.Zerakidze

Keywords: Thermo-geodynamics, Thermo-density, vertical displacements, thermoelastic, Mohorovichich, Paleoreconstruction, non-stationary.

Abstract. Tree-dimensional non-stationary geothermal and thermoelastic models of the Caucasus and the Black and the Caspian seas is developed and their geological-geophysical interpretation is given. Till 410 Ma temperature field was defined on the basis of the stationary model of the investigated region. Afterwards, from the period of formation of the most part of the sedimentary cover, computations were carried out on the basis of non-stationary thermal model. On the basis of thermal field the thermoelastic equations are solved and charts of vertical thermo-displacements have been calculated.

Earlier M. Alexidze et al. (1969, 1989, 1991) a three-dimensional stationary geothermal and thermoelastic models of the Caucasus and Black and the Caspian seas water areas have been produced. Besides charts of temperature and thermoelastic displacement were plotted for the “granitic”, Conrad and Mohorovicic discontinuities. These models revealed a number of interesting features in the geodynamic of the region. Nevertheless, they did not give an opportunity to consider the models in dynamics, taking into account process of sedimentation in time. Such a possibility gives the construction of three-dimensional non-stationary geothermal and thermoelastic models of the Caucasus and the Black and the Caspian seas water areas offered by authors of this paper. For the construction of three-dimensional non-stationary models of investigated region paleoreconstruction schemes of development of sedimentary cover of the Caucasus (Sholpo, 1978), of the Black sea area (Kasmin at al. 2000) and many different data about the Caspian sea area have been used. Numerical modelling of thermal and thermoelastic processes allows revealing temporal distribution of a number of thermogeodynamic events including formation of deep faults, thermoearthquakes and so on.

Before the origin of sedimentary complex thermal situation was considered as stationary: according to (V.N. Tikhonov, 1937) thermal flow of the whole Earth without sedimentary complex differs from stationary one by only 3%).

Reconstruction of 3D geothermal model

On the basis of seismic and gravimetric data the structure of the Earth’s crust is received for the region. It consist of sedimentary, granite and basaltic layers. According to geological age and physical property of the sedimentary layer, in its turn, is divided into seven layers (see below). On the surface the geographic relief is taken into account.

Data base is compiled for all these data. Thermal conductivity, heat capacity, density and magnitude of heat were determined for each layer. A three-dimensional non-stationary geothermic problem is formulated.

In order to realize this problem an algorithm has been developed.

Let’s consider non-stationary thermal conductivity equation

$$\frac{\partial \mathrm{T}}{\partial \mathrm{t}} = \frac{\partial}{\partial \mathrm{x}}\left(a\frac{\partial \mathrm{T}}{\partial \mathrm{x}}\right) + \frac{\partial}{\partial \mathrm{y}}\left(a\frac{\partial \mathrm{T}}{\partial \mathrm{y}}\right) + \frac{\partial}{\partial \mathrm{z}}\left(a\frac{\partial \mathrm{T}}{\partial \mathrm{z}}\right) + \frac{\mathrm{W}}{\mathrm{c}\,\rho} \quad (1)$$

Were T is temperature, t is time, x, y, z are spatial coefficients, λ is thermal conductivity, c is heat capacity, ρ is density, w - magnitude of radioactive heat, given off by sedimentary complex. If we assume that thermal conductivity a is constant for each layer, then we receive:

$$\frac{\partial \mathrm{T}}{\partial \mathrm{t}} = a_p\left(\frac{\partial^2 T}{\partial \mathrm{x}^2} + \frac{\partial^2 T}{\partial \mathrm{y}^2} + \frac{\partial^2 T}{\partial \mathrm{z}^2}\right) + \frac{\mathrm{W_p}}{\mathrm{c_p}\,\rho_p} \qquad (2)$$

were λ_p, c_p, ρ_p and w_p are corresponding coefficients of p layer.

$$a = \frac{\lambda}{\mathrm{c}\,\rho}$$

In order to solve the equation boundary and initial conditions are necessary: let's take for initial conditions

$$\left.\frac{\partial \mathrm{T}}{\partial \mathrm{x}}\right|_{\mathrm{x}=0,\mathrm{X}} = 0 \quad , \qquad \left.\frac{\partial \mathrm{T}}{\partial \mathrm{y}}\right|_{y=0,Y} = 0 \; ; \qquad (3a)$$

$$T\big|_{z=0} = T_0 \quad , \qquad T\big|_{z=H} = T_H ; \qquad (3b)$$

$$\lambda_{\mathrm{p}}\frac{\partial \mathrm{T}}{\partial \mathrm{n}} = \lambda_{\mathrm{p+1}}\frac{\partial \mathrm{T}}{\partial \mathrm{n}} \quad . \qquad (3c)$$

were λ_p is thermal conductivity coefficient and for the initial condition

$$T_{t=0} = T_0 \quad . \qquad (3d)$$

Boundary problem (1-3d) is solved for corresponding values and temperature distribution for discussed area is received.

Reconstruction of 3D thermoelastic model.

Warming up of non homogenous geological structure may yield considerable gradients of thermal stresses vertically, as well as laterally, because of differences in coefficients of thermal expansion of various formations.

These gradients may be very big in geosynclinicareas, such as Alpine orogenic belt and the Caucasus. We have undertaken the task of revealing these mechanisms on the basis of investigations of thermoelastic stresses. Heterogenous geological structure's heating up can result in significant gradients of thermal stresses $\Delta\sigma_T$ on vertical line $\Delta\sigma_Z$, as well as on lateral line $\Delta\sigma_L$, because of differences in coefficients of thermal expansion of various parts of the Earth's crust. These gradients may be particularly steep in folded areas, such as Alps, the Caucasus, etc., in view of deviations from horizontally – foliated structure. Because of complexity of surface and depth relief, due regard for thermal field's three – dimensionality in construction of thermal models of folded areas and in estimation of various geothermal effects becomes particularly important.

In the work (G.Gugunava, V. Sholpo et all.2003) a three-dimensional non-stationary thermal model of the Caucasus and Black Sea and Caspian Sea water areas was considered and its geologic-geophysical interpretation was given. Earlier, on the basis of the same data, a three-dimensional boundary problem of thermoelasticity theory was solved numerically (N. Muskhelishvili 1966).

In consequence of thermal field covering, in each point of medium shift vector U appears, with components U_1, U_2, U_3 (correspondingly 1-x, 2-y, 3-z) directed towards surface on the normal.

With that end in view, computations of non-stationary thermal condition of entrails of the Caucasian region and the Black Sea and the Caspian Sea water areas were used (G.Gugunava, V. Sholpo et all.2003).

Thermoelastic stresses of the investigated region were determined by numerical solution of the thermoelastic problem.

$$\mu\left(\frac{\partial^2 U_1}{\partial x^2}+\frac{\partial^2 U_1}{\partial y^2}+\frac{\partial^2 U_1}{\partial z^2}\right)+(\lambda^*+\mu)\left(\frac{\partial^2 U_1}{\partial x^2}+\frac{\partial^2 U_2}{\partial x\partial y}+\frac{\partial^2 U_3}{\partial x\partial z}\right)=\frac{\partial(\beta T)}{\partial x} \tag{4}$$

$$\mu\left(\frac{\partial^2 U_2}{\partial x^2}+\frac{\partial^2 U_2}{\partial y^2}+\frac{\partial^2 U_2}{\partial z^2}\right)+(\lambda^*+\mu)\left(\frac{\partial^2 U_1}{\partial x\partial y}+\frac{\partial^2 U_2}{\partial y^2}+\frac{\partial^2 U_3}{\partial y\partial z}\right)=\frac{\partial(\beta T)}{\partial y} \tag{5}$$

$$\mu\left(\frac{\partial^2 U_3}{\partial x^2}+\frac{\partial^2 U_3}{\partial y^2}+\frac{\partial^2 U_3}{\partial z^2}\right)+(\lambda^*+\mu)\left(\frac{\partial^2 U_1}{\partial x\partial z}+\frac{\partial^2 U_2}{\partial z\partial y}+\frac{\partial^2 U_3}{\partial z^2}\right)=\frac{\partial(\beta T)}{\partial z} \tag{6}$$

$$\mathrm{U}_1=\mathrm{U}_2=\mathrm{U}_3=0 \tag{7}$$

$$\mu\left(\frac{\partial \mathrm{U}_1}{\partial \mathrm{z}}+\frac{\partial \mathrm{U}_3}{\partial \mathrm{x}}\right)=0 \tag{8}$$

$$\mu\left(\frac{\partial \mathrm{U}_2}{\partial \mathrm{z}}+\frac{\partial \mathrm{U}_3}{\partial \mathrm{y}}\right)=0 \tag{9}$$

$$\left(\lambda^*\left(\frac{\partial U_1}{\partial x}+\frac{\partial U_2}{\partial y}+\frac{\partial U_3}{\partial z}\right)+2\mu\frac{\partial U_3}{\partial z}\right)=0 \tag{10}$$

$$\mu_n\left(\frac{\partial \mathrm{U}_1}{\partial \mathrm{z}}+\frac{\partial \mathrm{U}_3}{\partial \mathrm{x}}\right)=\mu_{n+1}\left(\frac{\partial \mathrm{U}_1}{\partial \mathrm{z}}+\frac{\partial \mathrm{U}_3}{\partial \mathrm{x}}\right) \tag{11}$$

$$\mu_n\left(\frac{\partial \mathrm{U}_2}{\partial \mathrm{z}}+\frac{\partial \mathrm{U}_3}{\partial \mathrm{x}}\right)=\mu_{n+1}\left(\frac{\partial \mathrm{U}_2}{\partial \mathrm{z}}+\frac{\partial \mathrm{U}_3}{\partial \mathrm{x}}\right) \tag{12}$$

$$\lambda^*{}_n\left(\frac{\partial U_1}{\partial x}+\frac{\partial U_2}{\partial y}+\frac{\partial U_3}{\partial z}\right)+2\mu\frac{\partial U_3}{\partial z}=\lambda^*{}_{n+1}\left(\frac{\partial U_1}{\partial x}+\frac{\partial U_2}{\partial y}+\frac{\partial U_3}{\partial z}\right)+2\mu_{n+1}\frac{\partial U_3}{\partial z} \tag{13}$$

Equations (4-6) are the well-known equations of the elasticity theory (N. Muskhelishvili 1966). Boundary conditions (7-9) indicate that surfaces of the area under review are free from stresses.

Formulae (10-13) are ordinary adjoint equations in the elasticity theory, equality of normal and tangential stresses. Values of Lame coefficients λ^* and μ are given in table 1.

Table 1.

Parameter 10^9 N/m^2	Sediments	Granite	Basalt	Mantle
λ*	24.832	26.75	41.295	76.108
μ	16.224	32.375	41.063	70.587

For numerical solution of the formulated problem the method of finite differences was used, where U_1, U_2, U_3 - are displacement components, λ*, μ are Lame constants, β is pressure=3Kα, T is temperature, K is delitation modulus,

$$K = \frac{3\lambda^* + 2\mu}{3}$$

$$\alpha = (4 - 1{,}3 \cdot 10^{-3} \cdot T) \cdot 10^{-5}$$

While solving boundary problem (4-13), we receive components U_1, U_2, U_3 of displacement vector $\vec{U}$, and by its help we define stress components.

Analys and interpretation of the thermoelastic 3D model

The analysis of calculation maps of vertical thermodisplacements at 140 and 70 km depts. (410 million years) shows that already from these depths contours of Black and Caspian Seas and fault of the Caucasus are being formed. Already from these depths contours of the Black and the Caspian Seas and faults of the Caucasus are observed.

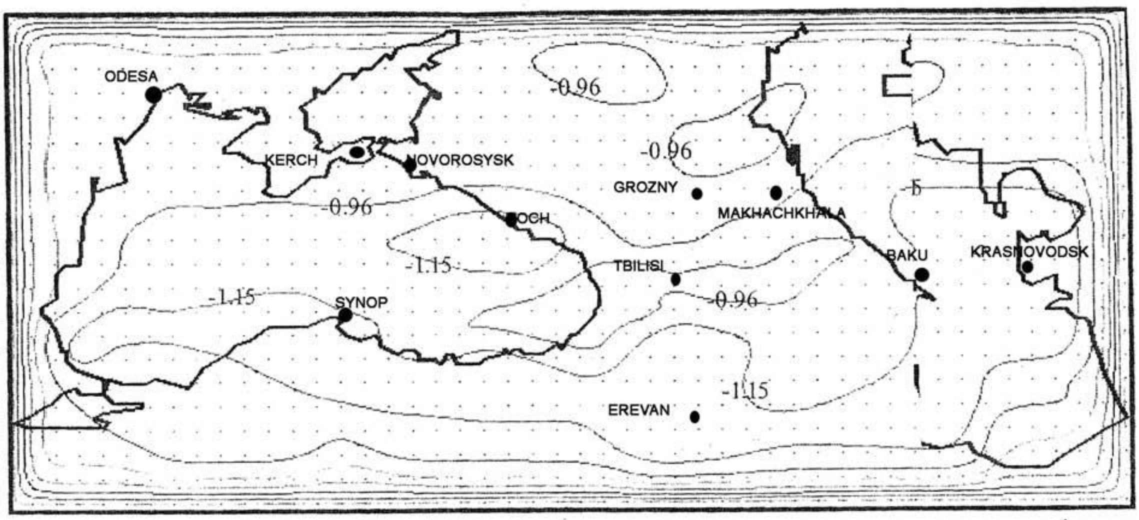

Pic.1. Thermo-vertical displacements (km) 140 km depth (410 million years)

Already over Moho discontinuity outlines of Black Sea depression and deep-sea part of Caspian depression occur on maps of vertical displacements, as well as on maps of thermodense anomalies (Pic.2).

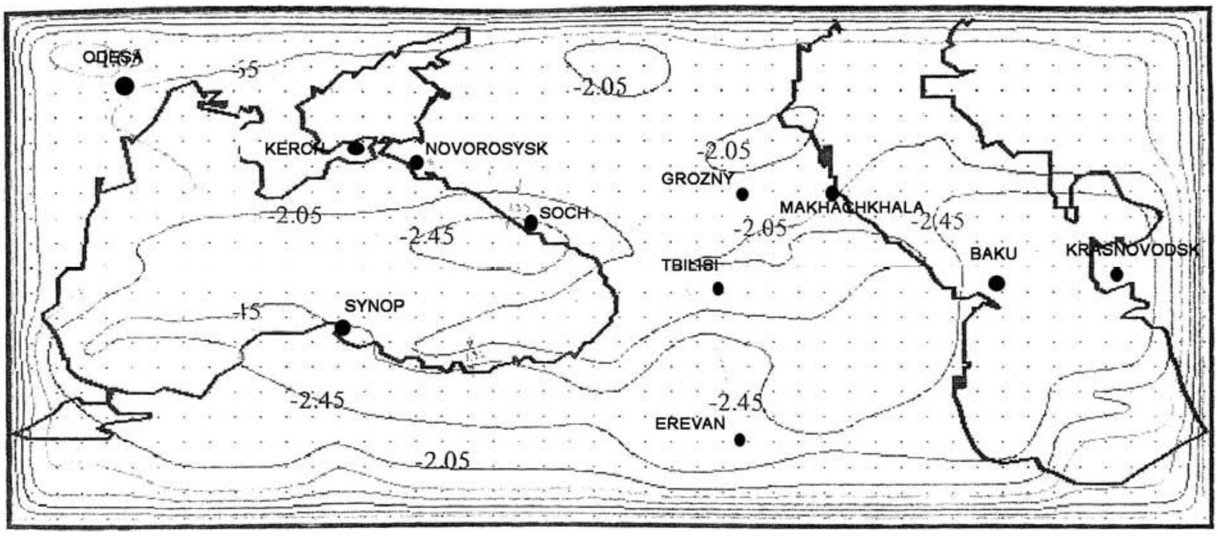

Pic.2. Thermo-vertical displacements (km) over Moho discontinoity

Isolines over Moho discontinuity (Pic. 2) represent elongated structure which is stretched from the Black Sea to the Caspian Sea, and they can not condition origin of discontinuity dislocations, i.e. deep faults, for which horizontal gradient of vertical displacements in 16 m/km is necessary.

Over Conrad discontinuity there are areas of thermodisplacements, which are forming deep thermo faults (Pic.3)

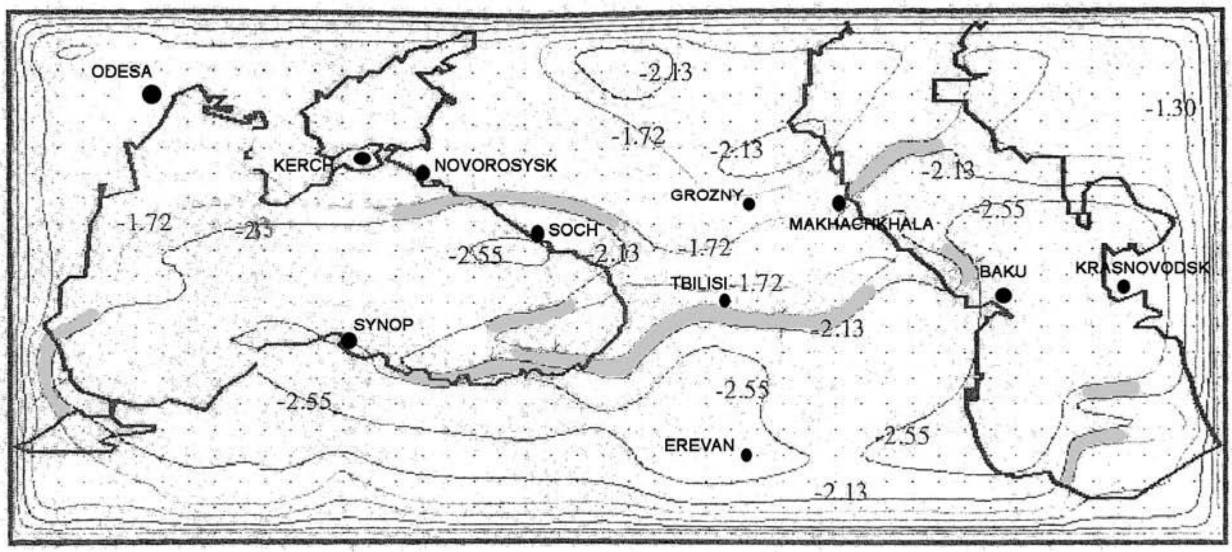

Pic.3 Thermo-vertical displacements (km) over Conrad discontinuity

Beginning from Granite layer surface, vertical displacements reach spatial critical values, at the same time isolines in some regions draw together so much that large areas of discontinuity dislocations occur (see Pic.4), crossing the whole Caucasus from sea to sea and almost utterly bordering the Black Sea and deep-sea part of the Caspian Sea.

In Transcaucasus in Devon, Carbon, Trias situation of vertical displacements is analogous of situation on granite layer surface.

In Lower Jurassic the system of discontinuity dislocations is branching even more, staying unchanged almost up to the Earth’s surface.

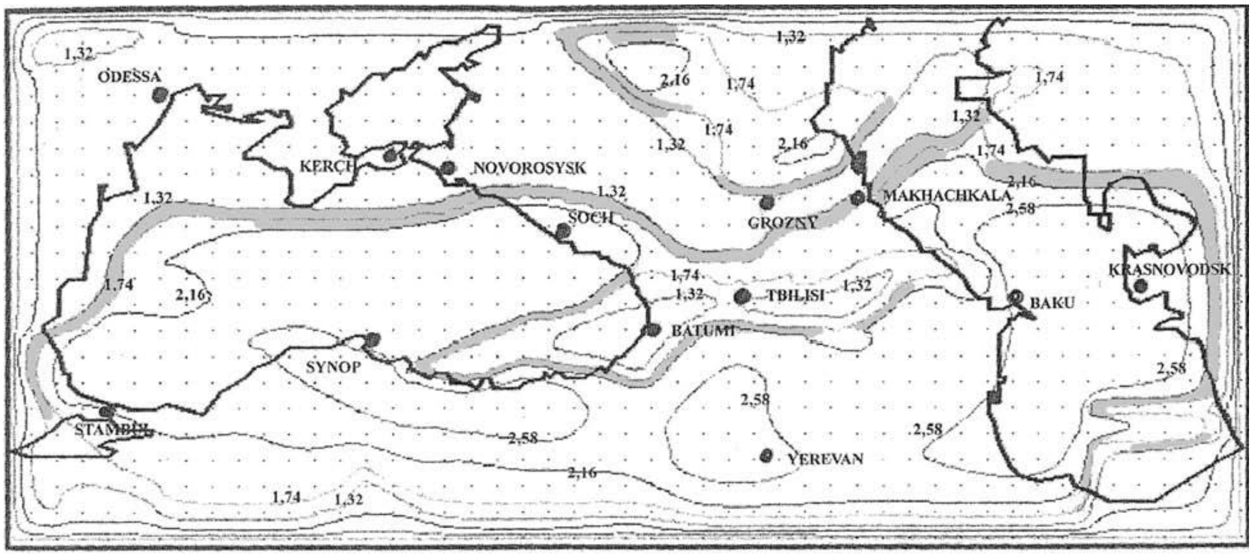

Pic. 4. Thermo-vertical displacements (km) over Granite layer surface

Areas of maximum approchement of isolines are shaded, which is indicative of possibility of deep faults occurrence.

West part of Achara-Trialeti zone and its prolongation to the South-West in the Black Sea are very interesting. In Achara region, on geological data basis, some deep faults are identified, which, according to our data, are clearly observed in water area of the sea.

Examination of the diagram of deep thermoelastic faults shows good correlation with geological observations in Achara. In this diagrams (Pic.4-5) faults have spindle-shaped prolongations in the South-East part of the Black Sea water area, which makes it possible to suppose sinking of Achara system faults in the Black Sea.

As model calculations of thermovertical displacements show, emersion of the territory of the Caucasus is observed, which manifests itself in uplift of crystalline substrate from 0,96 to 2,5 km before the origin of sedimentary complex. It seems that “chalk-forming” of the ocean “Tethys” in the Caucasus may be conditioned by thermoelastic vertical displacements in the mantle and the crust.

In the period of intensive uplift of central part of Black Sea and deep-water part of Caspian Sea water areas the fault of granite layer supposedly took place, which could explain the absence of this layer in the water areas.

Beginning from the surface of granite layer, along the contour of the Black Sea and deep-water part of the Caspian Sea (in the period of uplifting) ultimate strength of rocks was overcome (see Pic.4,5) which was manifested by discontinuity dislocations with deep fault formations.

When analyzing maps of distribution U_3 of vertical thermoelastic displacements of vector U , it is easy to notice that zones of anomalously high values of lateral derivatives U_3 (reaching 16 m/km and even more, considerably exceeding ultimate strength of rocks) agree well enough with data of majority of deep faults of the Caucasus and Black and Caspian Seas water areas. Faults of the Greater and the Lesser Caucasus, Black and Caspian Seas water areas, etc., are well observed on the maps.

Faults in anatolia region, conditioned by displacements of continental blocks, are transform and cannot be represented on the maps of vertical thermoelastic displacements.

Maps of thermal models, based on paleoreconstruction diagrams, show that within the Black Sea, beginning from Trias (shallow sea) till Upper Cretaceouse-Quaternary period, cristalline substrate comes to surface and only afterwards intensive deflection and accumulation of sediments begin.

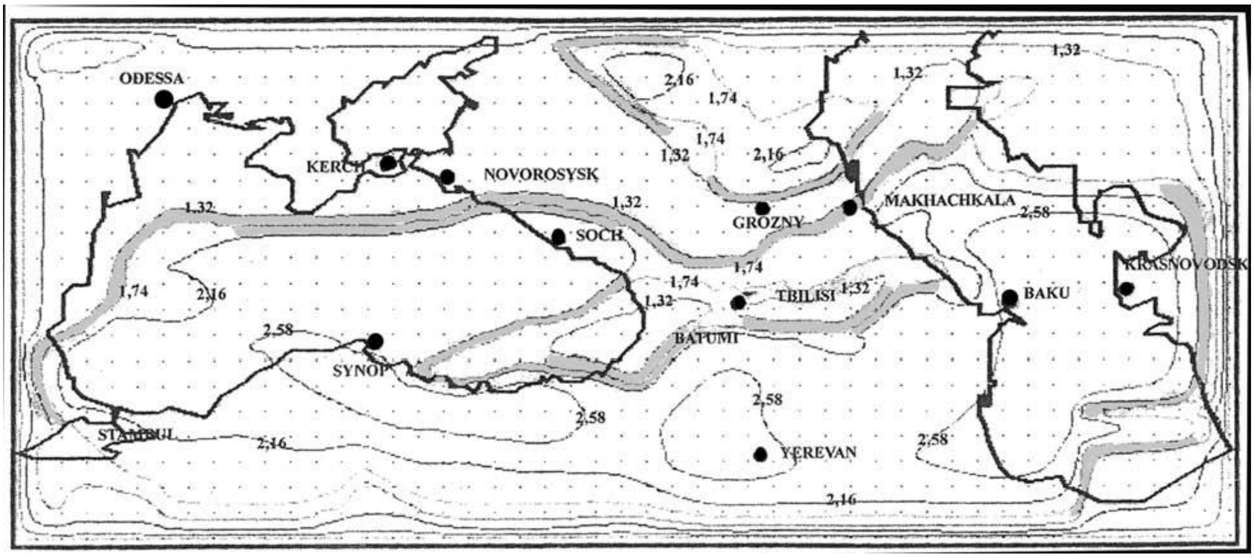

Pic.5. Thermo-vertical displacements (km) on the surface of Devonian, Carbonic, Triassic period

Before Upper Cretaceous mechanical connection between blocks of the Black Sea (and earlier, deep-water part of the Caspian Sea) and the whole surrounding lithosphere plate was utterly broken, after which sinking (a bit earlier) of Caspian block and in K_2 – Black Sea block, took place, which favoured sharp accumulation of sediments in them and further sinking also at the expense of accumulated sediments.

As for Stavropol and South Caucasus, here ultimate strength of rocks was not overcome (horizontal gradient is considerably lesser than 16 m/km); see Pic.2-5.

Problem of formation of Black Sea and Caspian Sea depression is of considerable interest. Most probably their nature is similar. There exist lots of hypotheses about origin of these structures. One more is offeres in the present investigation.

The Black Sea depression and Caspian depression are almost utterly bordered with deep faults, which penetrate into 70 km and deeper depths and also cross all formations of sedimentary complex, along which gradual accretion of faults towards surface took place owing to sinking heavy and cold foundation and growth of sediments weight which were accumulating in depressions. At the some time it should be taken into account that Black Sea and Caspian Sea “plates”, float on half-melt of elastico-viscous medium of upper mantle (astenosphere) and, owing to surrounding deep faults, begin to “sinking” deeper and deeper as sediments accumulate in depressions, untill all plates and buoyancy force get balanced.

In Upper Cretaceous, substrate, which is sunk under thick sediments and is not yet warmed up, represents low-temperature anomaly (at depth too); it follows that, irrespective of “screening” effect of sediments (as it is considered), this low-temperature body can not give surface high thermal flows at all.

Thus, at the first stage, against a background of general uplift, due to thermodisplacements along the whole plotting board, areas of Black Sea and deep-water part of Caspian Sea (see pic.2-5) experiance sharp uplift, which results deep faults along the whole contour of the seas. At second stage areas which are fringed with deep faults begin to come down.

Interesting picture, corroborating our model, is observed in the south of the Crimea peninsula, where, according to data of thermoelastic model, sublatitude structure of deep fault is observed, which coincides with geological data; “in the south submarine part of the Crimea structure is separated from deep-water hollow of the Black Sea by the fault which crosses the foot of continental slope (V.N. Hain, 1984, p.145). According to our data analogous picture is observed in the south of the Black Sea, in Anatolia region.

As to absence of deep thermoelastic faults inside the Black Sea, it may be explained by tectonic (purely mechanical) crushing of oblong plate of the Black Sea, which could not reflected on thermoelastic model.

It is to be supposed that analogous picture is observed in deep-water part of the Caspian Sea water area, which is of earlier genessis, but nevertheless, proceeding from the fact that calculations for coming to surface crystalline substrate give here too isotherm sinking, i.e. upper layeres of "granite" (where they do exist) and basalt as well, are considerably cooled. "Cold" sediments are being deposited on them again. That's why they can not be warmed up thus much as to give considerable heat flows on sea ground.

Undoubtedly initial origin impulse (in the period of 410 million years) of both depressions is of mantle origin. That fact that in the Caucasus contours of Black and Caspian Seas appear at Moho discontinuity testify to above said.

Conclusions:

1 large vertical displacements occur in the mantle; as for sedimentary complex, vertical displacements are insignificant;
2 we think that chalk-forming of ocean "Tetis" is connected with vertical thermodisplacement processes in the mantle and the crust;
3 it is possible that absence of granite layer in the Black Sea and deep-water part of the Caspian Sea is due to transgression in this period;
4 fractures arise at Moho discontinuity, continue in "basalt", develop intensively in "granite" and exist in sedimentary complex till these days, thus conditioning occurrence of contemporary earthquakes in the region;
5 along discontinuity dislocations around the Black Sea sedimentation begins only after Upper Cretaceous, and in the Caspian Sea a bit earlier and also with sharp accumulation of sedimentary rocks.

References

[1] Alexidze M.A., Buachidze G.N., Gugunava G.E., Kiria J.K., Chelidze T.L.. Three-dimensional stationary geothermal model of the Caucasus. Reports of ASGSSR, v. III N3, 1983 y. pp. 505-508.

[2] Alexidze M.A., Gugunava G.E., Kiria J.K., Chelidze T.L. A three-dimensional stationary geothermal model of the Caucasus geodynamic implications. Geodynamic and seismic source processes stress, strength and viscosity in the lithosphere. March-April. Potsdam (Abstract) 1989.

[3] Alexidze M.A., Gugunava G.E., Kiria J.K., Chelidze T.L.. A three-dinensional stationary model of the thermal and thermoelastic fields of the Caucasus. "Tectonophysics, T. 227, 1991, pp. 191-203

[4] Gugunava G.E., Sholpo V., Gamkrelidze E.P., Gogiashvili J.V., Kiria J.K., Chikovani N.G., Kolesnikov I.V. A three-dimensional non-stationary thermal model of the Caucasus and the Black and Caspian Sea area. Journal of the Georgian Geophysical Society. Issue A. Physics of Solid Earth. vol. 8A 2003.

[5] Hain V.N.. Regional geodynamics (Alpine Mediterranean belt), M. "Nedra:, 1984 y.

[6] Kazmin V.G., Shreider A.A., Finetti N., Chelikhov V.R., Bulichev A.A., Gilod D.A., Andreeva O.A. Al. Am. Shreider "Earlier stages of development of the Black Sea according to seismic data". Geotectonics, 200y. N 1. pp.41-68 (in Russian).

[7] Muskhelishvili N. Some basic problems of mathematical theory of elasticity. M. 1966.

[8] Sholpo V.N. (1978). Alpine geodynamics of the Greater Caucasus. M. "Nedra", p.126 and Doctor's dissertation of 1978 year.

[9] Tikhonov A.N. 1937y. On radioactive decay influence on the Earth's crust temperature. Reports of ANSSSR. "Geography and geophysics", N3 pp.431-458.

კავკასიის და შავი და კასპიის ზღვების აკვატორიის სამგანზომილებიანი არასტაციონალური თერმო–გეოდინამიკური მოდელი

გუგუნავა გ., ქირია ჯ., ქირია თ., ზერაკიძე ზ.

რეზიუმე

აგებულია კავკასიის და შავი და კასპიის ზღვების აკვატორიის სამგანზომილებიანი არასტაციონალური თერმო–გეოდინამიკური მოდელი, რომლის საფუძველზე ჩატარებულია რეგიონის გეოლოგო–გეოფიზიკური ინტერპრეტაცია. აგებულია წანაცვლების ვერტიკალური მდგენელის რუკები. დადგენილია ზოგიერთი რღვევის წარმოშობის თერმული ბუნება.

Journal of Georgian Geophysical Society,
Issue (A), Physics of Solid Earth, v.18a, 2015, pp. 49-58

Reinterpretation of Geophysical Data for the Study of Deep Structure of the Greater Caucasus

S. Ghonghadze, P. Mindeli, J. Kiria, N. Ghlonti, A. Esakia

Preface. The issue of orogenesis mechanism is one of the most difficult tasks to study in Geodynamics and it attracts attention of many specialists of different spheres of the Earth sciences. The region of the Greater Caucasus, considered in this paper, is a part of the greatest of the Earth the Alpine-Himalayan collision belt, alongside of which the highest mountain complexes are observed. In most cases the initial mechanism of orogenesis is collision – convergence of continental plates that leads to mutilation and thickening of the crust.

For the best conception of the deep mechanisms of regional geological processes it is important to use the information on geophysical investigations of the structure of the crust and mantle.

Many national and foreign scientists have been studying the deep structure of the Greater Caucasus. On the basis of existing gravimetric, magnetometric and seismometric data we attempted to process these materials qualitatively by new technologies of the latest computers and make conclusions on the issue.

We made comparative analysis between our data and the ones of the local and regional tomography processed by means of LOTOS software (headed by Kulakov) and other new geophysical methods of microseismic sounding (MSS) of A. V. Gorbatikov's and E. A. Rogozhin's works. In the *Figure 1* the gravimetric profiles, deep seismic sounding (DSS) and microseismic sounding (MSS) are shown.

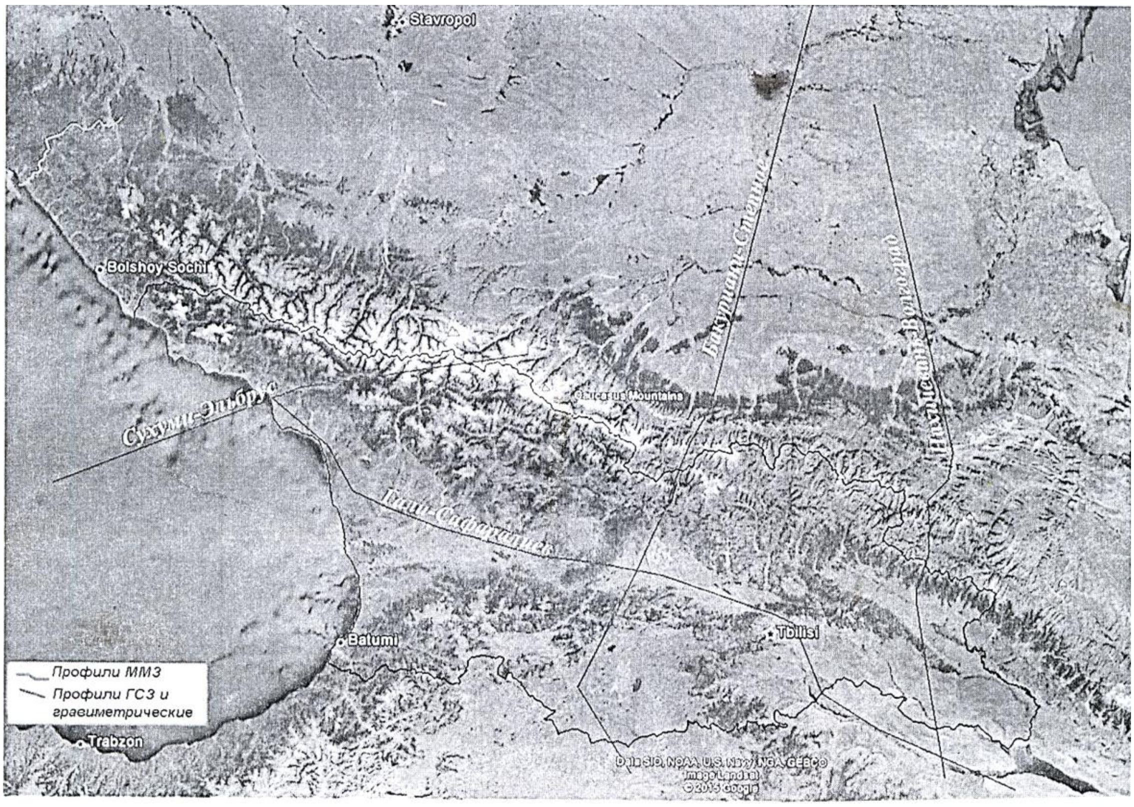

Figure 1. A scheme of the profiles.

Processing of gravimetric and magnetometric data. The single solution to the task taking into account the two deep seismic sounding profiles is involvement of anomalous gravity field, which contains information about the bottom of the Earth crust as the boundary with significant density jump.

Unfortunately, the observed gravity field expresses the influence of nearly all the inhomogeneity of the Earth. Thus, to distinguish the mantle structure it is necessary to maximally free the observed gravity field from external influences. Firstly, it is necessary to define and prevent the effects of the crust, which on the one hand is very important and on the other – may be reliably defined regardless of the gravity field by seismometric data (DSS). The residual anomalies of the gravity force, which with the precision of the crust model may be called the mantle anomaly, are the most relevant for the geodynamic structure and for determining the nature and intensity of processes.

The trend in the theory of interpretation of potential fields, which is connected with attempts to study in some cases the vertical distribution of magnetism and density according to the data of magnetic prospecting and gravity prospecting, was named as interpretation tomography. Interpretation tomography (Greek words *tomos* – to break, part, layer and *grapho* – to write, draw) is a system of study of geological structures either by gravity or by magnetic fields and enables obtaining their layered image. At present, in this trend there are several approaches offered by a number of researchers (though not all of them obviously call the object of their research as tomography in their researches) and they may be divided into two groups: approximation (Y.Y. Vashchilov, A.I.Kobrunov, A. P. Petrovsky, V.I.Segalovich, A.V. Ovcharenko, D.Oldenburg, Y.Lee, etc.) and filtration (P.S.Martishko, V.M.Novoselitsky, B.Y.Podgorny, I.I.Priezzhev, I.L.Prutkin, A.F.Shestakov, etc.).

It is obvious that precisely solving the task of the study of the vertical distribution of magnetism and density according to the data of magnetic prospecting and gravity prospecting is practically impossible. However, such works should be carried out hoping that the local situation in a certain region is more favourable than the common one. The filtration technology is implemented in the software *Oasis Montaj* created by Canadian company *GeoSoft* and is based on applying procedures of optimal filtration and approximation continuity of fields. For mathematical arrangement MAGMAP module applies filters in Fourier sphere or the sphere of wave numbers. Mathematically, the Fourier transformation *f(x,y)* is determined as follows:

$$\mathbf{f(\mu,\nu)=\int_{-\infty}^{\infty}\int_{-\infty}^{\infty}f(x,y)\cdot e^{-i(\mu x+\nu y)}dxdy}$$

the inverse relation

$$\mathbf{f(\mu,\nu)=\frac{1}{4\pi^2}\int_{-\infty}^{\infty}\int_{-\infty}^{\infty}f(\mu,\nu)\cdot e^{-i(\mu x+\nu y)}d\mu d\nu}$$

where μ,ν are wave numbers, accordingly in the directions x and y measured in radians per meter, on condition that x and y are expressed in meters. They are connected with spatial frequencies f_x and f_y expressed in period per meter.

The analytical continuation of the field in the upper semi-sphere is considered as a *pure filter* as it does not create any side effects that may require application of other filters or procedures for correction. Therefore, this filter is often used for elimination or minimization in regular grids of fields of non-deep sources or noises.

The Butterworth filter is quite suitable for the application of direct high or low quality filters for data, i.e. it enables easily regulating the smoothening degree of the filter and at the same time leaves the central wave number unchanged.

It is possible to obtain more general image of depths of certain points and sources of gravity and magnetic anomalies by analyzing the energy spectrum of the fields. *Figure 2* shows a scheme of the logarithm of the radial averaged amplitude spectrum of the anomalous gravity and magnetic fields depending on the spatial frequency received by means of the special option of the set of softwares *Oasis Montaj*, and also estimation by the same system of the source depths in different diapasons of spatial frequencies. The analysis of the gravity field scheme shows that the narrow frequency line in the low quality part of the spectrum is connected with the sources located very deeply, the special points of which correspond to the depths above 16 km. the most of the mentioned depths are 18 km. Thus, when considering the spectrum included in the anomalous gravity field the information is referred to the upper layer of the Earth crust with approximately 16 km thickness. In the scheme of the anomalous magnetic field it corresponds to the 18 km depth.

Let us note that the certain "vulnerability" based on the transformations of the geophysical field division methods was obvious from the moment of its appearance. The transformation fields enable only improving the obviousness of the influence of separate perturbing factors.

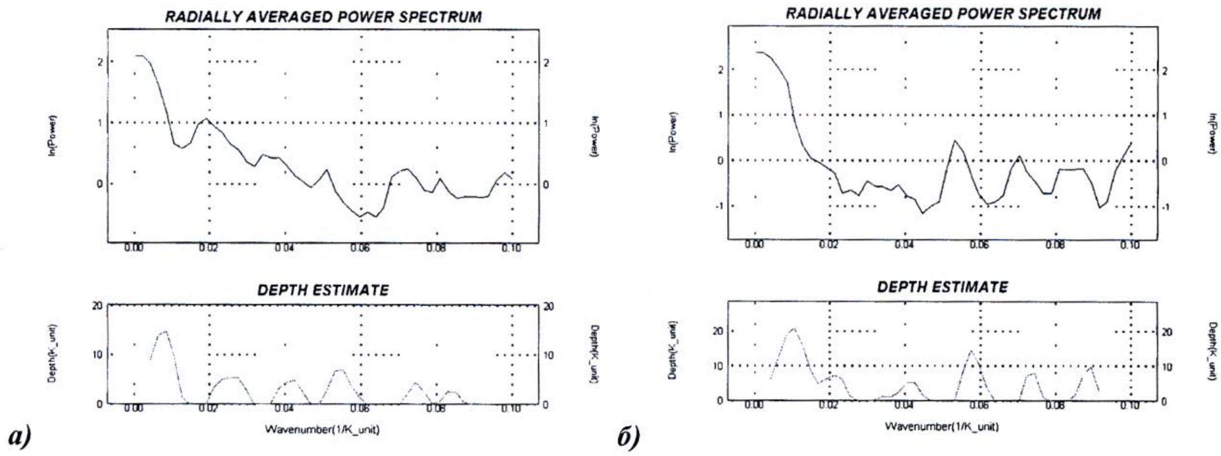

Figure 2. a) Estimation of source depths in different diapasons of spatial frequencies by the scheme of the logarithm of the radially averaged amplitude spectrum of the gravity field.

b) Estimation of source depths in different diapasons of spatial frequencies by the scheme of the logarithm of the radially averaged amplitude spectrum of the magnetic field.

The residual anomalies of the gravity field shown in the figure were obtained by recounting the anomalous field in the Bugge reduction with the density of the interlayer 2.67 g/sm^3 and correction of the relief up to 200 km at different heights up to 100 km. The error in the measurement for the image of 1:50 000 scale was 0.5 mGl and at the 1:200 000 scale – 1 mGl (*Figure 3*). Different height transformed fields were removed from the anomalous gravity field created by residual cover by the anomalies caused by the variations of depths up to boundary M and the regional fields connected with the influence of the most significant masses. The *Oasis montaj* software was used as an interpretation instrument taking into account the above recounted filters.

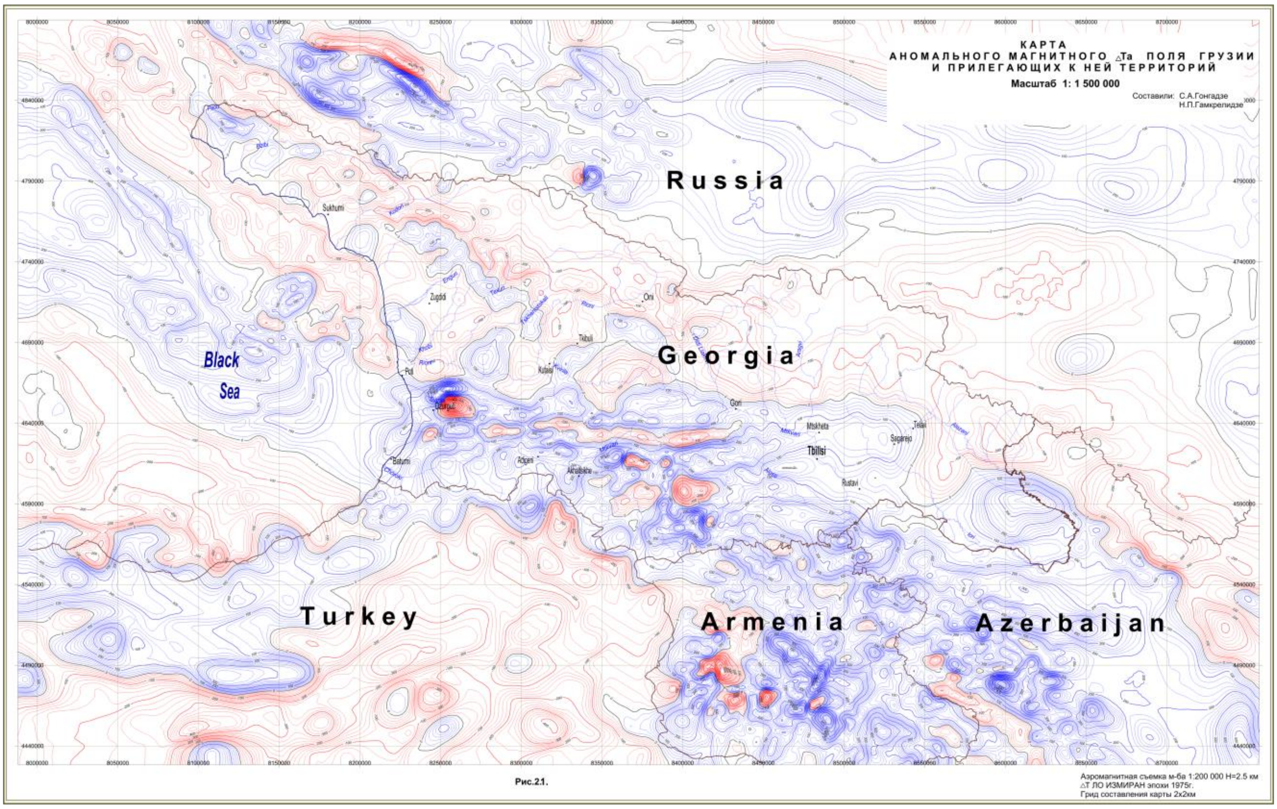

Figure 3. A Map of the anomalous gravity field of Georgia and its adjacent territories.

Figure 4 shows the horizontal sections at 15 and 45 km depths of the gravity and magnetic field for the transformed and residual field, on which the variation of the fields together with depth connected with low and high density inhomogeneities are shown.

Comparative analysis of the gravimetric and seismometric data of the local seismography and microseismic sounding method. For comparison the data of the local seismography are taken. The seismic data were processed by means of Local Tomography Software, LOTOS-09 (Novosibirsk). The algorithm of the tomography LOTOS-09 is used for the simultaneous application of P and S speeds of the structures and source coordinates. For the tomography a referent model of the Earth crust of the study area was used:

Depth	Vp	Vs	
0.000	4.53	2.78	speed in the residual layer
6.000	5.70	3.35	speed in the granite layer
21.000	6.43	3.70	speed in the basalt layer
44.000	7.98	4.70	speed on the Moho surface

The data of the P and S wave travels during the period of 1964-2007 are taken from the Catalague of the International Seismic Centre (ISC).

On the basis of the data shown in *Figure 4* showing also the results of the inversion of the real data of P and S anomalies for the 15 and 45 km depths the coincidence of the low anomalies with the fold-fault mountain ranges of the Greater Caucasus and the link between high anomalies and the intermountain depression of the Transcaucasus are obviously seen. It is especially well observed in the residual gravity field and inversion of the P-anomaly. In the sections for the 45 km depth area of the lowered values of the gravity field and the low anomalies of P-waves the dominating situation of the area is taken.

In the three profiles of the DSS of Bakuriani-Stepnoye, Nakhichevan-Volgograd and the one, as we called it, Sokhumi-Elbrus shown in *Figure 4* the vertical sections of the residual gravity and magnetic fields were constructed.

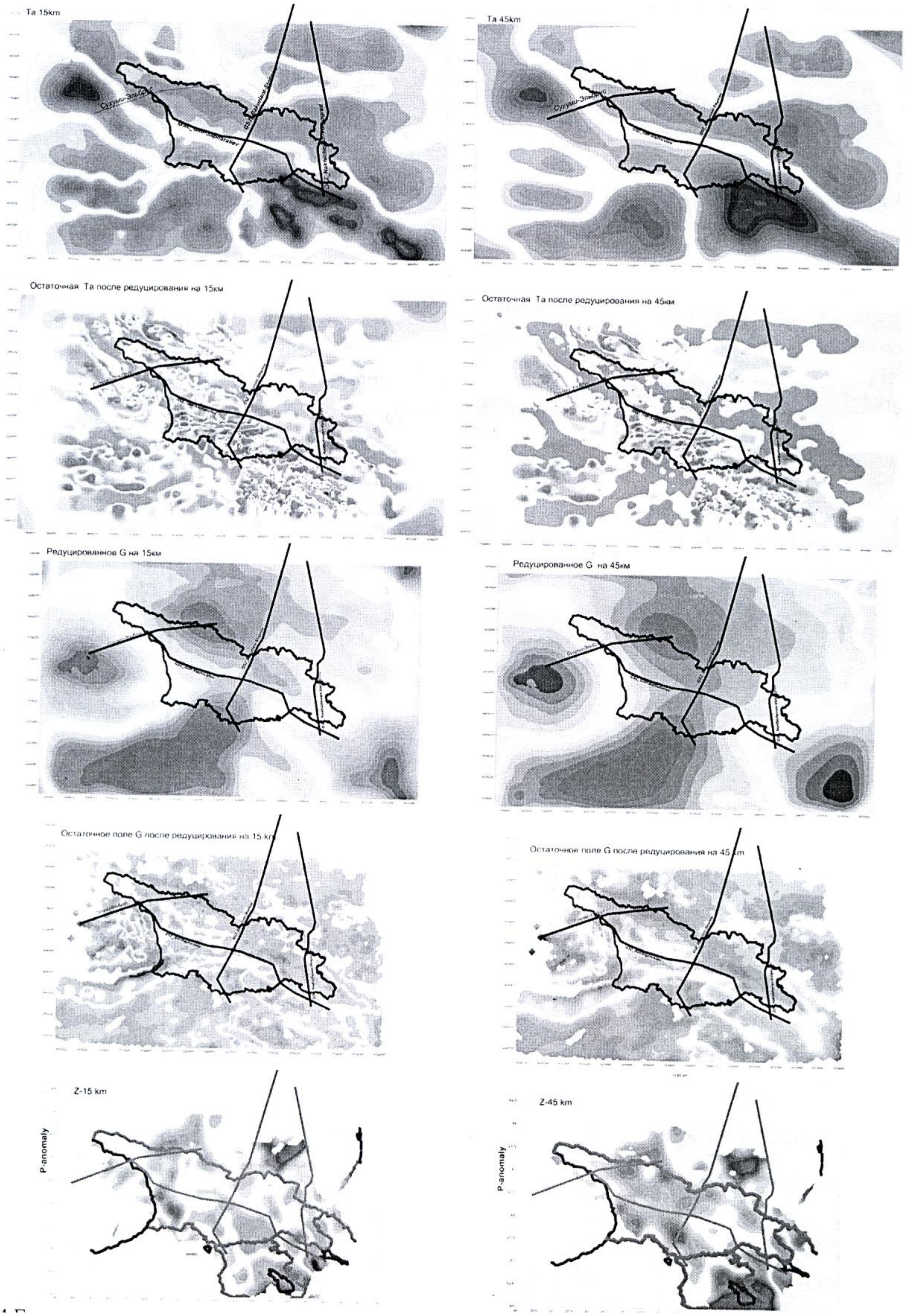

Figure 4. Horizontal section of the reduced and residual magnetic, gravity fields and the local seismotomography in 15 and 45 km.

In the Bakuriani-Stepnoye profile, in the residual gravimetric field the region of the Greater Caucasus is distinguished with alternation of the areas of high and low parameters, namely, vertical inhomogeneities. Only on the DSS tomography it is possible to mark horizontal conditional boundary for distinguishing of so called granite, basalt (the Conrad surface) layers and the Moho surface. *Figure 5* shows the interpretation of the Bakuriani-Stepnoye profile tomography, on which the three above mentioned horizons are distinguished. Several faults are illustrated by impairing the integrity of the speed inhomogeneity.

The same figure shows the model of the profile constructed by G.A. Pavlenkova (2012) as a new variant by means of the Zeld ray modeling software. This software, unlike the one we use, solves direct tasks.

There is a correlative connection between the two tomographies. Although, some differences in speed take place, both images coincide with each other (*Figure 5*).

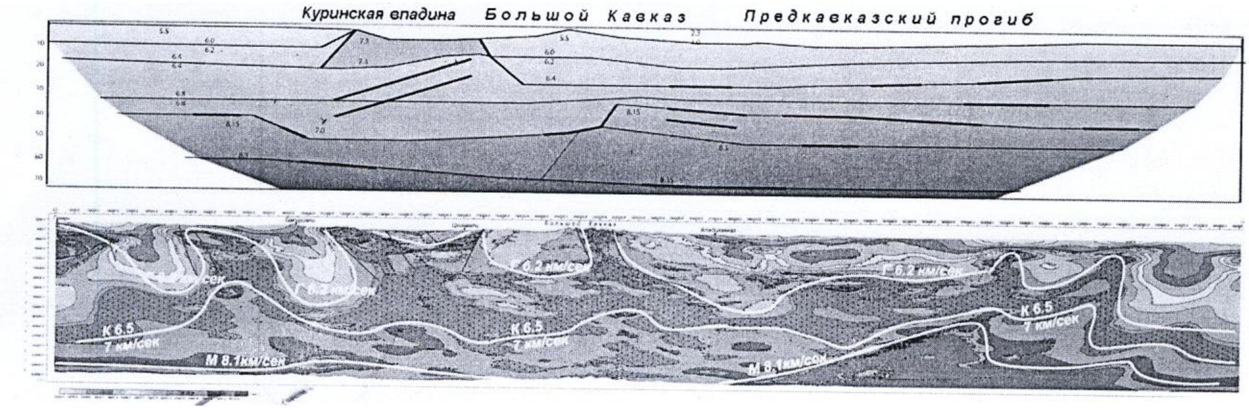

Figure 5. Interpretation of the Bakuriani-Stepnoye DSS profile seismotomography and the model of G.A. Pavlenkova with the new reinterpretation.

In the Nakhichevan-Volgograd profile (*Figure 6*) the Greater Caucasus is distinguished in the vertical section of the P-inversion in two areas, from the South by high values of the P-anomaly and to the North – by low ones. A qualified analysis shows the G alternation of the vertical low and high density inhomogeneities in the residual field as in the DSS profile. It is noteworth that a speed section for the P-inversion is constructed only for the 65 km depth as the reference model was given for up to 65 km and the residual fields - up to 100 km. The depth of the DSS method for the Bakuriani-Stepnoye profile is 70 km and for the Nakhichevan-Volgograd profile – 75 km. The interpretation of the CMRW (Correlation Method of Refracted Waves) tomography of the Nakhichevan-Volgograd profile enables distinguishing three conditional probable layers of granite, basalt and the Moho surface. When comparing this profile with the Pavlenkova model, similarity in speed boundaries is observed, though there are some differences.

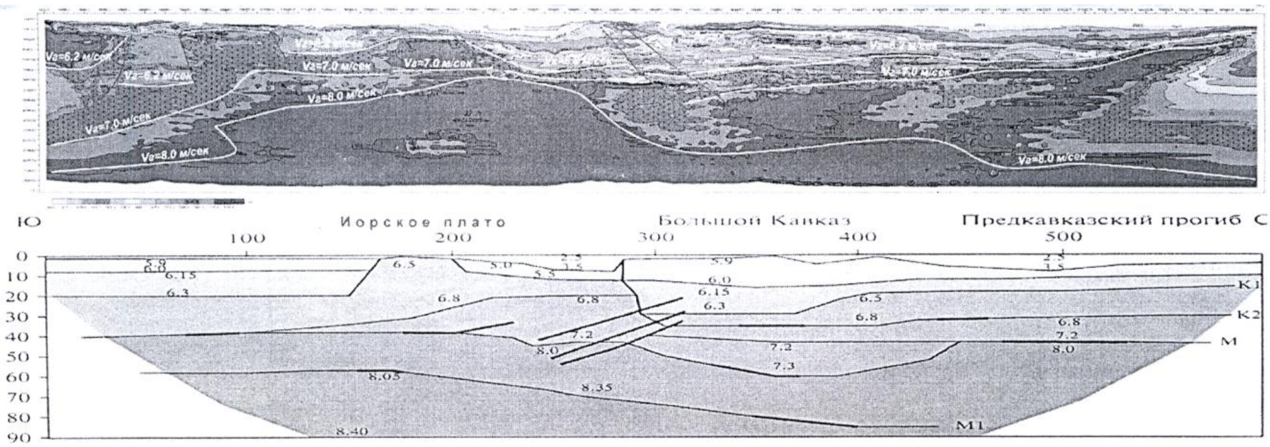

Figure 6. Interpretation of the Nakhichevan-Volgograd DSS profile seismotomography and the model of G.A. Pavlenkova with the new reinterpretation.

For comparison of the cross profiles of DSS Nakhichevan-Volgograd and Bakuriani-Stepnoye the interpretation of the longitudinal profile of Gali-Safaraliev, also called the profile from-sea-to-sea, was conducted. However, our data belong only to the 512 km long profile (*Figure 7*).

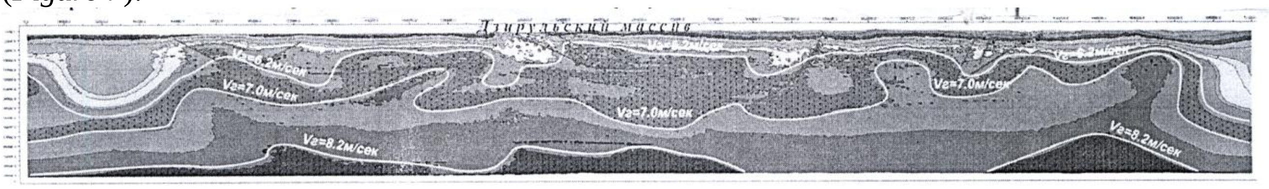

Figure 7. The seismotomography of the Gali-Safaraliev DSS profile

Here three boundaries belonging to the “granite” layer V=6.2 km/s, the “basalt” layer V=7.0 km/s and the Moho layer V=8.2 km/s are also distinguished.

Figure 8 shows the spatial layout of the DSS profile for determining the correlation of the distinguished conditional boundaries. When the cross profiles are crossed by the longitudinal profiles the horizons become interconnected.

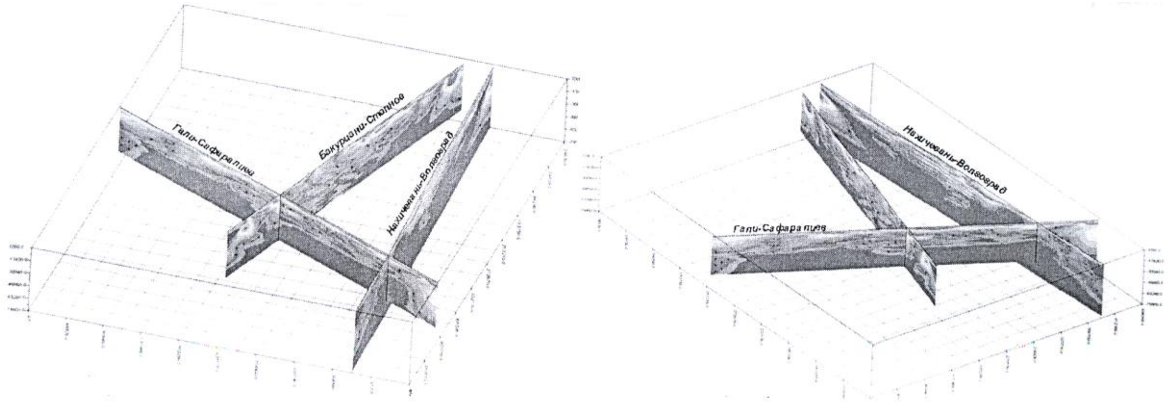

Figure 8.

The works were carried out by Balavadze B.K, Shengelaia G.Sh., Mindeli P.Sh, taking into account the data of the gravity filed, geologic-geophysical information and the interpretation results of the Bakuriani-Stepnoye and Nakhichevan-Volgograd DSS profiles. The schemes of the surface variation of the crystal foundation, the Conrad and Moho surfaces were constructed (*Figure 9*).

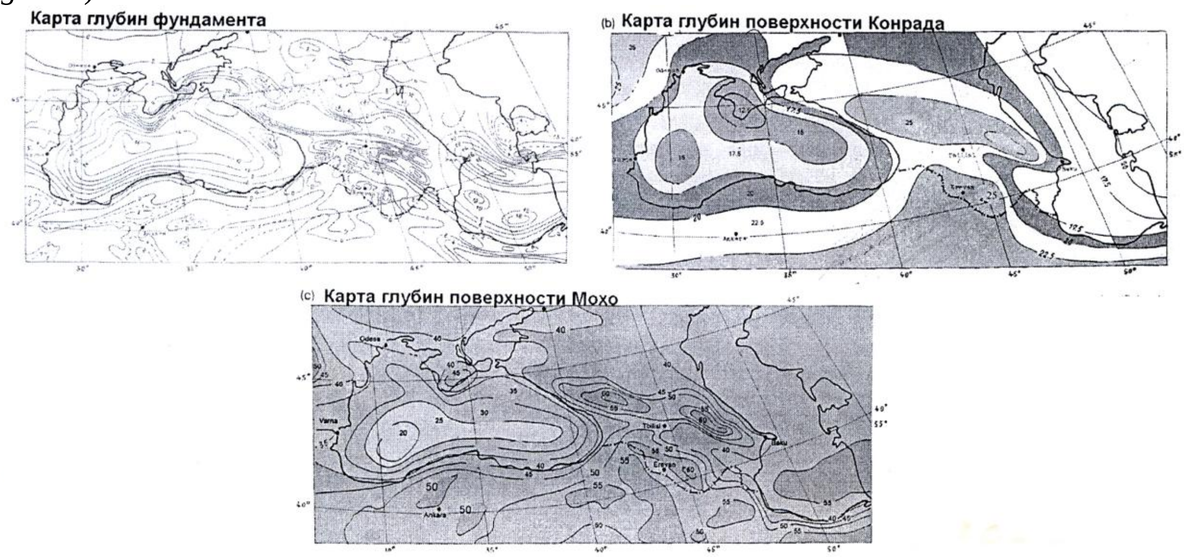

Figure 9.

It is obvious that the Greater Caucasus is mostly a unique deep geological structure. Tectonically it is characterized with block-folded structure. The formation of the Greater Caucasus is connected with the development of many geological processes on its adjacent territories.

The analyses of the reinterpretation of the DSS profile tomographies were conducted by Balavadze B.K, Shengelaia G.Sh., Mindeli P.Sh. In the structural maps of the granite, basalt and Moho surfaces some correlation dependence is observed: rising of the granite and Conrad surfaces in the zone of the Greater Caucasus and bending of the Moho surface.

It is noteworthy that in 1980-ies in the works by the magnetotelluric sounding method G.E. Gugunava suggested a generalizing model of the deep structure of the region. *Figure 9* shows the scheme of the locations of the points for observation of the electromagnetic complex.

As a result of the investigation of the Earth crust, or more correctly, at its boundary with the mantle so called conductive interhorizon was marked. It also revealed the correlation between the depth of the bedding of the conductive interhorizon and 600ºC isotherm, which on the territory of Georgia varies in the depths from 35 to 55-60 km. In the 300-350 km and 800-900 km depths the conductive layers of the upper mantle was revealed. The comparison of these results with our investigations of the gravimetric field made it obvious that under the Greater Caucasus in the Bakuriani-Stepnoye and Nakhichevan-Volgograd profiles the differential section from the 50 km depth completely changes with negative values of the field. In the Sukhumi-Elbrus profile the gravimetric field is completely negative and it decreases together with the depth that might be connected with the zone of volcanic activity. In the vertical sections of the regional seismotomography under the Greater Caucasus a low speed zone up to 400 km is distinguished. There is a correlative link among magnetotelluric, gravimetric and seismologic investigations.

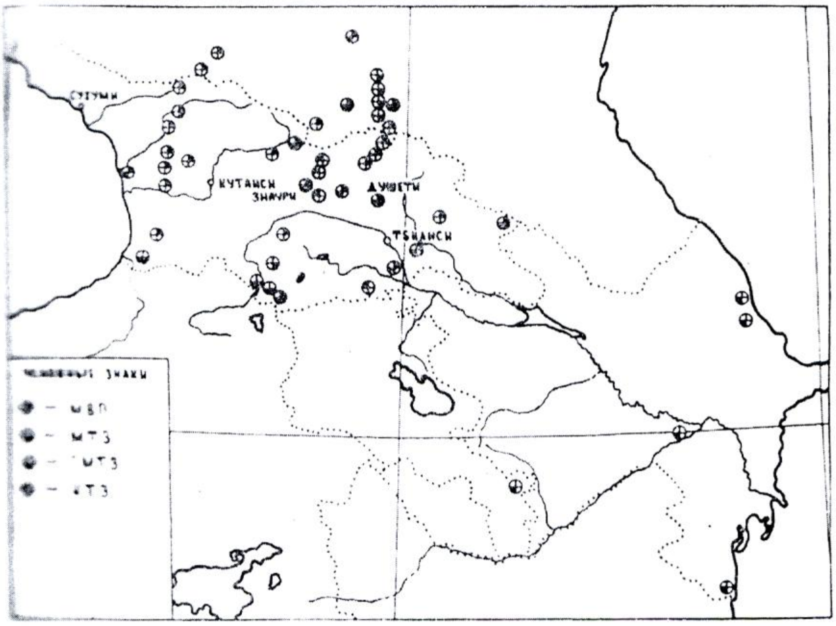

Figure 10. Scheme of the locations of the points for observation of the electromagnetic complexes (G.E. Gugunava, 1985)

Main conclusions. On the basis of the data shown in the *Figures 3, 4, 5, 6, 7* and *8* describing the results of gravimetric, seismometric DSS, MSS and the results of the inversion of the P- and S-anomalies up to the 100 km depth, despite the complex situation, it is possible to make conclusions about the interrelation between these anomalies and the geological structure of the Greater Caucasus:

The Greater Caucasus by all considered methods is distinguished with low speed and density parameters. In the seismotomography sections of the DSS and MSS profiles under the

Greater Caucasus the Moho boundary is sinking, a zone of thrust represented with fault series declining to the north-east (it is obviously seen in the DSS profiles due to the speed inhomogeneity variations) is distinguished. The conditional boundaries of the surfaces of granite (the thickness of the Bakuriani-Stepnoye profile granite is 40 km and over and the one of the Nakhichevan-Volgograd profile is up to 50 km), basalt and Moho (the cover bends up to 60 km) in the tomography images of the DSS are not continuous. All the Earth crust is disintegrated and is characterized with a block structure or zonality.

In the vertical sections of the gravimetric data and the MSS method the correlation between the speed and density parameters corresponding to the zonal division of the Greater Caucasus is seen.

A clear spatial link between the lowest values of the P and S speeds and the gravimetric anomalies in the Sokhumi-Elbrus profile is observed. It is obvious that this is connected with the areas of the Neogene-Quaternary volcanic activity.

Thus, according to the geophysical methods with the depth up to 100 km we may obtain some detailed image of the Greater Caucasus. In the DSS tomography sections a subduction process represented with the fault series of the main thrust declining to the north-eat of the Greater Caucasus is observed.

References

1. Adamaia S., Alania V., Chabukiani A., Kutelia Z., Sadradze N. Greater Caucasus (Cavcasioni): a long-lived North-Tethian back-arc basin. Turk J Earth Sci 2011; 20:611-28.
2. Balavadze B.K., Shengelaia G.Sh., Mindeli P.Sh. The gravity model of the Earth crust of the Caucasus. Monograph. The gravity model in the upper mantle of the Earth. Kiev, “Naukov Dumko”, 1979, p.p. 149-160 (in Russian).
3. Bloch Y.I. Interpretation of gravity and magnetic anomalies, 2009, p.p. 126-170 (in Russian).
4. Gamkrelidze N.P., Ghonghadze S.A., Mindeli P.Sh., Kiria J.K., Yavolovskaya O.V. Physics of the Earth crust of Georgia. Monograph. Institute of Geophysics, Tbilisi, 2012, (in Russian).
5. Gugunava G.E., Kiria J.K, and Bochorishvili T.B. Thermogeodynamic manifestations in the Caucasus and their genesis, eEarth Discuss., 4, 77-89, 2009.
6. Gorbatikov A.B., Rogozhin E.A., Stepanova M.Yy., Kharazova Yu., V., Andreeva N.V., Perederin F.V., Zaalishvili V.B., Melkov D.A., Dzeranov B.V., Dzeboyev <.A., Gabarayev A.F. Pecularities of the deep structure and modern tectonics of the Greater Caucasus in the Ossetian sector according to the complex of geophysical data, 2014. (in Russian).
7. Dolgal A.S., Sharkhimulin A.F. Gravitation tomography – practice – preceding theory? Geoinformatika, 2009. # 3, p.p. 59-64. (in Russian).
8. Strakhov V.N. Interpretational processes in Gravimetry and Magnetometry – realization of a unique approximation approach. I. The basic ideas and construction principles. Earth Physics, 2001, # 10, p.p. 3-18. (in Russian).
9. Koulakova I.Yu. A look at the processes under volcanoes through a prism of seismic tomography, A bulletin of the Russian Academy, 2013, vol. 83, # 8, p.p. 698-710. (in Russian).
10. Koulakov I., Zabelina I., Amanatashvili I., Meskhia V. Nature of orogenesis and volcanism in the Caucasus region based on results of regional tomography. Solid Earth. 2012. V. 3. P. 327-337.
11. Mindeli P.Sh. The gravity model of the lithosphere of the Caucasus and Eastern Mediterranean. Publishing house GCI, Tbilisi, 1999, p.133. (in Russian).

12. Mellors R., Jackson J., Myers Sc, Gok R, Priestly K., Yetirmishli G, et al. Deep earthquakes beneath the Northern Caucasus: evidence of active or recent subduction in western Asia. Bull Seismol Soc Am 2012; 102:862-6.
13. Mumladze Team Adam M. Forte, Eric S. Cowgill, Charles C. Trexler A. Niemi, M. Burak Yikilmaz, Louise H. Kellogg. Subducted, detached and torn slabs beneath the Greater Caucasus. GeoResJ 5 (2015) 36-46.
14. Pavlenkova G.A. The structure of the earth crust of the Caucasus according to the Stepnoye-Bakuriani and Volgograd-Nakhichevan Deep Seismic Sounding profiles (The results of reinterpretation of initial data). Earth Physics, 2012, # 5, p.p. 16-25. (in Russian).
15. Chelidze, T.; Gugunava, G.; Gamkrelidze, N.; Mindeli, P.; Kiria, J.; Ghongadze, S.; Yavolovskaya, O. The Deep Structure and 3D Thermo-geodynamics of the Caucasus by Geophysical Data. EGU General Assembly 2012, held 22-27 April, 2012 in Vienna, Austria. p.8242.

გეოფიზიკური ველების ახალი ინტერპრეტაცია დიდი კავკასიონის სიღრმული აგებულებისათვის

ს. ღონღაძე, პ. მინდელი, ჯ. ქირია, ნ. ღლონტი, ა. ესაკია

რეზიუმე

ჩატარებულია შედარებითი ანალიზი ჩვენს მიერ მიღებულ მონაცემებსა და რეგიონის ტომოგრაფიის ლოკალურ მონაცემებს შორის რომელიც მიღებულია პროგრამა ლოტოსის დამუშავებით.

მიღებულია სქემა კრისტალური ფუნდამენტის, კონრადის და მოხოროვიჩის ზედაპირების ცვლილებისა. ნაჩვენებია აგრეთვე, რომ დიდი კავკასიონი წარმოადგენს ერთიან გეოლოგიურ წარმონაქმს.

Journal of Georgian Geophysical Society,
Issue (A), Physics of Solid Earth, v.18a, 2015, pp. 59-66

Numerical modelling of groundwater system in the East Georgia's lowland

George Melikadze, Natalia Zhukova, Mariam Todadze, Sopio Vepkhvadze, Tornike Chikadze

Iv. Javakhishvili Tbilisi State University, M. Nodia Institute of Geophysics

Abstract

In order to assessment water pathway and origin, a numerical model of groundwater was elaborated for East Georgia's lowland - Alazani and Shiraki catchments. The model was calibrated in transient transport mode to tritium concentration measured in boreholes and springs located in East Georgia areas. Tritium was assigned as a single mobile species, not reacting with chemical elements and concentrated in water, what allowed determining the residence time of groundwater flow. The model estimated groundwater flow directions and velocities between recharge and discharge areas, as well as groundwater age for Alazani and Shiraki catchments.

Introduction

Eastern Georgia is the most important the agricultural area of Georgia. This territory, with semiarid climate and a big deficit of drinking water resource are crossing two large rivers Alazani and Iori. In order to reassessment water resource of this two catchments, a numerical model of groundwater layers was elaborated based on the obtain data. Modelling has been processed by special software VisualModflow Package.

Geological and Hydrogeological settings

The geological composition of the study region is complex and contains Jurassic, Cretaceous, Palaeogene, Neogene and Quaternary rocks. Most of the area belongs to the folded system of the Greater Caucasus, and a smaller part on the southeast (Garekakheti Plateau) belongs to the Transcaucasia Intermountain Area (1).

The folded system of the northern slope of the Greater Caucasus is formed by sediments of the Upper Lias up to Upper Cretaceous age. The folded system of the Kakheti Ridge, representing the southeastern branch of the folded system of the southern slope of the Greater Caucasus, is composed of sediments from Jurassic to Pliocene age (1). In turn, the northeastern and northwestern slopes of the Kakheti ridge are formed by Alazani series of Neogenic and Pleistocene continental sediments. Their maximum thickness is 2 km and the dominant components are gravels, conglomerates and sands. Gravels are typically formed by large size boulders of sandstone and limestone material. The Alazani valley between the Greater Caucasus and the Kakheti ridge is filled with Quaternary sediments and sediments of the river Alazani. It consists of sandy-gravel and clay-loam sediments, forming several water-bearing horizons down to approximately 500 m in three principal aquifers – Kvareli, Gurjaani and Telavi. The total thickness of sediments of the Alazani valley, lying on the surface of crystalline rocks, is between 2 and 4 km.

The Garekakheti Plateau is formed by tertary sediments with outcrops of Upper Jurassic rocks (Dedoplitskaro Hill). The synclines on the Shiraki Plain are filled by Quaternary sediments of the Krasnokolodski suite. They consist of argillaceous sands, conglomerates and gravels. The sands are partly gypsiferous. The largest Shiraki syncline is of considerable extension up to 50 km, and the sediments are approximately 1000 m thick (1).

The aquifers of the Alazani basin are generally abundant in artesian groundwaters due to recharge from Cretaceous and Jurassic formations of the southern slope of the Greater Caucasus and the northern slope of the Kakhetian ridge, the growing population and industrial and agricultural activities require new insights into the monitoring, assessment and development of these resources. The dynamics of the ground waters are greatly affected with the peculiar composition of Shiraki Massif, which is the component of the Iori Plateau dividing the basins of the rivers Iori and Alazani in the lower current. To the north the Shiraki Massif is distinctly divided from the Alazani valley with the eroded tectonic batter of 400m of height. Within the plain the modern relief is characterized with considerable sloping towards the axial part. Besides, bending can be observed along the axis of the syncline as well, thus, in spite of the general regional sloping in the south- east direction, the plain is contoured as a locked depression (2-3).

In conditions of the entire lack of the hydrographic network in the area the ground water supply takes place at the expense of atmospheric precipitation, which is proved by the given regime observations. Besides we suppose the possibility of some injection of the ground waters from below by the downstream waters. The horizon of the ground waters is dated for the fourth sediments and is mapped quite sharply by the given measurements of the boreholes. On the map hydroisogyps the picture of water movement from the relatively raised peripheral parts of depression towards the lower and locked central part where ground waters are closer to the ground surface is quite distinctly depicted (6m at the middle sedimentary depth of 25m) and on the whole are spent on evapotranspiration. A great width of the crumby continental layers krasnokolodski suite (Akchagil- afsheron), lain in a large syncline, is a main aquifer, and contains pressure ground waters (4-5).

Field work

More than one hundred water points (springs, boreholes, dug wells) were sampled during expedition (6). Major ions, ^{18}O, ^{2}H and ^{3}H were measured at each site. Physico-chemical parameters (Temperature, pH, DO, EC) were obtained directly in the field, by the WTW Multi 340i set. Hydrodynamical properties of aquifer rocks (hydraulic conductivity, storativity, etc), have measured, which was necessary for numerical modelling will be evaluated.

Additional monthly monitoring of ^{18}O, ^{2}H and ^{3}H in rainwaters and streamwaters was established in the study area. From the GNIP (^{18}O, ^{2}H) stations in the recharge area in Tianeti (since January 2013), the central area in Telavi (since May 2012), and the discharge area in Dedoplitskaro (since January 2013) and Lagodekhi (since July 2013). While the information on temperature, rainfall amount and air humidity at Telavi is supplied by the adjacent meteorological station, the rain samplers at Tianeti, Dedoplitskaro and Lagodekhi were complemented by air temperature and humidity sensors HOBO. New GNIR (^{18}O, ^{2}H) stations include Alazani/Shakriani (since May 2012) and Iori/Tianeti (since January 2013), both equipped with HOBO water level sensors. Available meteorological datasets and discharge data from official meteorological and hydrological stations were obtained from the office of Hydro-Meteological service of Ministry of Environment and Natural Resources Protection in Tbilisi.

Modelling

A mathematical model of groundwater hydrodynamics was elaborated for the area based on the conceptual model, which based on the provisional data (geological, geophysical, hydrogeological, hydrological, etc). Model of the aquifer have been processed by special software VisualModflowPro package.

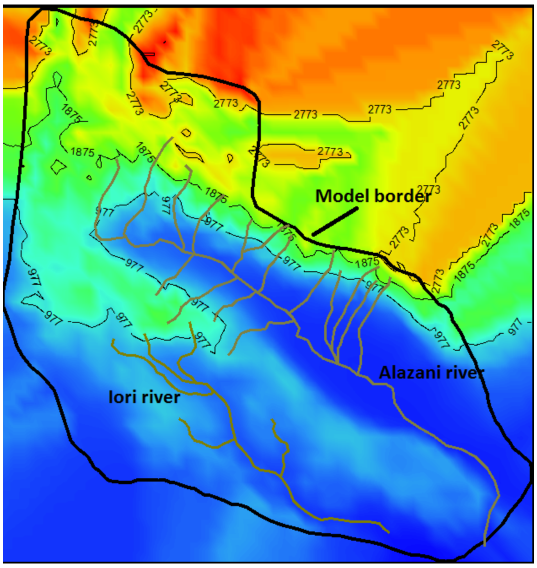

Fig.1 Model boundary

On the Fig.1 we can see the border of the area includes Iori and Alazani rivers. For creation conceptual model available geological profiles were used. On the base of these data 3D model were created. Model is rather complicated. It includes many layers (See Fig. 2).

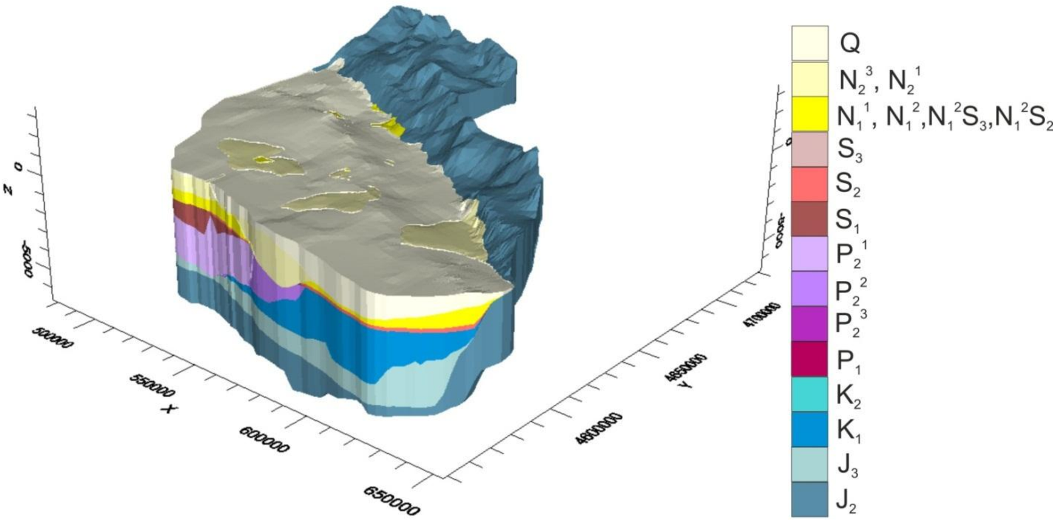

Fig. 2 Conceptual model

Conceptual and numerical model were developed in Visual Modflow Flex 2012 and Visual Modflow Classic 2011 programs. Conceptual 3D model consists of 14 layers (Q, N, J, S3, S2, S1, P21, P22, P1, K2, K1, J3, J2). Each layer represents a porous material with different infiltration properties. Data from geological profiles and maps where used to recreate layers. Upper layers (Q and N) are designed as unconfined. Each layer, as single hydro stratigraphic unit, was determined by hydraulic conductivity, specific storage, and effective porosity (Tab 1.).

Tab. 1. Hydrologic property of layers

Layers	Hydraulic conductivity (m/s)	Specific storage (m^{-1})	Effective porosity
Q	7.6042×10^{-5}	3×10^{-6}	0.05
N	1.6204×10^{-6}	5×10^{-5}	0.03
J	1.8519×10^{-6}	9×10^{-4}	0.07
S3	2.257×10^{-6}	9×10^{-4}	0.05
S2	3.8588×10^{-6}	7×10^{-4}	0.05
S1	4.653×10^{-6}	6×10^{-4}	0.05
P21	0.8557×10^{-6}	5.5×10^{-5}	0.04

P21	0.9520×10^{-6}	2×10^{-5}	0.04
P22	0.7900×10^{-6}	3.2×10^{-5}	0.05
P1	2.8471×10^{-6}	4×10^{-6}	0.06
K2	1.5824×10^{-6}	4.5×10^{-6}	0.06
J3	1.2511×10^{-6}	3×10^{-6}	0.07
J2	1.0047×10^{-6}	2×10^{-6}	0.075

Rivers were used as boundaries of the model area. They were assigned as specific flow boundary conditions (Tab. 2).

Tab. 1. Size of rivers

River	Riverbed thickness (m)	River width (m)	Riverbed conductivity (m/day)
Alazani	5	50	20
Iori	3	30	10

Visual Modflow Flex supports the standard Drain Boundary Package; we used it to simulate the boreholes under artesian conditions. 20 drain boundary conditions were added to the model. Next table shows parameters which were assigned to drains. Debit rate depends on the position of well screen.

Tab. 3 Boreholes' data

Artesian boreholes screen geology	Debit rate (L/sec)
Q	Up to 165
N	Up to 60
P	Up to 70
J	Up to 10

Conceptual model were converted to numerical one and further development. Debits rate of artesian wells where used for to calibrate model in steady-state mode. Precipitation value (800 mm/year) was assigned to upper right zone of model. Location of artesian wells marked as triangles on the Fig.3

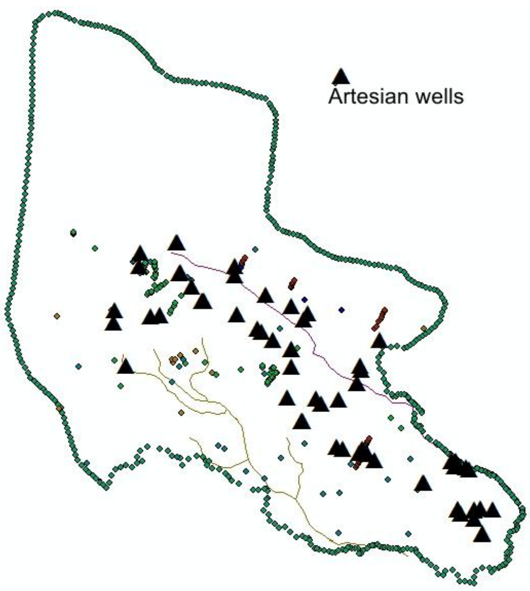

Fig. 3 Location of artesian wells.

Had calibrated water table of the study area, based on the initial heads values. Had indicated dry area in the centre of model (Fig. 4).

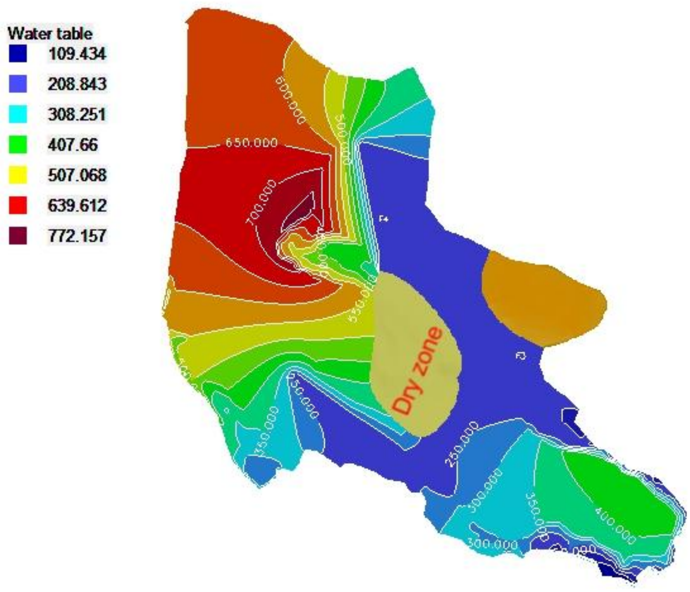

Fig. 4 Water table

In the model was fixed water level in absolute elevation on the difference layers and was simulated Flow velocities for Alazani-Shiraki area together (Fig. 4).

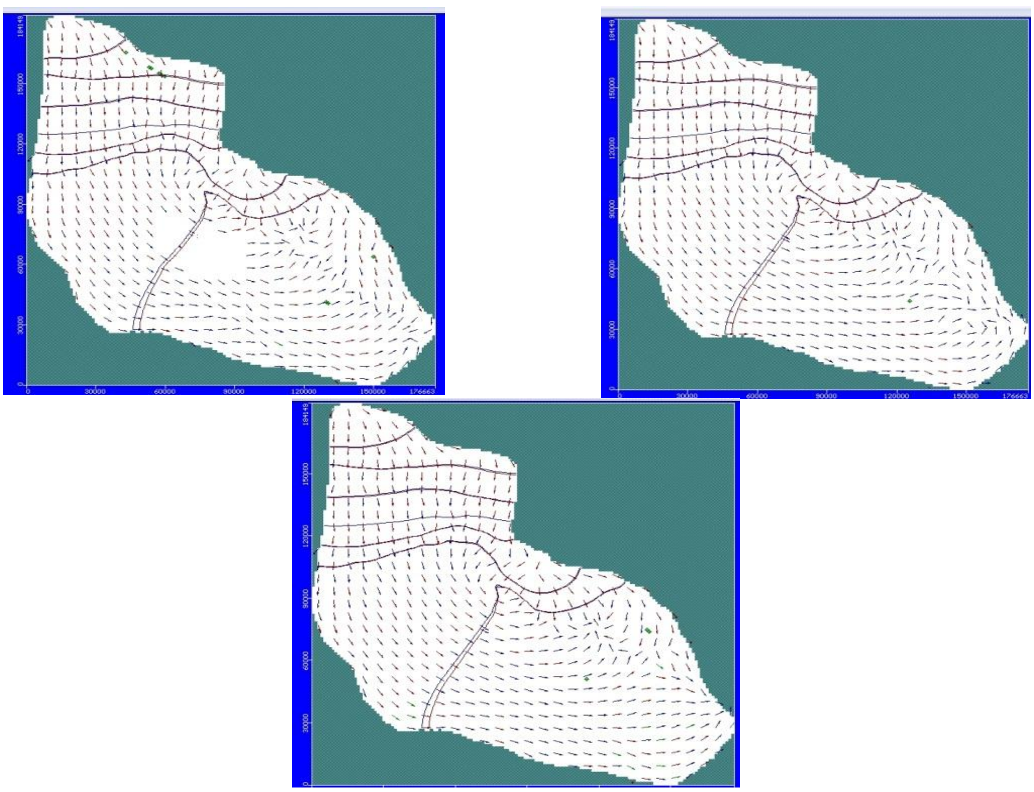

Fig. 4 Flowvelocities of a) 1st layer; b) 10nd layer; c) 20rd layer

Fig. 4 shows us flow velocities intensity and direction of simulated water system. As we can see water does not enter the system in upper horizon of central area .This part is weakly water-bearing and does not infiltrate water down. In the right zone water is discharged in the rivers. Middle horizon is recharged by groundwater flows. Intense of flow is increasing in the 10rd layer and keeps at the same stage up to 20rd layer.

In order to calculate residence time of groundwater flows was used to Particle toolbox. From the mountain area groundwater moves to the Alazani site, average water age between 2 locations is about 90 days. From the Shiraki hills water moves to Alazani wells (Kasritskali and others), water age between 2 locations is about 90 days (Fig.5). From the lower area of central Shiraki hill water moves to the right direction and archives Alazani valley during 6 months.

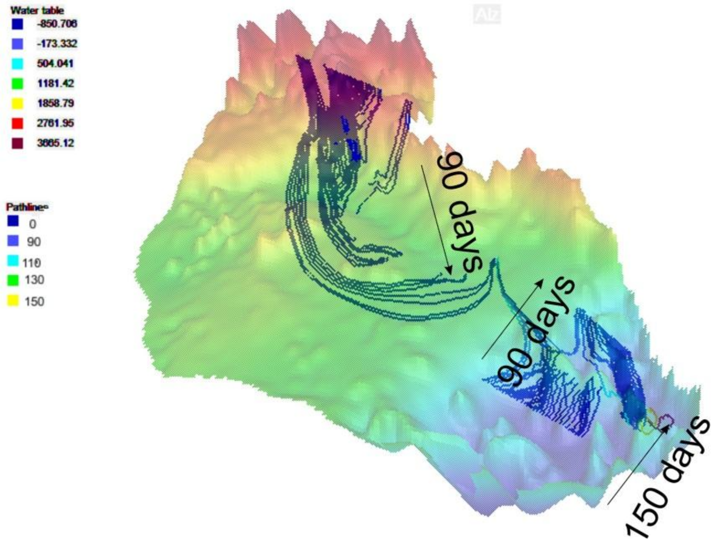

Fig. 5 Groundwater flow pathway and residence time

As we can see, zone# 2 (see Fig. 6) upper mountain area is recharged more intense than zone#3, but water discharged in general in the zone#3. Groundwater discharge of wells is rather slight compared to rivers. Furthermore, was calculating total flow budget in the model (Fig.7).

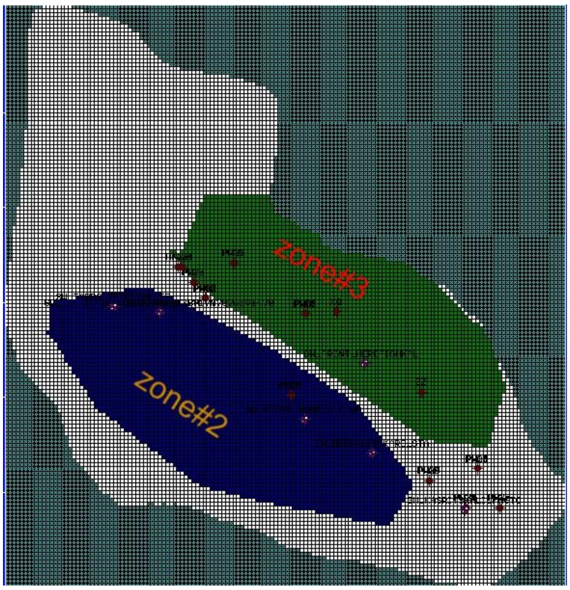

Fig. 6 Groundwater zone

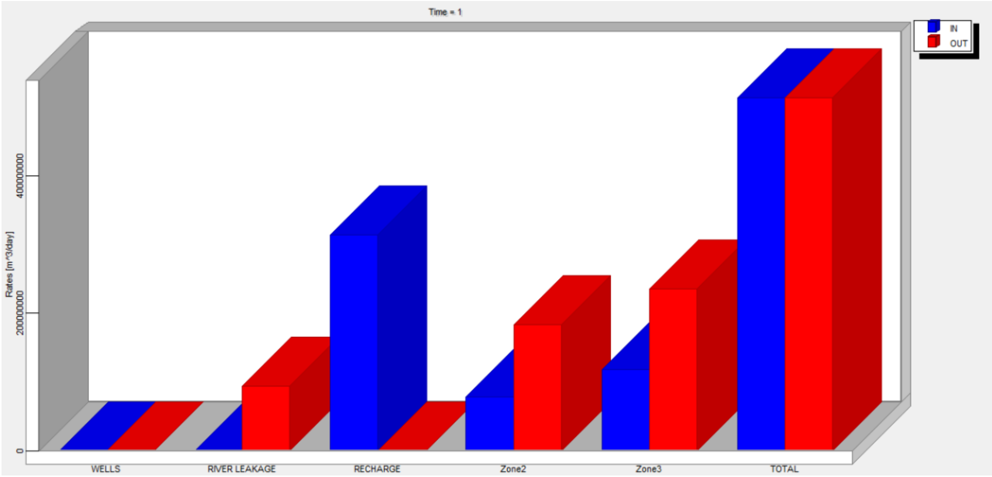

Fig. 7 Flow Budget, Blue is discharge, Red is recharge

Conclusions

Bases on the model the residence time of groundwater flows from the study areas of Alazani valley to the Shiraki area, average water age between 2 locations is about 4 months. Grounwater has confirmed the evolution in mineralization from Northwest to Southeast, with major increase in the Shiraki syncline area. Therefore, are observed changes of total mineralization in the vertical cross section of the boreholes. It is recommended to enhance the use of waters from the karstic formations such as the Kvareli and Dedoplitskaro Plain for alternative drinking water sources in the regions.

References

1. Gudjabidze, G.E. 2003. Geological Map of Georgia. Scale 1:500.000. Georgian State Department of Geology, Tbilisi.

2. Bagoshvili, G.N. (1990). Report on hydrogeological survey 1:50000 on the southern slope of the Greater Caucasus. Ministry of Geology of USSR, Tbilisi, 2 volumes, 95 and 163 pp. (unpublished, in Russian)

3. Beselia, B.N. (1988). Prelimiary survey on the appearance of groundwaters Quaternary alluvial-prolluvial confined and Upper Lurassic and Lower Cretaceous aquifers between the rivers Chelti and Durudji. Ministry of Geology of USSR, Tbilisi, 3 volumes. (unpublished, in Russian)

4. Buachidze, G. 2005. Transboundary Artesian Basin of Georgia. Presentation at the conference EURO-RIOB 2005, Namur, Belgium, 29 Sept-1 Oct 2005. http://www.riob.org/IMG/pdf/Euro-RIOB_29sept2005_Buachidze.pdf

5. Buachidze, I.M., and Zedginidze, S.N. 1985. Hydrogeology and Perspectives of Groundwater Use in the Alazani-Agrichai aquifer. Tbilisi, 335pp. (in Russian).

6. Melikadze G, at al., Preliminary result of stable isotopes monitoring in the Alazani-Iori catchment , Journal of Georgian Geophysical Society, Issue (A), Physics of Solid Earth, v.17a, 2014, pp. 39-46

Acknowledgments: The authors thank the Rustaveli National Scientific foundation for financial support of the project #31/27 “Environmental Isotopes Testing in Alazani-Iori Catchments (East Georgia) For Provision of Sustainable Use of Groundwater Resources” and Institute of UNU-FLORES in Dresden for purchased some laboratory and field equipment.

აღმოსავლეთ საქართველოს დაბლობი რაიონების მიწისქვეშა წყლის სისტემების ციფრული მოდელირება

გიორგი მელიქაძე, ნატალია ჟუკოვა, მარიამ თოდაძე, სოფიო ვეფხვაძე

თორნიკე ჭიკაძე

ივ. ჯავახიშვილის სახ. თბილისის სახელმწიფო უნივერსიტეტი, მ. ნოდიას გეოფიზიკის ინსტიტუტი

აბსტრაქტი

მიწისქვეშა წყლების გენეზისის შესწავლია მიზნით შემუშავდა საკვლევი რეგიონის ციფრული მოდელი. ის შედგება 20 ფენისგან. თითოეული ფენა შედგება სხვადასხვა გამტარებლობის ფოროვალი გარემოსაგან. მოდელში განსაზღვრული იქნა კვებისა და განტვირთვის არეალები. ასევე დაფიქსირდა წყლის გადაადგილების გზები, სიჩქარე და მიწისქვეშ მოძრაობის პერიოდი.

Journal of Georgian Geophysical Society,
Issue (A), Physics of Solid Earth, v.18a, 2015, pp. 67-74

Preliminary result of monitoring hydrological cycle in the Gudjareti catchment

George Melikadze, Natalia Zhukova, Mariam Todadze, Sophio Vephkvadze

Mikheil Nodia Institute of Geophysics of Ivane Javakhishvili Tbilisi State University

Abstract

This article summarizes the existing meteorological, hydrological and snow data in , installation of the monitoring network, collection of water samples, and snow hydrology fieldwork in the Gudjareti catchment. In the frame new project was organizing additional network in the catchment Mitarbi, provided a lot of new data on snow hydrology in the studied area that was not available before. Measurements at different altitudes were useful. Although snowfall represents just about 30% of annual precipitation, snowmelt water is an important source of water for the rivers (maximum contribution about 50%). Snowmelt affects river runoff at least 2-3 months. Yet, stable water isotopes in the snowmelt water significantly differ among the sites and they are different from those in the snow cover.

Introduction

The study area is situated in the southwestern part of Georgia, in the Little Caucasus Mountains, the Adjara-Trialeti range. The altitude ranges from about 800 m a.s.l. at the Borjomi city to about 2900 m a.s.l. at the highest mountain peaks. Mean annual mean air temperature is 8.3°C in Borjomi (altitude 794 m a.s.l.), 4.4 °C in Bakuriani (altitude 1703 m). Mean air temperatures of the warmest months (July, August) in Borjomi, Bakuriani and the slopes of the study area are 19°C, 14°C and 9-10°C, respectively. Mean air temperatures in January are 2.8, -5.5 and -9°C, respectively. The mean annual precipitation amount in the area varies from 650 to 950 mm in Bakuriani (3).

The The first hydrometeorological monitoring and sampling network in the Borjom-Bakuriani area was established through the projects of the International Atomic Energy Agency (IAEA) “Using Isotope Techniques to Assess Water Resources in Georgia” (2007-2009) and “The Role of Snow in Hydrological Cycle of the Borjomula-Gudjaretis-Tskali Rivers Basin, Georgia” (2010-2013). This network is now being used in the framework of the project "Snow resources and the early prediction of hydrological drought in mountainous streams 2013 – 2016" funded by the Swiss National Science Foundation (2014-2017). This project includes monitoring in a newly equipped small experimental catchment Mitarbi since September 2014. The main goal of this project is assessment the role of snow in the generation of low flows and a better prediction of hydrological droughts in mountainous catchments.

Sampling methodology

The sampling methodology of this study focuses on data generation that describes the altitudinal evolution of the main climatic characteristics in the study area. The following sampling and monitoring concept was set up (Fig. 1):

- Monthly composite samples of precipitation (P) are collected in Hellman raingauge at four elevations- Tsagveri, Tba, Bakuriani and Mitarbi (new station). Air temperature (T) and air humidity (H) data (hourly time interval) are measured along by the HOBO sensor. Three water level gauges (WL) were installed at the Borjomula, at the Gudjareti and Mitarbi (new station) river. The gauges are equipped with the pressure transducer HOBO diver, providing hourly measurements.

- Sampling in monthly step are carried out on the three rivers, two springs Daba and Sadgeri, and the Tba borehole, for analyses of stable isotopes ^{18}O and ^{2}H.
- Snow course measurements (Snow Depth, Snow Water Equivalent) are conducted at 5 locations (elevations), along with samples for analysis of stable isotopes ^{18}O and ^{2}H.
- Snowmelt water sampling (SC) is conducted at four locations: Tba, Bakuriani, Tsagveri and Mitarbi (extended funnel gauge, plastic and tin snow lysimeters). Passive (Frisbee) samplers are placed at three locations –Tba, Tsagveri and Bakuriani.

During the first project year, monthly trips to the catchments were performed for water and snow sampling for the stable isotopes determination, sites maintenance and data acquisition of groundwater level and meteodata.

Analyses of ^{18}O and ^{2}H were performed by the Picarro Laser Water Isotope Analyzer at the Institute of Geophysics of Ivane Javakhishvili Tbilisi State University.

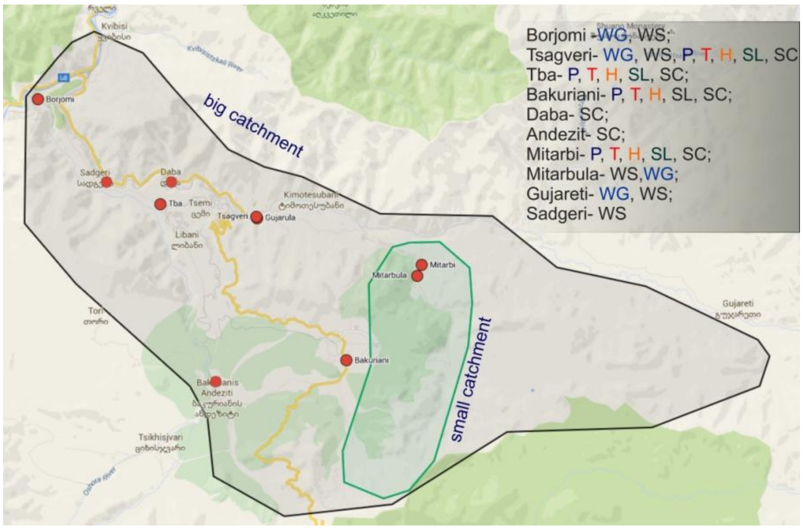

Fig. 1. Monitoring and sampling points in the studied area.

Monitoring results

During two years of monitoring, a good correlation of air temperature among three main experimental sites in the study area was observed Monitoring results show that winters of 2014 and 2015 were short.

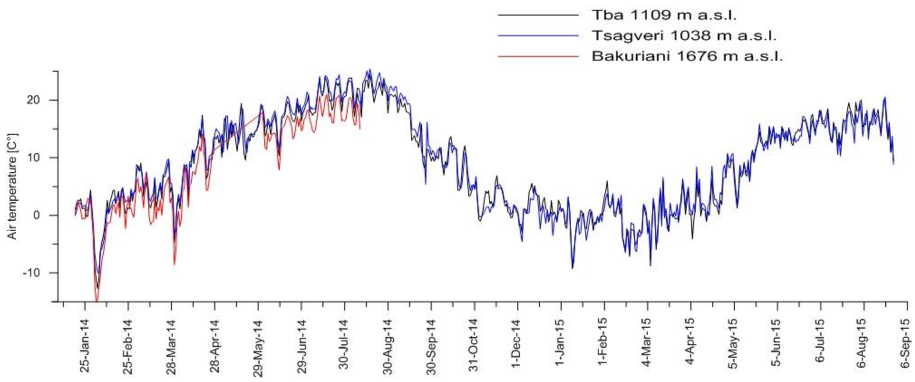

Fig.2 Air temperature monitoring data, 2014-2015.

The precipitation data for 2014 and 2015 (Fig.3) show that about 30% of annual precipitation is snow-solid.

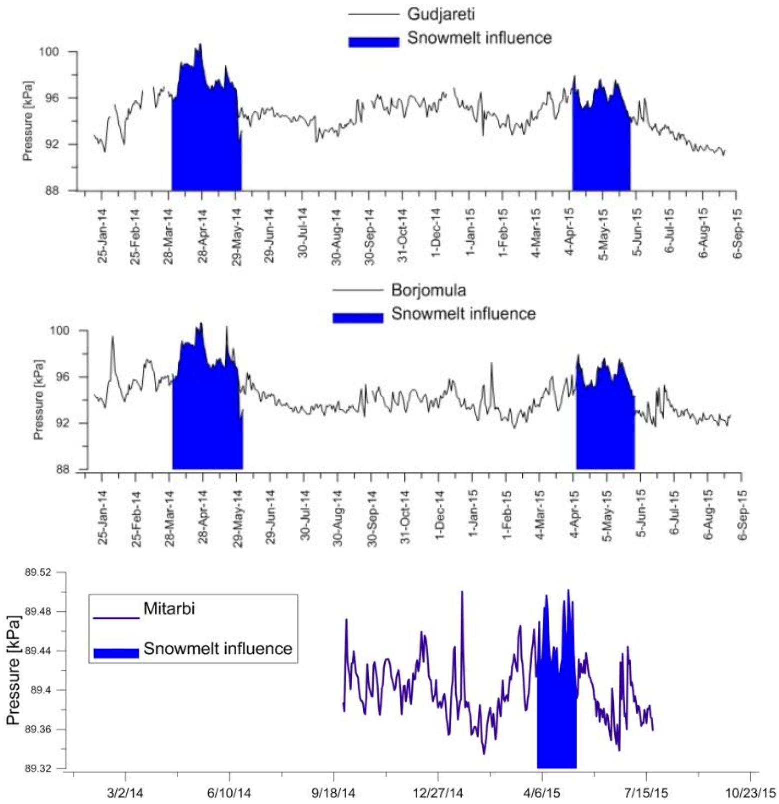

Fig. 3. River water level monitoring data 2014-2015, with indicated snowmelt periods.

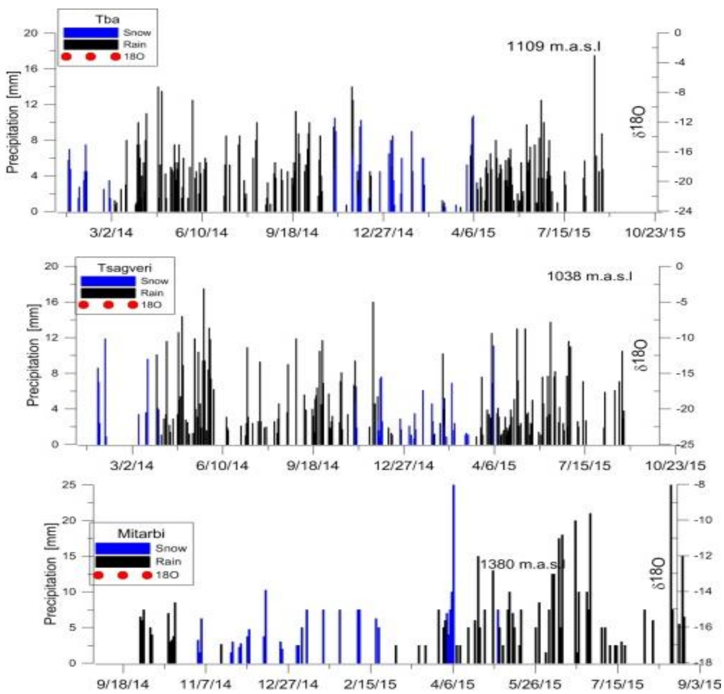

Fig. 4. Monitoring data 2014-2015, precipitation of rain and snow and its ^{18}O-content

Based on the figures 3 of river water level we can conclude that snowmelt periods for 2014 and 2015 were not long. The snowmelt period in 2014 started on February 15 and finished in the middle of March. The snowmelt period in 2015 started in the end of March and ended in April.

Fig. 4 shows that, maximum snow water equivalent (SWE) is observed in the lower part of the study area, representing about 60-80% of solid precipitation. The duration of the melting period varies between 2-3 weeks.

Fig. 5 shows the variability of ^2H in precipitation at different altitudes, rivers and groundwater. Groundwater does not differ isotopically from the rivers. It indicates that both the rivers and shallow groundwater come from the same source. As expected, the groundwater is generally isotopically heavier than river water. Snow cover during the snowmelt becomes isotopically enriched.

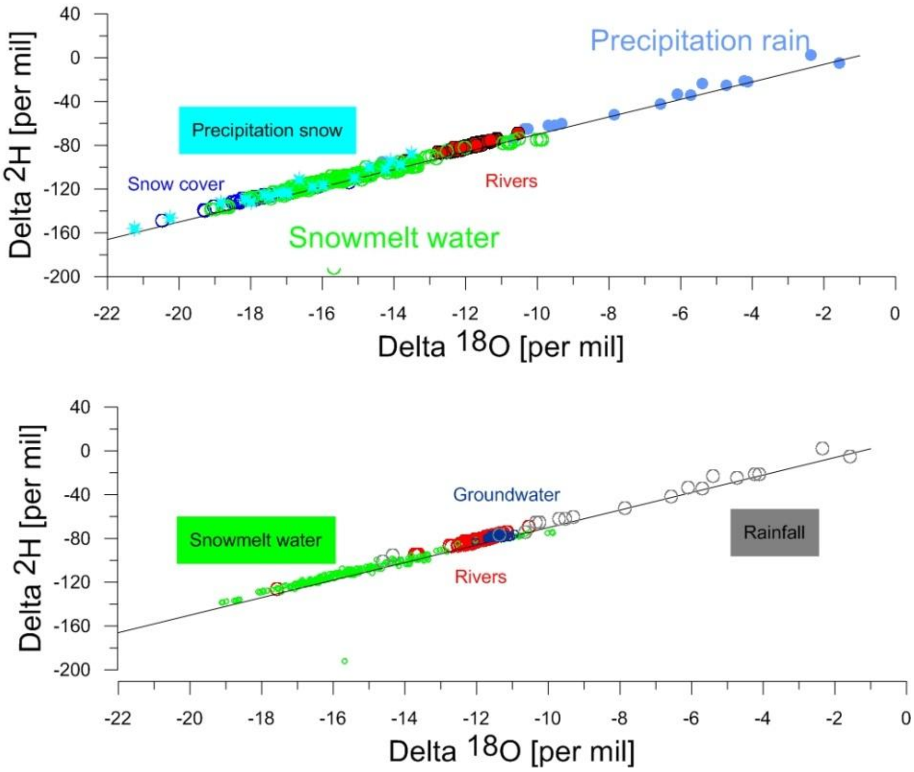

Fig 5 Isotopic composition of waters in the study area

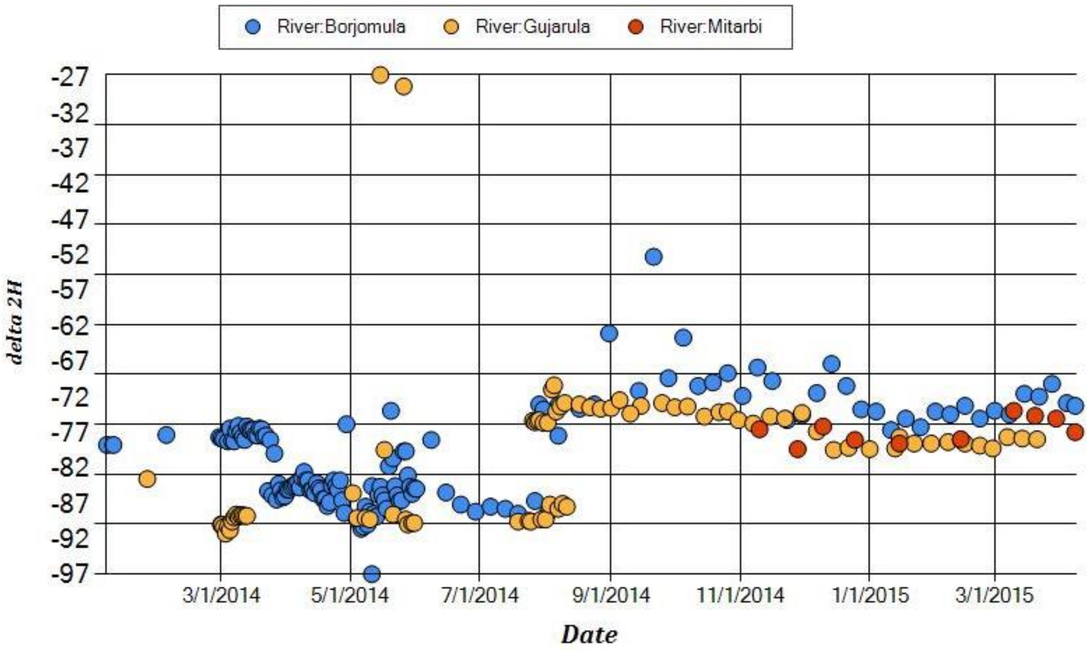

Fig. 6 Monthly ^{2}H isotopic composition of rivers in the study area, 2014-2015

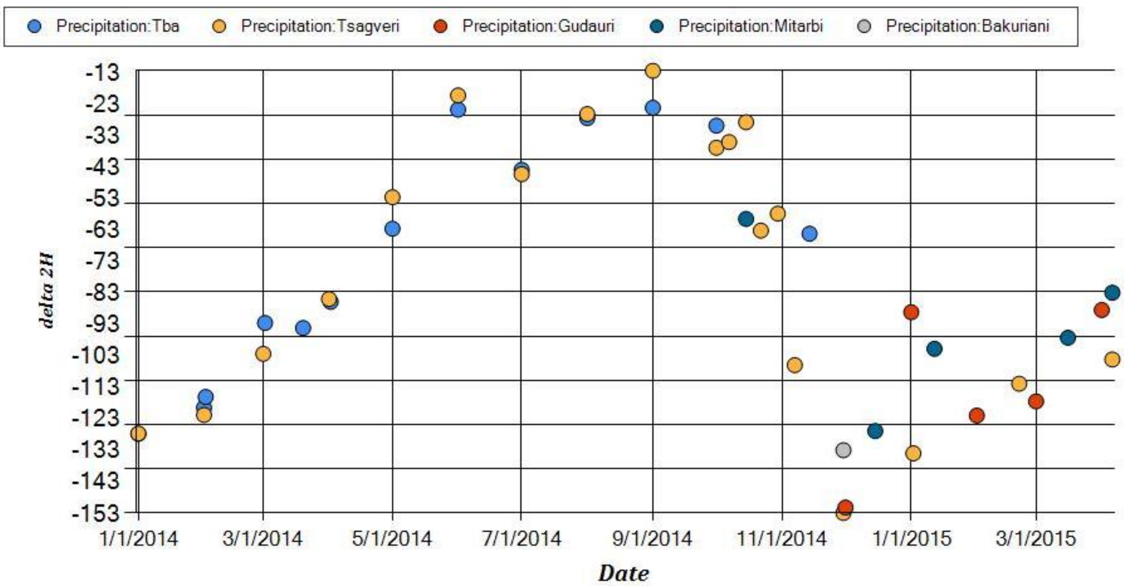

Fig. 7 Monthly ^{2}H-content in precipitation in the study area, 2014-2015

Fig. 7 reveals the typical seasonal variation of the isotopic composition of precipitation.

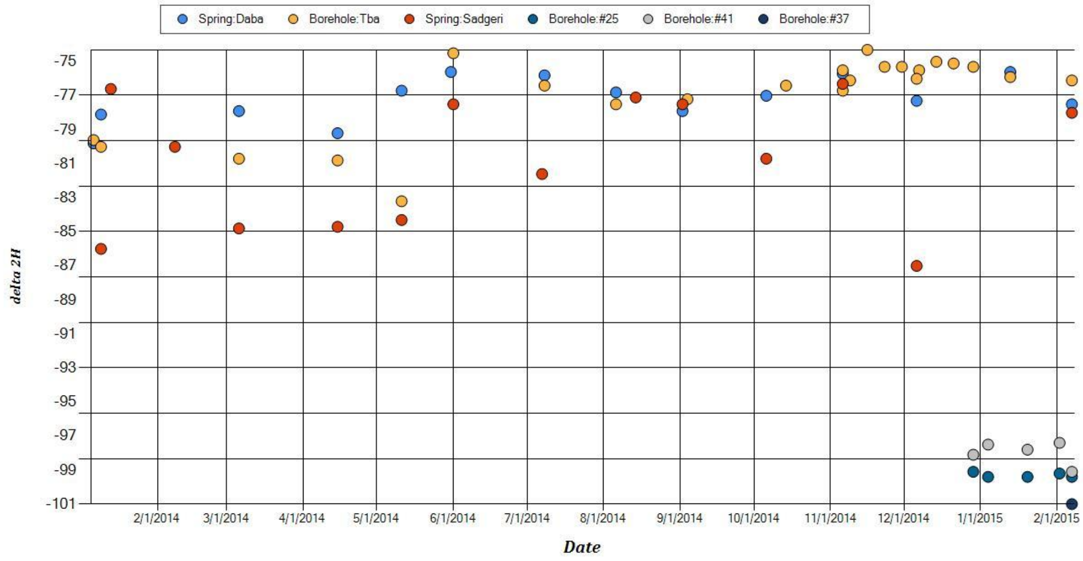

Fig.8 Monthly ^{2}H – content in groundwaterin the study area, 2014-2015.

Fig. 8 shows that the variations of isotopic composition of groundwaters Tba, Daba and Sadgeri are similar. Groundwaters in the boreholes 25, 37 and 41 are isotopically depleted, indicating old mineral (paleo) waters. This phenomenon is shown also on Fig. 9

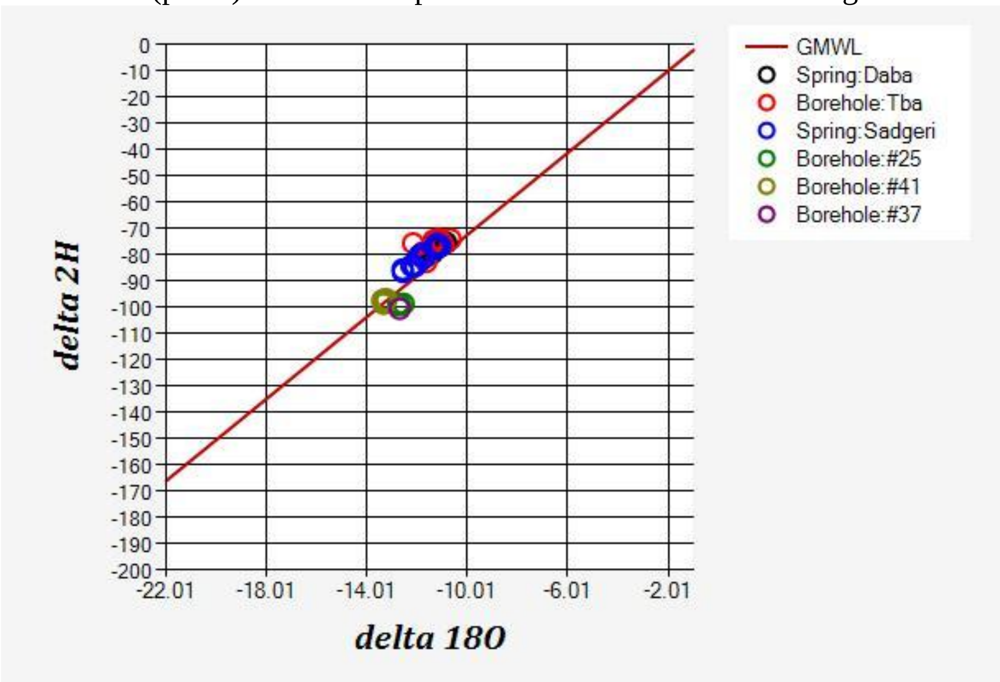

Fig. 9 Relationship ^{2}H-^{18}O in groundwaters from springs and boreholes in the study area, 2014-2015

Historical runoff data were assessed (Fig.10) in order to estimate potential evapotranspiration a better simulation of low flows and mitigation of hydrological droughts.

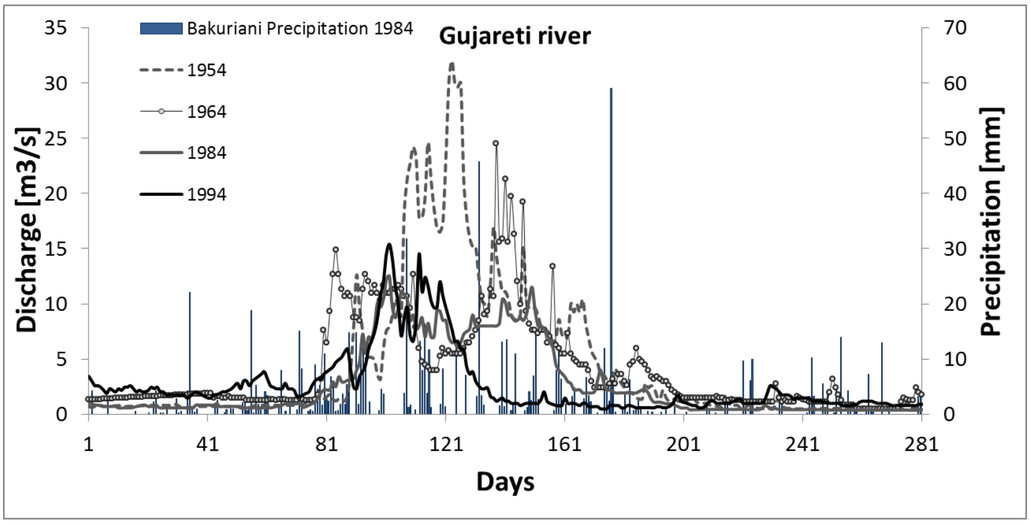

Fig. 10 Gudjareti River discharge at Tsagveri.

Peak stream flows occur in response to snowmelt and snowmelt mixed with rain. A decreasing magnitude of flow peak can be also observed on Fig.10
.

Data of 2014-2015 show that air temperatures increased approximately around the middle of March, but a more intensive snowmelt started a few days later. Water levels in the rivers increased as a response to the snowmelt and later the typical snowmelt runoff regime (diurnal variability of runoff) evolved. Isotopic composition of snowmelt water sampled at Bakuriani by means of the smaller tin and the larger plastic lysimeters were mostly similar, except the beginning of the snowmelt period.

Snowmelt water at Tsagveri (lower altitude) during more intensive snowmelt was isotopically lighter than at Tba (higher altitude, but more exposed to sunshine radiation).

River water reacted to increased snowmelt input in the middle of March, following rainfall on March 19 and continuation of snowmelt since March 26 of 2015.

Conclusions

- The moitoring network established in the project has provided a high amount of new data on snow hydrology in the studied area (solid-liquid precipitation, hourly variability of water levels in the rivers, snow cover characteristics, stable water isotopes,…).
- Although snowfall represents only about 30% of annual precipitation, snowmelt water is an important source of water for the rivers (maximum contribution about 50%).
- Snowmelt affects river runoff during at least 2-3 months.
- Snowmelt is thus important also for water availability in dry summer period.
- Stable water isotopes in the snowmelt water significantly differ among the sites and they are different from those in the snow cover.

Acknowledgments: Authors acknowledge the financial support of **the programme** SCOPES, Swiss National Science Foundation grant No: 781 "Snow resources and the early prediction of hydrological drought in mountainous streams" (2014 – 2017) and Institute of UNU-FLORES in Dresden for purchased some laboratory and field equipment.

References:

1. George I. Melikadze, Tamaz Chelidze, Natalia Jukova, Peter Malik,and Tomas Vitvar, 2011, Using Numerical Modeling for Assessment of Pollution Probability of Drinking Water

Resources in Borjomi Region (Southern Georgia),Climate Change and its Effects on Water Resources, Issues of National and Global Security (Edit Baba, A., Tayfur, G., Gunduz, O., Howard, K.W.F., Fridel, M.J., Chambel, A.), 2011, NATO Science Series. Springer. ISBN: 978-94-007-1145-7. Chapter 29, pp.267-275.
2. GEORGE I. MELIKADZE, NADEZHDA DOVGAL , NATALIA ZHUKOVA, USING NUMERICAL MODELING FOR BORJOMI-BAKURIANI DRINKING WATER RESERVOIR, Workshop materials “Exploration and exploitation of groundwater and thermal water systems in Georgia,, 124 -132, 2010, Tbilisi, GEORGIA,
3. G. Melikadze, N. Kapanadze, M. Todadze, “Assessment the role of snow in hydrological cycle of the Borjomula-Gudjareti-Tskali rivers basin”, Journal of Georgian Geophysical Society, Issue A. Physics of Solid Earth, vol. 16A 2013.
4. W. Dansgaard. Stable isotopes in precipitation. Tellus 1964, 5, 436.
5. I. D. Clark, P. Fritz. Environmental Isotopes in Hydrogeology, Lewis Publishers, New York, 1997.

გუჯარეთის მდინარის აუზში ჰიდროლოგიური ციკლის მონიტორინგის პირველადი შედეგები

გიორგი მელიქაძე, ნატალია ჟუკოვა, მარიამ თოდაძე, სოფიო ვეფხვაძე

აბსტრაქტი

სტატიაში გაანალიზირებულია არსებული მეტეოლოგიური, ჰიდროგეოლოგიური და თოვლის საფარის მონაცემები. ხორციელდებოდა ექსპედიციები წყლის და თოვლის საფარის სინჯების აღების მიზნით. ახალი პროექტის ფარგლებში დამატებით მიტარბის მდინარის აუზში ორგანიზება გაუკეთდა სამონიტორინგო ქსელს, რომლის მეშვეობითაც მოპოვებული იქნა უახლესი მასალა თოვლის ჰიდროლოგიაში, რომელიც არ არსებობდა მანამდე. სხვადასხვა სიმაღლეზე განხორციელებული გაზომვები გამოდგა წარმატებული. თოვლის ნალექმა შეადგინა მთლიანი ნალექების მოცულობის 30%. ის წარმოადგენს მდინარეების მკვებავი წყლის მნიშვნელოვან წილს (მაქსიმალური წილი 50%). თოვლის დნობის შედეგად მდინარეების წყალუხვობა გძელდება 2–3 თვე. დადგინდა, რომ თოვლის ნადნობი წყლის იზოტოპური შემადგენლობა განსხვავდება სხვადასხვა სიმაღლეზე და ასევე, განსხვავდება თოვლის საფარის იზოტოპური შემადგენლობისაგან.

Journal of Georgian Geophysical Society,
Issue (A), Physics of Solid Earth, v.18a, 2015, pp. 75-83

Methodology of detection of distribution in geodynamic field of the Earth during preparation the earthquakes

Tamar Jimsheladze, George Melikadze, Genadi Kobzev, Aleksandre Tshankvetadze, Marina Devidze, Nino Kapanadze,

Iv. Javakhishvili Tbilisi State University, M. Nodia Institute of Geophysics

Abstract

This article discusses the processing techniques of hydrodynamic observations for the purpose to study the geodynamic processes during preparation of seismic events that includes in itself both the complex field observation and cameral data processing using specialized software package.

Introduction

The Regime network of hydrodynamic observations in Georgia currently is presented by 15 observation boreholes. They were selected among many boreholes as the sensitive to the geodynamic stress ones. The criterion of sensitivity was their ability to capture the Sun-lunar tidal and atmospheric pressure variations as well as their location characterizing the main geological units.

Field observation methodology

Field observations include a real-time monitoring of groundwater level and atmospheric pressure. To conduct qualitative observations the equipment which provides measurements with a predetermined frequency and data transmission upon request is used. We use the data logger XR-5 produced in USA, which has 8 analog and two pulse ports. There are selected the appropriate water level, atmospheric pressure and temperature sensors. The data are registered with a frequency of once per minute. Using GSM communication systems data is transferred from the data logger located at the observation point.

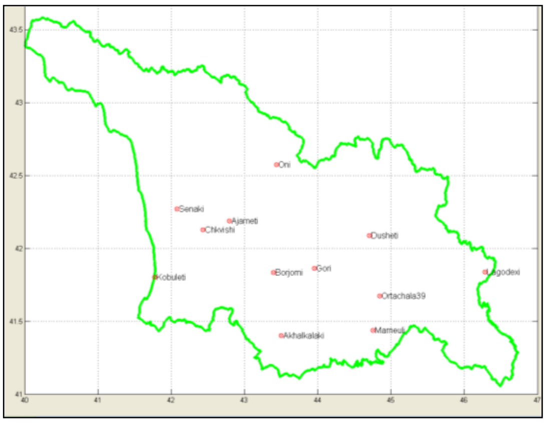

Figure 1. Location of hydrodynamic regime boreholes on the territory of Georgia

Data analyze

Water level variations as a multiple value includes both the influence of exogenous (tidal variations, atmospheric pressure and precipitation) and endogenous (earthquake, seismic movements) factors (1-6). Therefore, when analyzing the data of water level should be taken into account all influencing factors of Earth stress and accuracy of measuring devices and others.

In calculating the actual deformation quantities reaching borehole after the earthquake, the Dobrovolsky's (7) equation is used:

$$e=10^{1,3M-8,19}/R^3 \; ; \; R=\sqrt{(x^2+y^2+h^2)} \;, \qquad (1)$$

Where x and y – are earthquake coordinate, h and M – depth and magnitude respectively.

Let us assume that the water level variation in the borehole *water level* can be represented as a linear equation:

$$water\_level(x)=a*tidal(x)+b*atmosphere(x)+c. \qquad (2)$$

To find three unknown coefficients (a, b, c), included in the linear equation we must compose and solve a system with three equations (three or more equations). In order to compose one such equation is enough to have the measured values for *water level* and *atmosphere*. The Values of tidal variations are calculable- generated by a separate program. We can assume that these coefficients (a, b, c) are valid only for a limited period of time.

For the observation data processing by us was composed the computer program "StationsMany". The program is written in the medium of MatLab (authors of the program G. Kobzev and G. Melikadze). To generate the tidal variations is used program GRAV (8).

The program "StationsMany" is designed to study the behavior of water level in one or more boreholes, it is possible to analyze the reaction of water during earthquakes and to help with search for earthquake precursors. The program allows visualizing water level variations, atmospheric pressure, tidal-variation. It also allows finding unknown coefficients (a, b, c) of the equation (2) for any chosen time interval.

In the mentioned program is given the possibility to upload earthquake data, to conduct a selection among them by the number of parameters: the magnitude, the distance from the borehole, the energy which came from the earthquake to the borehole. It is also possible to choose an earthquake area.

The program creates an exogenous theoretical signal and compares it with the actual signal. Comparison allows you to characterize each exogenous (atmospheric pressure, tidal variation) parameters separately. This allows studying the effect of each on the level of water in the aquifer.

Water level variations that are caused by changes in atmospheric pressure and tides of the earth's crust are considered as "background" values. They change their form during earthquake preparation.

We have also developed the second method of studying the behavior of water level - with the help of "velocity". The proposed concept of "velocity" removes the seasonal trend of water level, which is usually presented when measuring the water level variations in boreholes and create a number of problems in the processing of data. The "velocity" of groundwater level change is determined by the equation for the difference of water levels in two points of time:

$$Speed(\mathrm{m+i})=(water(\mathrm{m+i})-water(\mathrm{i}))/\mathrm{m}, \quad \mathrm{i}=1,2,3,\ldots \qquad (3)$$

Where m - fixed number of minutes, for example, m = 180 minutes.

And finally, the third technique displayed in the program is «RestDance», which allows fixating violations in the geodynamic regime calculating the difference in amplitudes of the variations in water level and tidal variations, as well as the time shift between extremums of these variations.

In the study of the groundwater regime in observation wells we have been focused on the period of preparation for earthquakes, as well as post-seismic stress.

Results

To demonstrate the technique of data analysis, we consider the change of parameters during earthquake preparation period.

In seismically quiet period the water level variations are caused only by the external factors, but in the earthquake preparation process we observe the changes in the nature of variations. During this period, there are irregularities in the changing of "background running" water level before and after the earthquake.

We studied the earthquake, which occurred on the territory of Azerbaijan May 26, 2015, 1:20, magnitude 4.6, and its impact on the borehole Ajameti located at a distance of 360 km from the epicenter of the earthquake, and also the earthquake in Georgia July 27, 2015, 6:58, magnitude 4.1, and its impact on the borehole Marneuli located at a distance of 75 km from the epicenter of an earthquake.

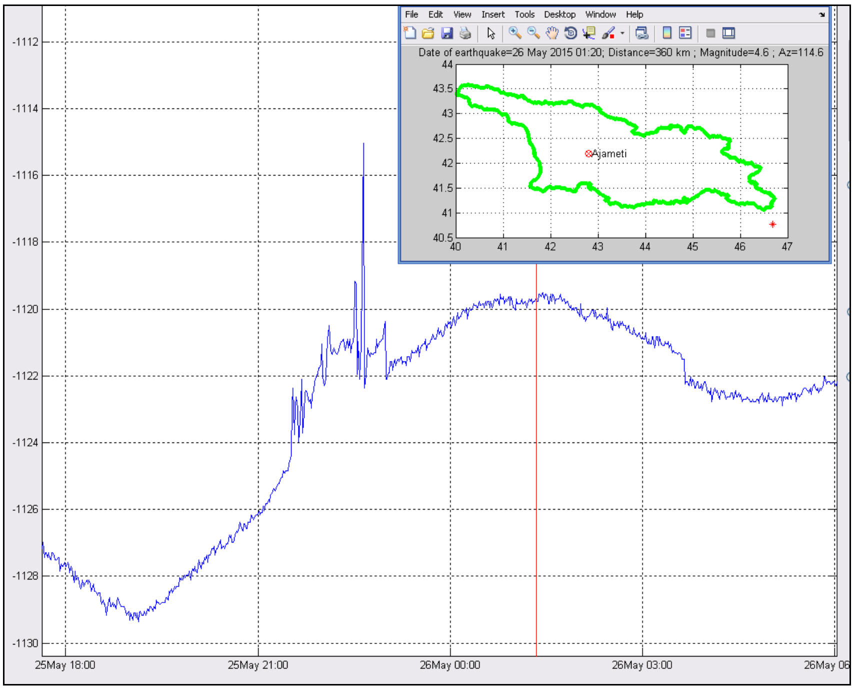

Fig. 2. Water level variation in the borehole “Ajameti”. The vertical line indicates the time of the earthquake: 26 May 2015, 1:20, 4.6 magnitude, 360 km away. On the abscissa - the date in hours.

On the Fig. 2 at the upper right corner is shown the location of the borehole “Ajameti” (circle) and the epicenter of the earthquake (the star, the lower right corner).

On The graph of the water level can be seen significant violations that took place in the borehole before the earthquake. They had being continued on May 25 from 21:30 to 23:00 on the amplitude of up to 3 cm. The earthquake occurred on May 26, 2015, 1:20. Anomaly appeared 3 hours 50 minutes before the earthquake, and lasted for 1 hour 30 minutes). Next May 26 at 3:40 there was a drop in water level about 1 cm. After was observed the normalization of the behavior of the water level.

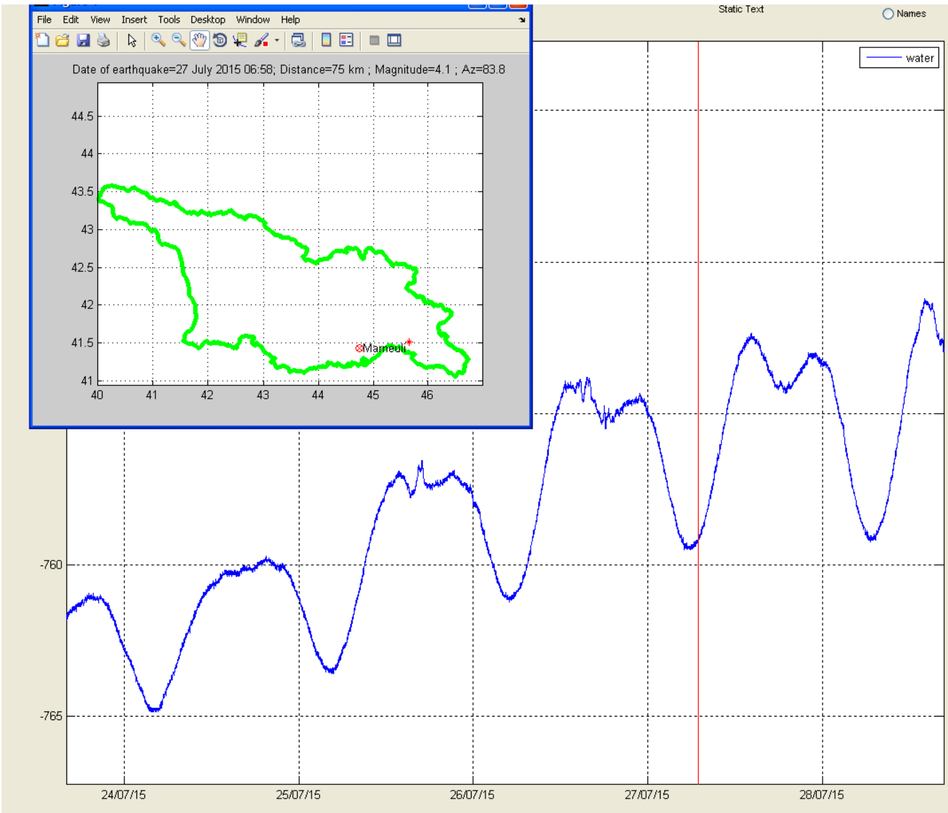

Fig. 3 Water level variations in the station "Marneuli" (in cm). The vertical line marks earthquake July 27, 2015, 6:58, 4.1 magnitude, 75 km away.

Fig. 3 shows the location of the borehole "Marneuli" (circle) and the epicenter (star to the East). Now let us have a look at the changes in water level, using the method of velocity, ie, comparing the velocity of change of water and tidal-variations.

There are marked two lines on the figure: the line of the water level variation velocity and the line of tidal-variations velocity. It is noticeable that the graph of velocity of tidal-variation has a "smooth" look as tidal variations are theoretically -generated by program GRAV.

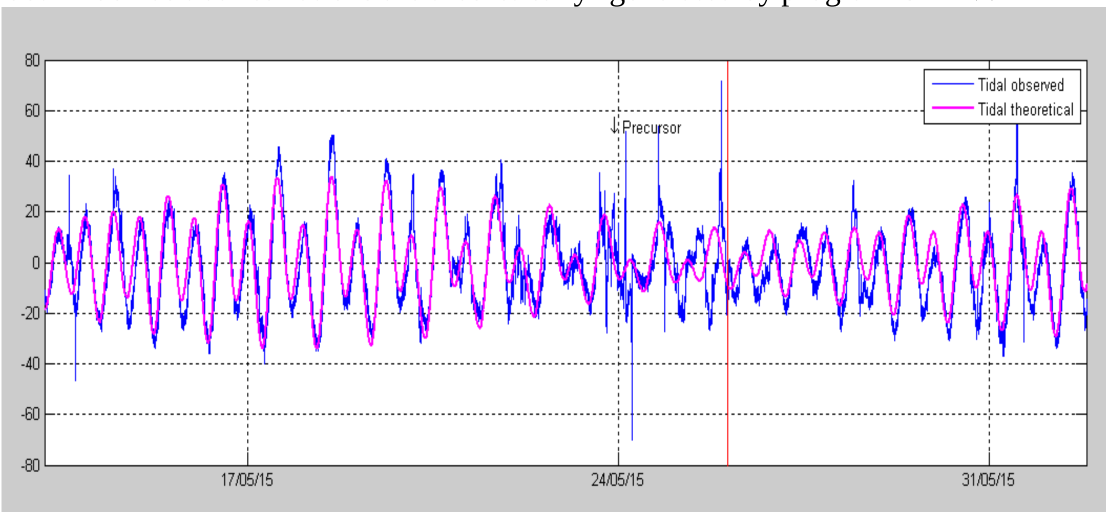

Fig. 4 The velocity of change in water level and tidal (tidal, smooth line). According to the data of borehole Ajameti

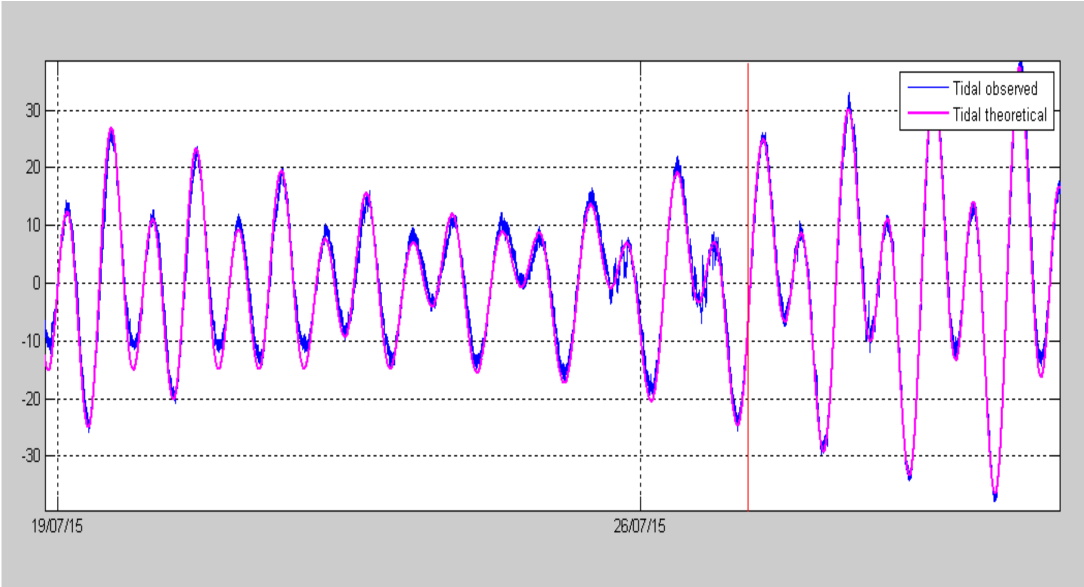

Fig. 5 Velocity of changes in water level and tidal (tidal, smooth line).
According to the data from borehole Marneuli

Figure 4 and 5 can distinguish three plots. At the first station, there is a good match between these velocity lines. In the second section, there is a marked discrepancy between these lines, which becomes significant before the earthquake. After a few days again, there is a good match between the lines.

We also observe the violations on the plots of apmlitude differences and quotients:
We can compare the water level and tidal amplitude variations using program «RestDance». Under the amplitude variation we will assume the following: On the graph of tidal variation we find the point t_0, in which the daily absolute maximum and minimum is reached.

Fig. 6 . Graph of the water level with marked points where were reached the minimum and the maximum of tidal according to the data in borehole “Ajameti”

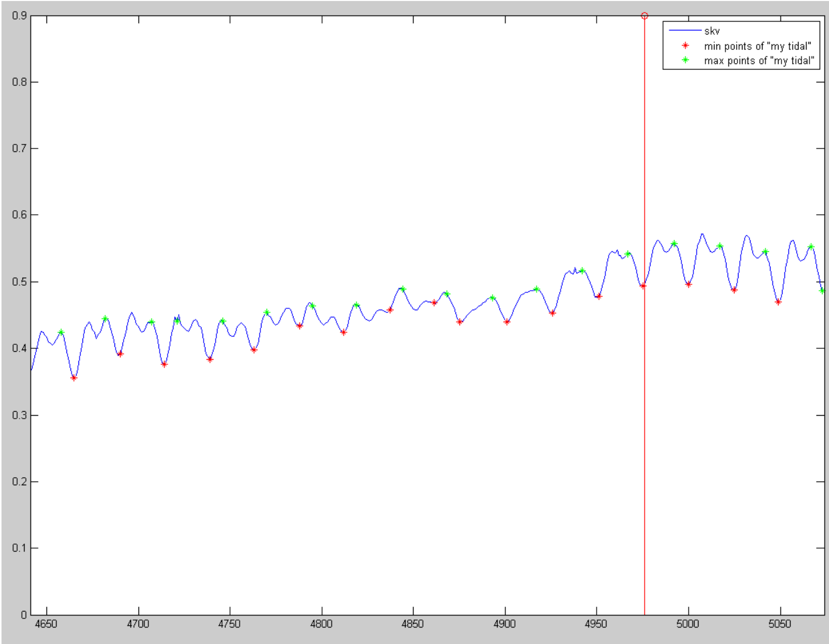

Fig. 7. Graph of the water level (hourly data) with points where were reached the minimum and the maximum of tidal data for borehole Marneuli.

Next, we find the first point (time)) t_1>t_0 , when the tidal reaches the greatest value. Tidal amplitude at t_0 is AT=tidal(t_1)- tidal(t_0). For water level amplitude will be AW=water(t_1)-water(t_0). The figure above shows the results of dividing the amplitudes of water AW / AT. The figure below shows the results of subtracting the amplitude AW-AT.

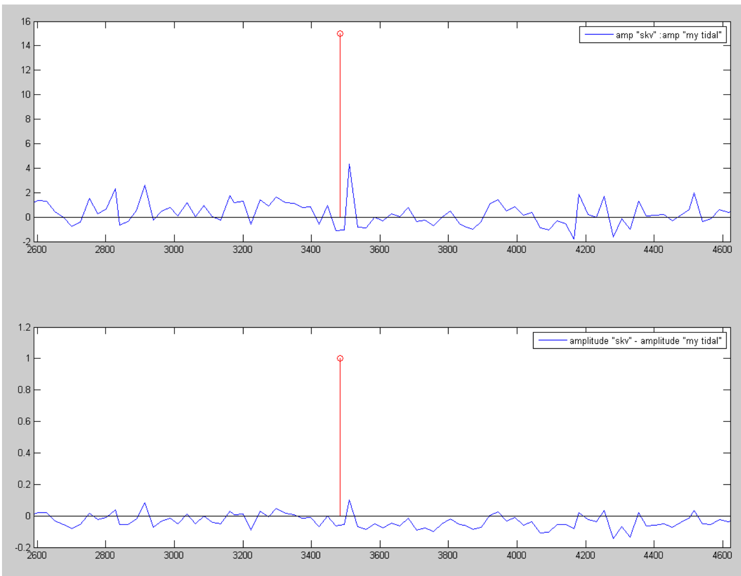

Fig. 8 Upper Graph AW / AT: amplitude of water divided by the amplitude of the tidal.

The lower figure Graph AW-AT: the amplitude of water minus the amplitude of tidal according to the data from "Ajameti" well

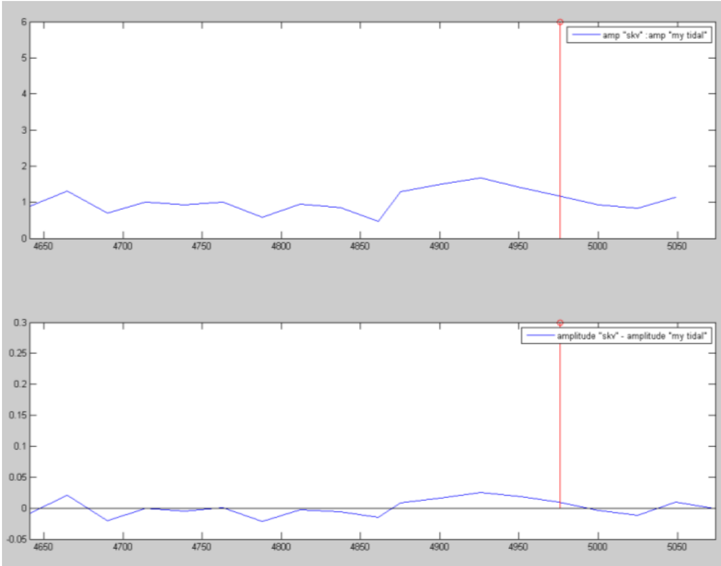

Fig. 9 Upper Graph AW / AT: amplitude of water divided by the amplitude of the tidal. The lower figure Graph AW-AT: the amplitude of water minus the amplitude of tidal according to the data from "Marneuli" borehole

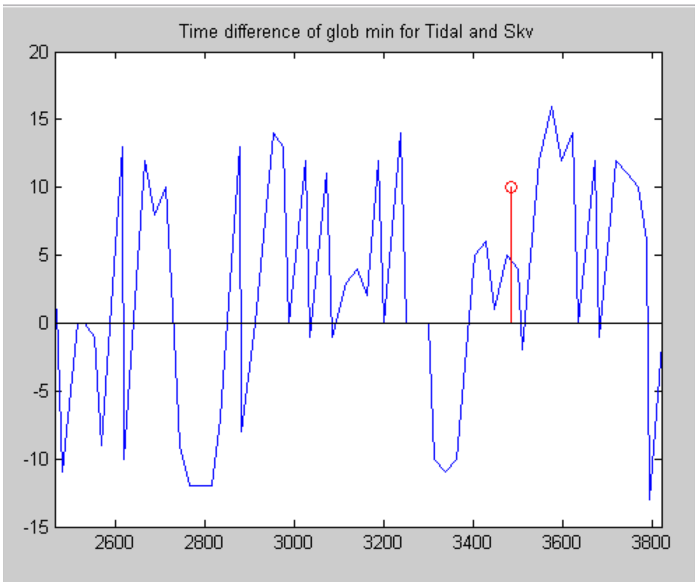

Fig. 10 The response to the earthquake of May 26, 2015, Mag. 4.6 (Azerbaijan); "Ajameti" borehole

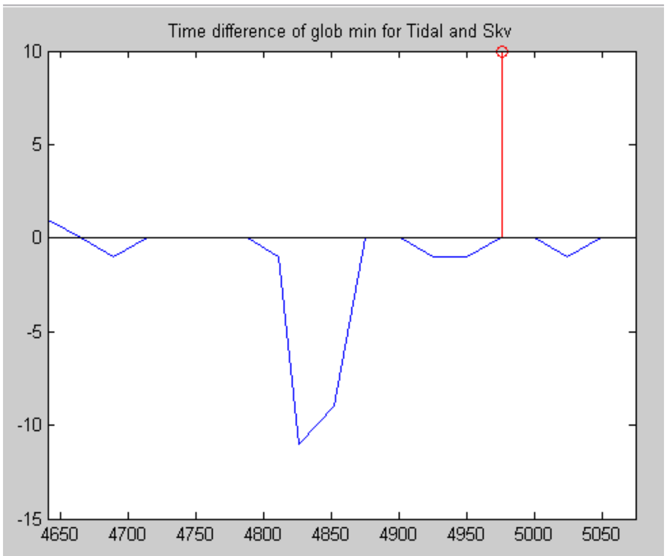

Fig. 11 The response to the earthquake of July 27, 2015, Mag. 4.1 (Georgia); "Marneuli" borehole

Conclusion

Has been developed the methods of detection of underground water geodynamic anomalies related to the seismic activity. For the same period of time all three methods detected abnormal changes which proves the suitability and the credibility of the methods.

Acknowledgments: The authors thank the Rustaveli National Scientific foundation for financial support of the project #156/13 "Spatial and Temporal Variability of Geodynamical Field and Its Influence on the Deep Aquifers and Geomagnetic Field".

References

1. Bella, Biagi P., Melikadze G. et al. - Anomalies in geophysical and geochemical parameters revealed on the occasion of the Paravani (M=5.6) and Spitak (M=6.9) earthquakes (Caucasus). Amsterdam, Tectonophysics 202 Elsevier Science Publishers B. V.,1992, p.p. 23-41

2. P. A. Hsieh, I. D. Bredehoeft, I. M. Farr. Determination of Aquifer Transmissivity from Earth Tide Analysis. Water resources research. vol. 23. 10. 1987, p.p. 1824-1832.

3. P. A. Hsieh, I. D. Bredehoeft, S. A. Rojstaczer. Response of Well-Aquifer Systems to Earth Ties: Problems Revisited. Water resources Research vol. 24. No. 3. 1988, p.p. 468-472.

4. Melikadze G., Popov E. A technique of Hydro-geological supervision with the purposes of the forecast earthquake on territory of Georgia. A series geology «Gruziinti» N7, 1989.

5. Melikadze G., Adamchuk Y, Todadze M Search informational harbingers of earthquakes on the territory Georgia. A series Geology «Gruziinti» N10, P., 1989

6. Melikadze G., Matcharashvili T., Chelidze T., Ghlonti E. Earthquake related disturbance in stationarity of water level variation. Bulletin of the Academy of sciences of the Georgian, 165 № 1, 2002

7. Dobrovolsky et al., Добровольский И.П., Зубков С.И., Мячкин В.И. Об оценке размеров зоны проявления предвестников землетрясений. - В сб.: Моделирование предвестников землетрясений. - М.: Наука, 1979

8. Rojstaczer S. Intermediate period response of water wells to crustal strain: Sensitivity and noise level, J. Geophys. Res., 93, 13,387-12,402. 1988.

მიწისძვრის მომზადების პერიოდში დედამიწის გეოდინამიურ ველში დარღვევების გამოვლენის მეთოდიკა

გიორგი მელიქაძე, თამარ ჯიმშელაძე, გენადი კობზევი, ალექსანდრე ჩანკვეტაძე, მარინა დევიძე, ნინო კაპანაძე

ივ. ჯავახიშვილის სახ. თბილისის სახელმწიფო უნივერსიტეტი, მ. ნოდიას გეოფიზიკის ინსტიტუტი

აბსტრაქტი

სტატიაში განხილულია ჰიდროდინამიური დაკვირვებების შედეგების დამუშავების მეთოდიკა სეისმური მოვლენის მომზადების პერიოდში ჰიდროდინამიური პროცესების შესწავლის მიზნით, რაც გულისხმობს როგორც კომპლექსურ საველე დაკვიევებებს, ასევე მონაცემთა კამერალურ დამუშავებას სპეციალური კომპიუტერული პროგრამების პაკეტის საშუალებით.

Journal of Georgian Geophysical Society,
Issue (A), Physics of Solid Earth, v.18a, 2015, pp. 84-89

RADIOGENIC COMPONENT THERMAL FIELD OF THE CAUCASIAN REGION

E. Sakvarelidze[1], I. Amanatashvili[2], G.Kutelia[3], V. Meskhia[4]

1 *Head of Laboratory of Geophysics, Ivane Javakhishvili Tbilisi State University, Chavchavadze av., 1, Georgia, Tbilisi.*
2 Professor, Georgian Technical University, Kostava St.,77 , Georgia, Tbilisi
3Professor, Ivane Javakhishvili Tbilisi State University, Chavchavadze av., 1, Georgia, Tbilisi.
4 Professor, Ilia State University, Kakutsa Cholokashvili St., 3/5, Georgia, Tbilisi.

Abstract

Results of research thermal field of the Caucasus are given in this work. ***Radiogenic component of the heat flow was calculated*** *for all studied territory. Values of mantle components of heat flows for folded systems, for intermountain depression (the Georgian block) and for the Black and Caspian seas are estimated. Deep temperatures at the bottom of a sedimentary complex, Conrad and Moho borders. Maps of distribution of a heat flows and deep temperatures are. created.*

The research of thermal model of the Earth represents the big interest because the internal heat of the Earth plays the basic role in the history of its development, define its tectonic, seismic and volcanic activity. The physical state of matter in the Earth substantially depends on the temperature. The internal heat of the Earth has significant influence on other physical fields - electric, magnetic, thermal, a seismic velocity field and others and also plays the important role in processes of rock formation and minerals' deposits, and in particular oil and gas deposits. The main problems in the study of the thermal regime of the earth are to determinate the geothermal flow, the geothermal gradient and the calculation of deep temperatures. The heat flow carries the information about the processes occurring in the depths associated with the release of the energy or absorption. Unfortunately, the experimental data on the heat flow is very small, because these measurements are mainly carried out in the existing wells, the number of which is not enough to create an accurate picture of the flow distribution across the surface of the Earth. There is a lack of data, especially for the seas and oceans. We decided to fill up this lack of data on the heat flow with theoretical calculations of the flows for the considered region. We understand that the data obtained in this way give the average picture of the distribution of the flows, excluding their anomalous values.

Influence of tectonic processes on a thermal field is shown up doubly. On the one hand, at the same time with strengthening of tectonic activity changes the structure of a lithosphere, therefore there is a redistribution of sources of heat and change of processes of transfer of heat , distribution of temperatures and heat flows, that leads to emergence of zones of the raised and lowered flows. On the other hand, during the periods of tectonic activity from a subsoil arrives additional thermal energy, that leads to increase in crust of temperatures and heat flows. Connection between a thermal state and dynamic of a subsoil is shown first of all in compliance of zones of the maximum tectonic activity and zones of tension of crust and also zones of the increased values heat flows and vigorous magmatic activity. Owing to uneven distribution of heat flows and deep temperatures in Earth there are horizontal temperature gradients therefore thermoelastic tension is created. After achievement of limit values of this tension there can be a gap and an earthquake. Therefore one of the main objectives of an assessment of seismic danger of seismic active regions is studying of a thermal field of the region and allocation of its abnormal zones. Identification of temperature anomalies in the crust can serve as a proof of the presence of thermal stresses, which should be considered in the future when assessing the seismic activity of the region.

In the presented work the results of studying of a heat flow distribution and calculations of temperatures of the Crust of the tectonically and seismic active Caucasian region are given. The distribution of a heat flow is made on the basis of the experimental data and also on the basis of the calculated flow values.

Temperature calculation was performed by solving the heat equation. Study region was covered with equal-step grid and in its node bedding depths of boundary surfaces are known. The temperature calculations were performed at the nodes of the lattice at the bottom of the sedimentary complex, and at the border of Conrad and Moho. The calculations take into account the dependence of the coefficient of thermal conductivity of rocks on temperature.

The calculation of deep temperatures in the crust associated with the availability of data on the heat flows in places temperature calculation. Experimental data about heat flows are insufficient for calculation of temperatures in all considered region. We have carried out calculations of the heat flow in the Caucasian region for definition of deep temperatures in the given work. The geothermal flow represents the sum of mantle and radiogenic components, it is distributed unevenly across all studied territory. Local anomalies are created by following factors: presence of rocks and ores of the raised radioactivity, exothermic and endothermic processes in oil-and-gas bearing horizons, a coal deposit, modern volcanism and tectonic movements, circulation of the underground waters, different sizes of the heat conductivity of rocks.

The calculations of a mantle component of radiogenic heat flow were performed on the basis of a deep structure of the investigated region. We used block parameterization with sloped dividing boundary surfaces. Bedding depth of boundary surfaces at any point is computed by linear interpolation of quantities which exits at surrounding grid nodes. We consider the following three-layer medium as the initial model of the Earth crust structure: I – sedimentary, II- granite, III- basalt layers [1] and cover the investigated region with an equal-step grid and its node bedding depths of boundary surfaces are known. In contrast to flat-parallel medium, in our case boundary surfaces are inclined, which reflects real medium comparatively precisely. If we express the initial model of medium structure in geographical information systems (GIS, Arc Viev) as tomograms, we'll receive such picture (Fig.1).

The average value of radiogenic thermal emission (radiogenic heat sources density) for a sedimentary layer have been taken equal to 1,25 μWt/m^3, for a granite layer 1,6 μWt/m^3, and for basalt – 0,4 μWt/m^3. Radiogenic component of the flow was calculated by the formula:

$$Q_1 = A_1H_1 + A_2H_2 + A_3H_3\,, \quad (1)$$

where A_1, A_2 и A_3 - radiogenic heat source density for a sedimentary layer, for a granite layer and for basalt respectively; H_1, H_2 and H_3 – thicknesses of the layers.

The estimation of mantle component a heat flow $\mathbf{q_m}$ for the main structures of the Caucasus is carried out ($\mathbf{q_m}$= q- Q_1, where - heat flow). The average size of a mantle component of geothermal flow by our calculations is equal to: for the Black Sea 20 mWt/m^2, for folded systems 25 mWt/m^2, for intermountain depression (the Georgian block) 15 mWt/m^2, for the Caspian Sea 15 mWt/m^2.The temperature distribution in the Crust was obtained by solving three-layered model of the stationary heat equation

$$\frac{d}{dz}\{\Lambda_i(T_i)\frac{dT_i}{dz}\} = -A_i, \quad (2)$$

where Λ_i -thermal conductivity, A_i - radiogenic heat sources density T_i - the temperature, i-denotes the number of layer.

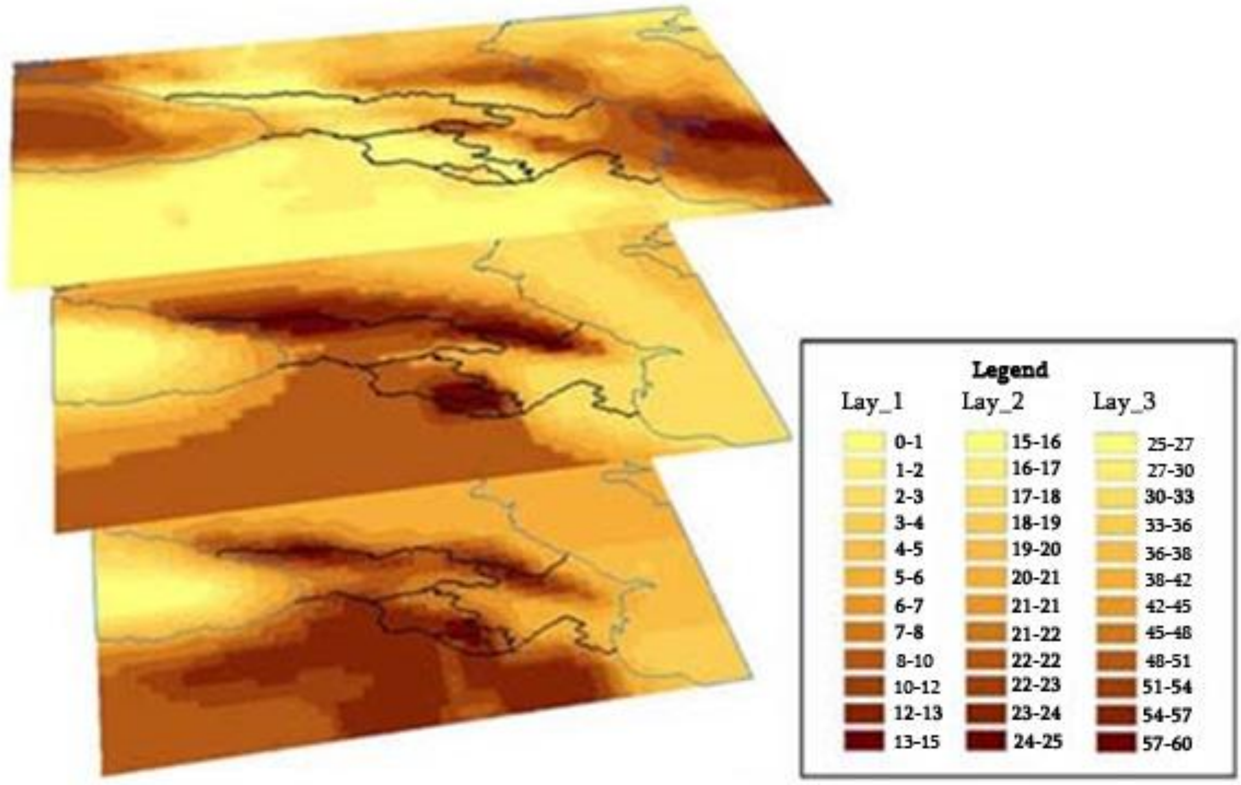

.Fig.1 Distribution of depths (km) of the sedimentary complex, granit and basalt layers in tree – layered model.

We considered the temperature dependence of the value Λ_i. The problem is solved in consideration of the dependence of thermal conductivity on the temperature, of our previous experiments [2]

$$\Lambda_i = \frac{1}{\rho_{0i} + \alpha_i T_i} \quad (3)$$

where $\rho_{0i}(m°C/Wt)$ and $\alpha_i(m/Wt)$ were obtained experimentally by us for different rocks [2]. ρ_{0i}- thermal resistance of the rocks at 20^0C, and α_i - the tangent angle of inclination ρ_i(T) function to the axis of abscissa.

The boundary conditions on the Earth's surface, on the bottom of the sedimentary complex and on the border of Conrad represented as follows; on the Earth's surface we consider temperature as zero and heat flow corresponding to the flow in calculating points. On the bottom of the sedimentary complex and on the border of Conrad we consider continuity of the temperature and heat flow. Calculation of deep temperatures for the Caucasian region was held earlier [3],[4],[5],[6] with the available experimental data heat flows. In the present paper the calculation of temperatures in Caucasian region was conducted using experimental [5] and calculated by us heat flow using the formula (1), by other words, in points where there is no experimental data, we used the calculated values of the heat flow. Similar researches are performed by us for the Black Sea region[7].

The results obtained are presented in form of maps on figures 2,3,4,5. Fig.2 presents distribution of heat flow, fig. 3-5 depict maps of distribution deep temperatures at the bottom of the sedimentary complex, and on the border5 of Conrad and Moho.

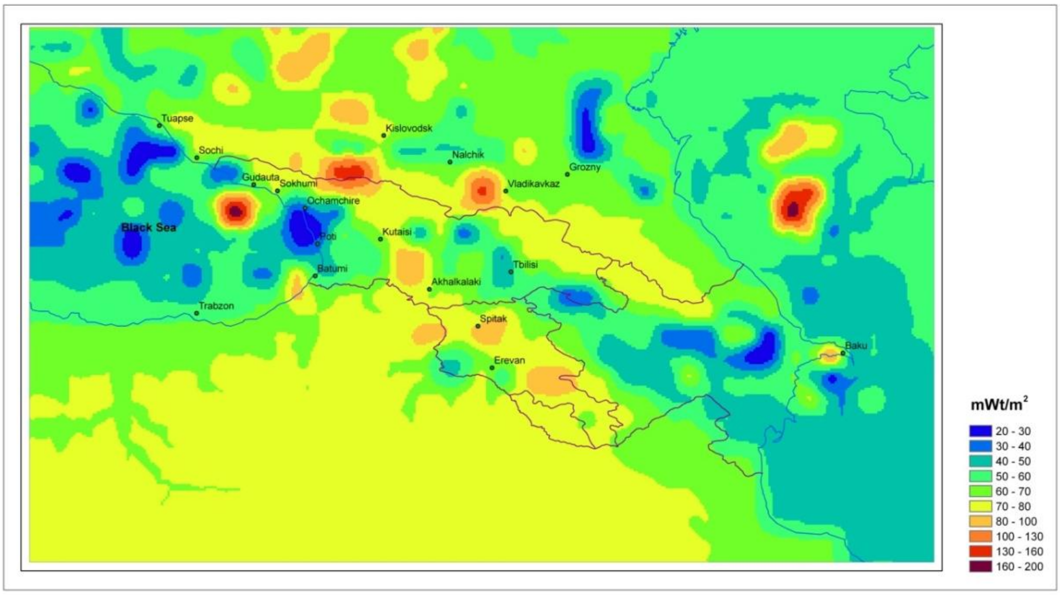

Fig.2 Distribution of the heat flow.

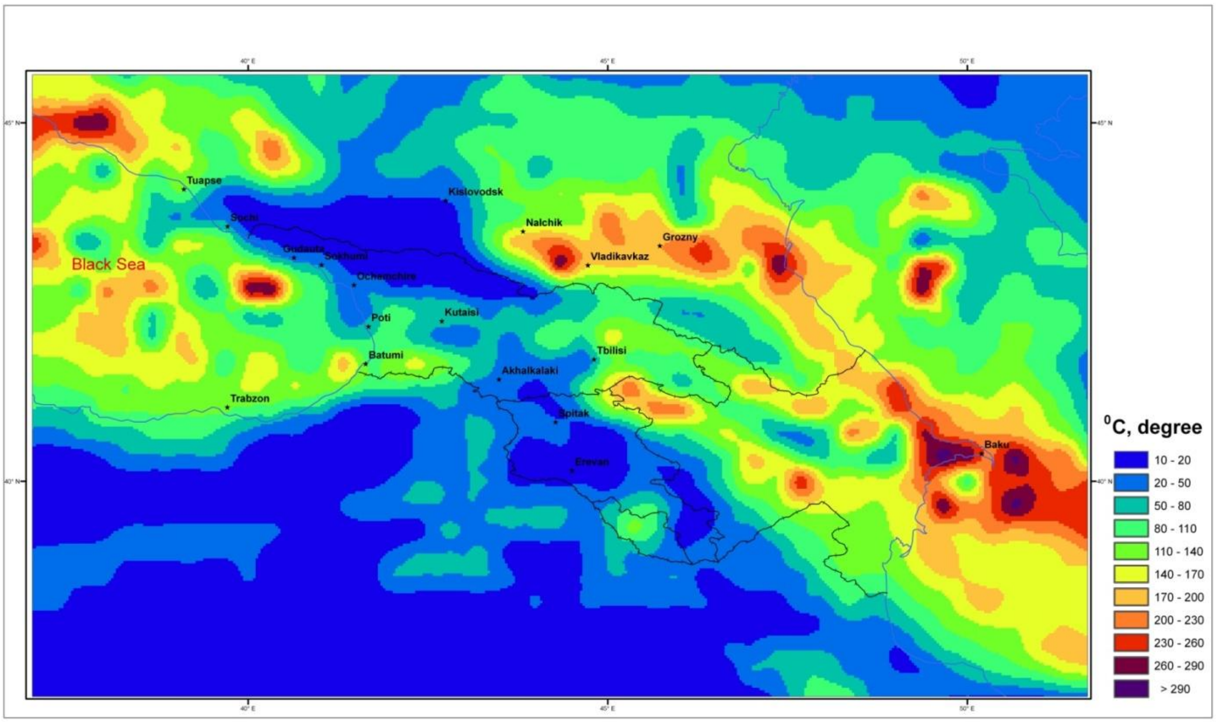

Fig.3 Distribution of deep temperatures on the border of sedimentary complex

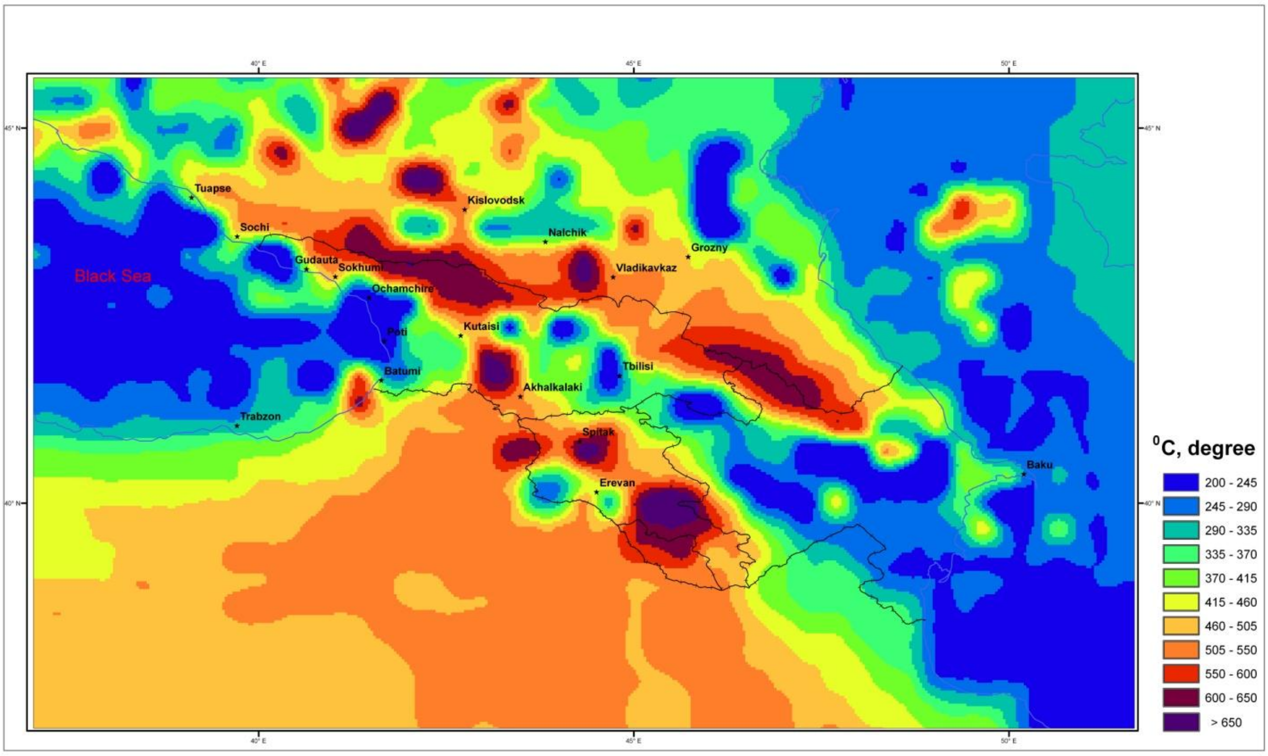

Fig.4 Distribution of deep temperatures on the border of Conrad

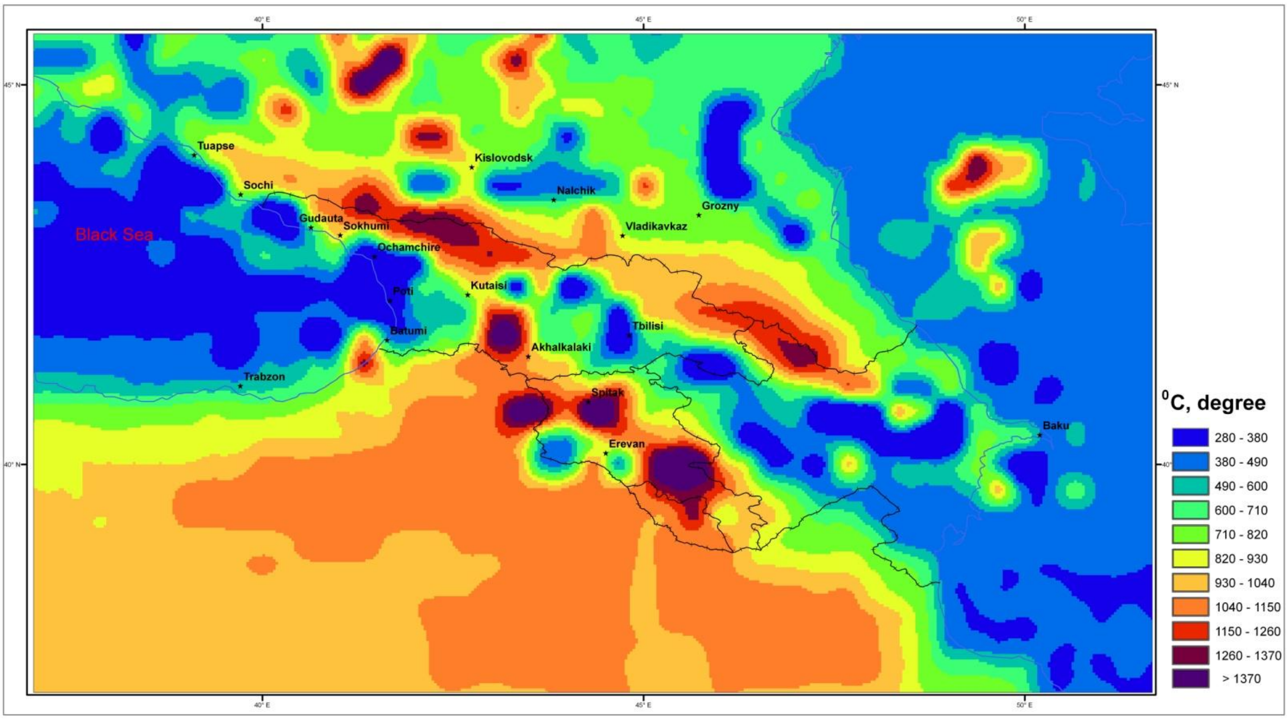

Fig.5 Distribution of deep temperatures on the border of Moho.

References

1. B. Balavadze, P. Mindeli. Main Results of Geophysical Studies of the Black Sea Crust Structure, "Nauka", Moscow, 1966.
2. E. Sakvarelidze. Thermophysical Properties of Rocks in the Temperature Range 20- $500°C$.

   Heat Flows from the Crust and Upper Mantle Earth. M. Nauka, 1973.
3. E. Sakvarelidze, N. Mamulia. Some Resultss of the Investigation the Heat Regim of the Crust for the Water Area of the Black Sea. Bull.of the Georg Acad.of Scianses, 161,1, 2000

.4.ე.საყვარელიძე, ნ.მამულია. დედამიწის ქერქის სითბური რეჟიმის შესწავლის ზოგიერთი შედეგი საქართველოს ტერიტორიისათვის. საქ. მეცნიერებათა აკადემიის მოამბე, 140, 2, 1990.

5.M.Alexidze, G.Gugunava, D.Kiria, T.Chelidze A Three-dimensional Stationary Model of the Thermal and Thermoelastic Fields of the Caucasus. Tectonophysics 227,191-203, 1993.

6.R. Kutas. The Field of Head Flows and Thermal Model of the Earth's Crust, Kiev, Naukova Dumka, 1978.

7. E.Sakvarelidze, I.AmanataSvili,V.Meskhia Thermale Regime of the Crust of the Eastern Black Sea and adjacent Territory. Journal of Shipping and Ocean Engineering, David Publishing Company, USA, Vol.4, Number 5-6, June 2014, p. 152-160

კავკასიის რეგიონის სითბური ველის რადიოგენური კომპონენტი

ე. საყვარელიძე, ი. ამანათაშვილი, გ.ქუთელია, ვ. მესხია

რეზიუმე

ნაშრომში მოყვანილია კავკასიის რეგიონის სითბური ველის კვლევის შედეგები. შესწავლილი ტერიტორიისთვის გამოთვლილი არის სითბური ნაკადების რადიოგენური მდგენელები. შეფასებულია ნაკადების მანტიური მდგენელების მნიშვნელობები მთიანი რაიონებისთვის, მთათაშორისო დეპრესიისთვის (ქართული ბელტი) და შავი და კასპიის ზღვებისთვის. გამოთვლილია სიღრმითი ტემპერატურები ქერქის დანალექი კომპლექსისთვის, კონრადისა და მოხოს საზღვრებისთვის. აგებულია სითბური ნაკადების და სიღრმითი ტემპერატურების განაწილების რუკები.

Journal of Georgian Geophysical Society,
Issue (A), Physics of Solid Earth, v.18a, 2015, pp. 90-94

Short-period AGWs of the measopause region observed by all-sky imager over Abastumani

Giorgi Sh. Javakhishvili

E. Kharadze Abastumani Astrophysical Observatory at Ilia State University; K. Cholokashvili Ave 3/5; Tbilisi 0162; GEORGIA
javakhishvili@iliauni.edu.ge

Abstract

The short-period (about 5-10 min) atmospheric gravity waves (AGWs) were observed in the mesopause region over Abastumani in by the hydroxyl infrared all-sky imager. The specifics of their propagation are given. The importance of these small-scale AGWs for monitoring the wave-like processes in the mesopause and study the lower-upper atmosphere coupling in the Caucasus region caused by orographic effects are also noted.

1. Introduction

Atmospheric gravity waves (AGWs) play important role in the lower and upper atmosphere dynamical processes [1,2]. It is important to study the generation of these waves, the influence of their propagation and dissipation on the atmospheric structure and behavior as well. Luminous layers of the upper atmosphere, including hydroxyl OH bands (maximum luminous layer about 87 km height), sensitive to propagation AGWs [3, 4, 5]. The observed mesopause short-period (with duration 5-10 min) and longer period waves activity express the properties of the seasonal variations of the regional and global scale dynamical phenomena [6, 7]. The modern imager systems allow us to study two-dimensional pictures of AGWs propagation in the upper atmosphere including mesopause [8].

In this work the parameters and two-dimensional picture of the short-period AGWs propagation in the mesopause observed from Abastumani Astrophysical Observatory by the hydroxyl infrared all-sky imager are demonstrated which are obtained for the first time in the Caucasus region. The importance of these phenomena is noted for study the lower and upper atmosphere coupling processes under various helio-geophysical conditions. By use of dispersion equation for AGWs, the importance of background wind velocity for their vertical propagation and identification of a possible source of their generation in the lower atmospheric layers are noted.

2. Short-scale mesopause region AGWs observed by hydroxyl infrared all-sky imager and its possible theoretical description

The mesopause hydroxyl OH bands are one of the brightness objects in the upper atmosphere nightglow spectrum [7, 9. 10, 11]. The sufficient part of hydroxyl emission is in the infrared region of its spectrum. The mesopause temperature is estimated by OH bands emission [Fishkova, Shefov]. Ground based observations of the nightly behavior of the hydroxyl emission intensities show the propagation of atmospheric waves and their properties in the mesopause region [7]. The monitoring of dynamical processes by the hydroxyl infrared all-sky imager (wavelength >1500 nm) have been carried out in

Abastumani Astrophysical Observatory since September 2014. The field of view of the imager system covers the region over the Big and Small Caucasus and Black Sea within the radius of 150 km in the mesopause, which could play an important role in dynamical processes in this region.

In the wave-like processes observed by all-sky imager system the presence of waves with 6-10 min periods are noted. Such short-period AGW-type waves appear occasionally and the duration of their presence do not exceed 40-45 min. Such short-period waves - so called ripples [3,4,7] - can be excited in situ by nonlinear as well as possibly other processes, also can be coupled with lower atmospheric variations, including orographic effect.

In figure 1 the pictures of temporal development of the short-period AGWs observed from Abastumani by the hydroxyl infrared all-sky imager on September 1-2, 2014 (upper panels) and on August 11-12, 2015 (lower panels), are shown. In analogy with [8, 12, 13, 14] for 1-2.09.2014 observation, the estimated wave period is T≈7.5 min, horizontal wavelength ≈7 km and phase velocity of horizontal propagation (to the North-East) ≈15 m/s. For 1-2.08.2015 observations, the estimated wave period is T≈9.8 min, horizontal wavelength ≈13.5 km and phase velocity of horizontal propagation (to the to the North-East) ≈23 m/s.

The waves demonstrated in figure 1 correspond to the propagation of short-period AGWs in the mesopause region. The observed phase velocities (15 m/s and 23 m/s) of these waves are close to background wind velocities characteristic to the mesosphere and lower thermosphere regions and can influence their propagation and evolution [3, 4, 7].

The propagation of AGWs with ω_g frequency in the isothermal atmosphere in the case of presence the horizontal (x directed) background wind with velocity u_o can be described by the following

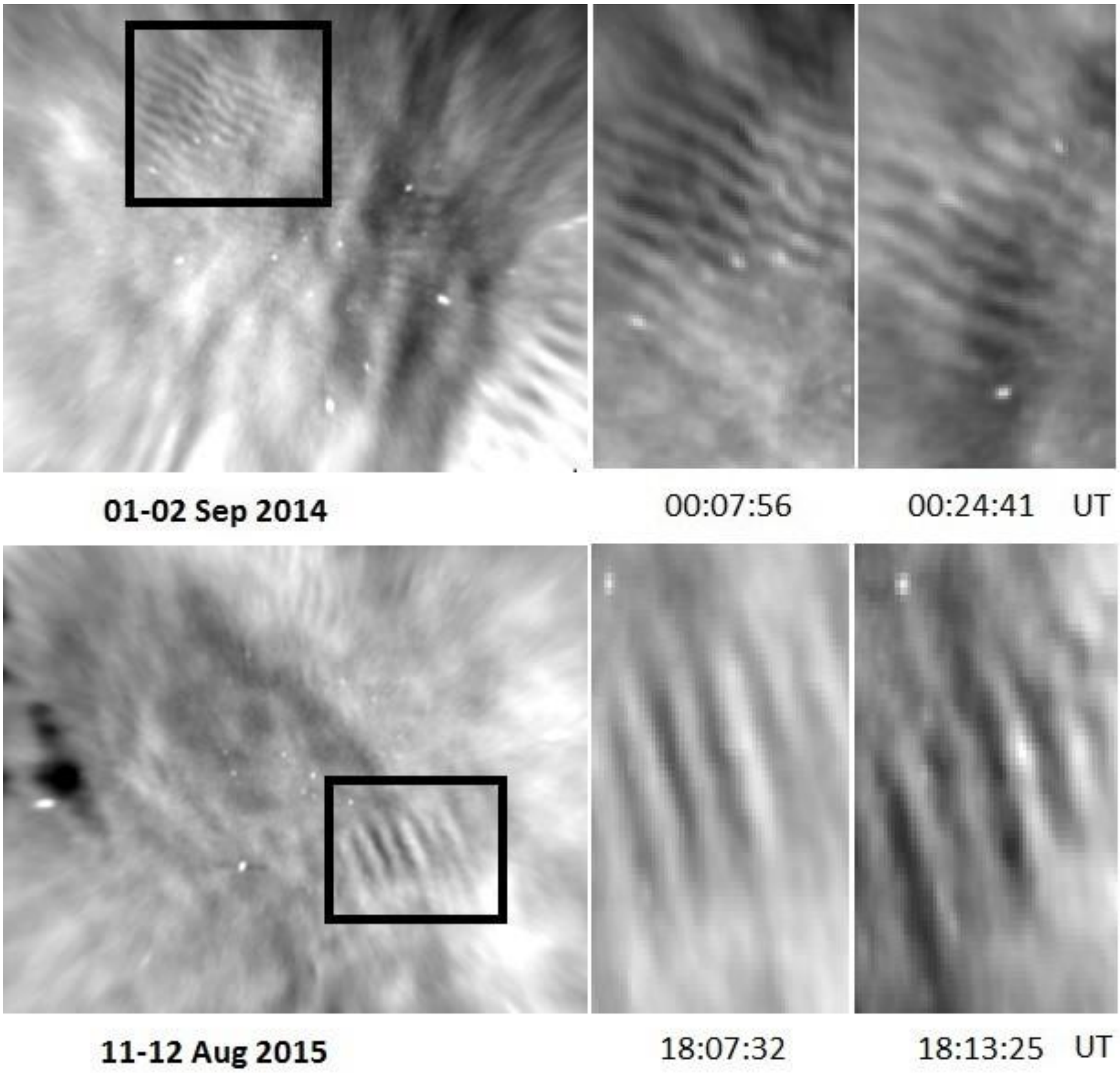

Fig. 1. The short-scale atmospheric gravity waves in the mesopause region observed from Abastumani by the hydroxyl infrared all-sky imager on September 1-2, 2014 night UT= 00:07:56, UT=00:24:41 (upper panels) and August 11-12, 2015 night UT= 18:07:32, UT=18:13:25 (lower panels).

dispersion relation [1,3]:

$$\omega_g = k_x u_o + \left\{ \frac{1}{2} c_s^2 \left(k_x^2 + k_z^2 + \frac{1}{4H^2} \right) - \sqrt{\frac{1}{4} c_s^4 \left(k_x^2 + k_z^2 + \frac{1}{4H^2} \right)^2 - \omega_b^2 c_s^2 k_x^2} \right\}^{\frac{1}{2}} . \tag{1}$$

Here $\omega_b = \left[(\gamma - 1) g / (\gamma H)\right]^{1/2}$ is the isothermal Brunt-Väisälä frequency. $\mathbf{g}$ is the acceleration due to gravity, $c_s = (\gamma g H)^{1/2}$ is the speed of sound, γ is the ratio of the specific heats $(\gamma = 1.4)$, H is atmospheric scale height, $k_x = \dfrac{2\pi}{\lambda_x}$, and are horizontal and vertical wavenumbers, λ_x and λ_z are the horizontal (*x* directed) and vertical wavelengths, respectively.

The maximal frequency of AGWs (cut-off frequency) described by Eq. (1) is the Brunt-Väisälä frequency ω_b and corresponding minimal period for the mesopause region is about 5 min for atmospheric scale height *H*=5 km. In the case of absence of the background horizontal wind ($u_o = 0$) we can estimate the vertical λ_z wavelength of the observed AGWs, Eq. (1), the direction of propagation and consequently a possible source of its generation in the lower atmospheric layers.

In the figure 1, in case of short-period AGWs of the mesopause region, the dispersion Eq. (1) for the vertical wavenumbers (in case $u_o = 0$) give the values $\lambda_z = 6\,km$ (1-2.09.2014) and $\lambda_z = 8\,km$ (11-12.08.2015) are demonstrated. According to Eq. (1), the background wind velocities around $u_o = 10 - 40\ m/s$, typical for the mesosphere-lower thermosphere heights [15], can change AGWs frequency by $\Delta\omega_g = k_x u_o$, which is about the same order as AGWs frequency $\omega_g = \omega_g(u_o = 0)$, in case of absence of the background horizontal wind.

Figure 1 shows that the short period AGWs activity can cover the whole field of view of the all-sky imager above Abastumani. In this case it is possible to estimate mean background wind and its horizontal inhomogeneity, which influence wave propagation, as well as their dissipation [5]. So, the mesopause region observations, using modern imager technique, allow us to reveal short and long scale variations characteristic for this region, which cannot be described by current global circulation models [15] and is the field of our future investigation.

3. Conclusion

The monitoring of the mesopause over Caucasus by all-sky imager in the hydroxyl infrared band from Abastumani shows that short-period AGWs propagate quite frequently in this region. The two-dimensional images of AGWs evolution gives possibility to find location of their generation, taking into account background wind. It also shows their importance in investigation the lower and upper atmosphere coupling caused by orographycal effects of the Caucasus region. The importance of the observed short-period AGW in the region caused by orographic effects are noted to study the lower-upper atmosphere coupling.

Acknowledgements

This work has been supported by ShotaRustaveli National Science Foundation grant No 31/56.

References

[1] Hines, C.O., *Can. J. Phys.*, 1960, v.38, pp. 1441–1481.

[2] Didebulidze, G.G., Pataraya A.D. *J. Atmos. Sol.-Terr. Phys.*, 1999, v.61, pp. 479-489.

[3] Didebulidze G.G., Chilingarashvili S.P., Kvavadze N.D., Sharadze Z.S., *Phys. Chem. Earth B.*, 2000, v. **25**(5/6), pp.443-446.

[4] Didebulidze, G.G., Chilingarashvili, S.P., Toroshelidze, T.I., *J. Atmos. Sol.-Terr. Phys.*, 2002, v.64, pp.1105-1116.

[5] Didebulidze, G. G., Kafkalidis, J. F., Pataraya, A. D. *J. Atmos. Sol.-Terr. Phys.*, 2004, v. 66, pp. 715-732.

[6] Yue, J., Nakamura, T., She, C.-Y., Weber, M., Lyons, W., Li, T. *Ann. Gephys.*, 2010, v. 28, pp. 1401-1408.

[7] Khomich, V.Yu., A.I. Semenov, and N.N. Shefov. *Airglow as an Indicator of Upper Atmospheric Structure and Dynamics,* 2008, Springer, Berlin Heidelberg.

[8] Taylor, M.J., Ryan, E.H., Tuan T.F. and Edwards E., Evidense of preferential directions for gravity wave propagation due to wind filtering in the middle atmosphere, J. Geophys. Res., 1993, 98(A4), pp. 6047-6057.

[9] Фишкова Л.М., 1983. *Ночное излучение среднеширотной верхней атмосферы Земли,* Тбилиси, «Мецниереба».

[10] McDade, I.C., Murtagh, D.P., Greer, G.H., Dickinson, P.H.G., Witt, G., Stegman, J., Thomas, I., Jenkins, D.B., *Planetary and Space Science*, 1986, v.34, pp.789–800;
[11] Mcdade, I.C., Llewellin, E.J., Murtagh, D.P., Greer, G.H., *Planetary and Space Science*, 1987, v. 35 (9), pp.1137–1147.
[12] Cai, X., Yuan, T., Zhao, Y., Pautet, P.-D., Taylor, M. J., Pendleton, W.R. *J. Geophys. Res*.: Space Physics, 2014, v. 119 (8), pp. 6852-6864.
[13] Bossert, K., Fritts, D.C., Pautet, P.-D., Taylor, M. J., Williams, B.P., Pendelton, W.R. J. Geophys. Res.: Atmospheres, 2014, **v.** 119(16), pp. 9765-9778.
[14] Nielsen, K., Taylor, M. J., Hibbins, R. E., Jarvis, M. J., Russell, J. M. *J. Geophys. Res*., 2012, v. 117, D05124, doi:10.1029/2011JD016261.
[15] Picone, J.M., Hedin, A.E., Drob, D.P., Aikin, A.C., *J. Geophys. Res*., 2002, v. 107(A12), http://dx.doi.org/10.1029/2002JA009,430.

აბასთუმანთან სრული ცის იმიჯერული სისტემით დამზერილი მეზოპაუზის რეგიონის მოკლეპერიოდიანი ატმოსფერული გრავიტაციული ტალღები

გიორგი ჯავახიშვილი
ე.ხარაძის აბასთუმნის ასტროფიზიკური ობსერვატორია
ილიას სახელმწიფო უნივერსიტეტი

რეზიუმე

აბასთუმნიდან ჰიდროქსილის ინფრაწითელი ზოლის სრული ცის იმიჯერული სისტემის გამოყენებით მეზოპაუზის რეგიონში დამზერილია მოკლეპერიოდიანი (დაახლოებით 5-10 წთ პერიოდის ხანგრძლივობით) ატმოსფერული გრავიტაციული ტალღები (აგტ) და ნაჩვენებია მისი გავრცელების ზოგიერთი თავისებურებანი. აღნიშნულია ამ მცირემასშტაბოვანი ტალღების მნიშვნელობა, როგორც მეზოპაუზაში ტალღური პროცესების მონიტორინგისათვის, ასევე კავკასიის რეგიონში ოროგრაფიული ეფექტებით გამოწვეული ქვედა და ზედა ატმოსფეროს კავშირების შესასწავლად.

Journal of Georgian Geophysical Society,
Issue (A), Physics of Solid Earth, v.18a, 2015, pp. 95-97

Preliminary testing results of an equipment for Georadiolocation model studies

C. Tskhvediashvili

Supervisor - D. Odilavadze

Introduction

Georadiolocation is a non-invasive geophysical approach, which is underground, near subsurface (<50 m) is the electric heterogeneity study ([1], [3]). This is achieved at high and superhigh frequency (38MHz-2GHz) electromagnetic field generating discrete impulses (Zond 12e), radiation and reflected impulse registration (Prizm 2.5, [2], [4]). Georadiolocation found wide application in archeology, in geotechnics, road construction, glaciologyand in many other areas. [2]

As a rule, the dimensions and characteristics are unknown while working in field conditions and they are investigated according to their radio-type. The paper discusses radio-types of different, pre-selected set of objects and the straightforward task. Known objects are carefully studied and radio-type analysis allows us to discuss the size and characteristics of the object.

Description

Experiments were carried out on the device model (see Figure.1), which was filled with dry sand. Beach access relative dielectric ε = 5.0, which was determined as a result of the experiment. Measurements were used georadari Zond 12e (see Figure. 2).

Figure.1 Equipment for modeling (modeling facility)
size: 116 x 85 x 60 (centimetre)

Figure.2 GPR Zond 12e

Results

Experiment 1 - Results obtained by the method of parabola comparative method revealed that the relative dielectric penetration of the sand used in the experiment is 5.1, which corresponds to a clean, dry sand e (see Figure.3).

Experiment 2 - The case of a 3 ertnamet drive to imitate a stone foundation. Distance from the surface to the first stone is 6 cm. In order to eliminate external perturbation of the bottom we used zero amplification, and for visible presentation we amplified the upper side by 12db-up and twice used Fourier transform (see Figure.4).

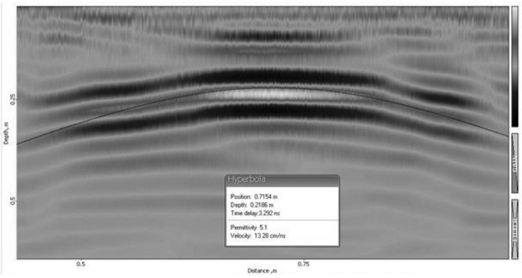

Figure.3 metallic inclusion

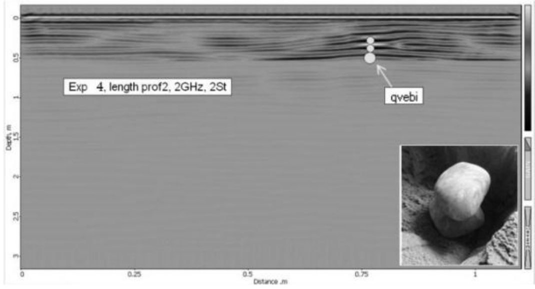

Figure.4 foundation imitation

Experiment 3 (see Figure.5) under 0,5 m depth the zero amplification is used, and the upper side is strengthened by 12db. 2 mil- radio-type is seen here and it is marked in the diagram, while in the middle the image resulted in waves interference appears as a "reflector".

Distance between tubes reducedby 10 cm, and the radiograms obtained by theExperiment 4 - (see Figure.6) shows that the equipment considered a powerful reflection as a whole body. In this diagram as well we used the zero amplification in order to eliminate the effect of the tank bottom, while the upper part was strengthened by 18db for better visualization

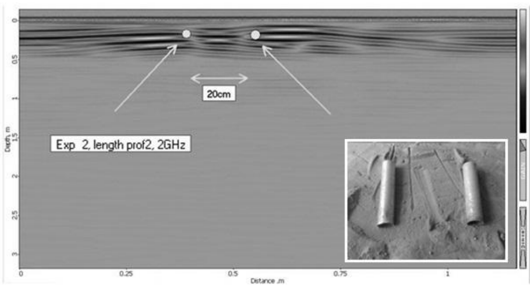

Figure.5 Two tube

Distance between opposite walls - 20centimetre. size: diameter - 6.5centimetre; length - 33.5centimetre; thickness - 0.5centimetre; depth - 13centimetre.

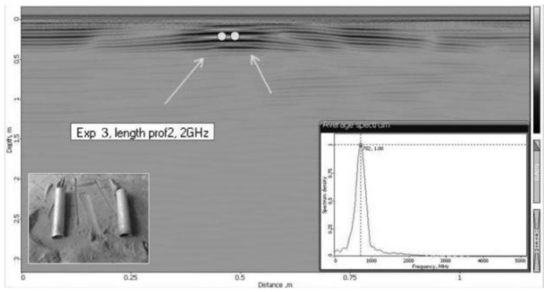

Figure.6 Two tube

Distance between opposite wall - 10centimetre. size: diameter - 6.5centimetre; length - 33.5centimetre; thickness - 0.5centimetre; depth - 13centimetre.

Conclusion

As a result of the investigation by means of the georadiolocation device, we determined the dielectric conductivity of the model environment (the sand from Sachkhere, the relative dielectric conductivity - 5, corresponds to the data base value), as well as for examined models (alluvial sediments, metallic, air containing cavity models) radio-types were obtained, as a result of which we determined their dimensions by the model device. On the basis of layout of similar models we verified resolvability of the device.

References:

[1] А. К. Манштейн “Малоглубинная ГеофизикаА” (2002)
[2] A. Neal “Ground-penetrating radar and its use in sedimentology: principles, problems and progress. Earth-Sciebce Reviews” (2004)
[3] М.Л. Владов, А.В. Старовойтов “Введение в Георадиолокацию” (2004)
[4] Software “Prizm 2.5 User’s Manual” (2010)

სამოდელო დანადგარზე წინასწარი გეორადიოლოკაციური კვლევების შედეგები

გ. ცხვედიაშვილი

რეზიუმე

ჩატარებული კვლევებით გეორადიოლოკაციურ დანადგარზე, დადგენილ იქნა სამოდელო გარემოს დიელექტრიკული განვლადობა (საჩხერის ქვიშა, ფარდობითი დიელექტრიკული განვლადობა - 5, ემთხვევა პროგრამული უზრუნველყოფის ბაზაში მითითებულ მნიშვნელობას), ასევე გამოკვლეული მოდელებისათვის (ალუვიური ნალექის, მეტალური, ჰაერის შემცველი სიღრუვის მოდელები) მიღებულ იქნა რადიოსახეები, რის შედეგადაც დადგინდა მათი ზომები სამოდელო დანადგარზე. მსგავსი მოდელების ურთიერთგანლაგების მიხედვით შემოწმდა ხელსაწყოს გარჩევისუნარიანობა.

Journal of Georgian Geophysical Society,
Issue (A), Physics of Solid Earth, v.18a, 2015, pp. 98-102

Spatial and Temporal Distribution of the Earthquakes in Seismically Active Regions of the World in 2000-2015

T. Kiria

Abstract

The research enables proving the hypothesis that there are some regions, where events are better distributed in time and space regarding normality and there are also regions, in which the earthquakes are not distributed normally in time (only 10%-15% according to the statistics). Finally, we may assume that there are seismic regions with strongly similar, more or less similar and very different statistical structures. The theme for the following research is making cluster analysis of other regions and constructing a mathematical model in order to reveal triggered earthquakes.

Methodoology

The research is based only on the global. statistical data of earthquakes with magnitude 5 and more (catalog http://www.isc.ac.uk). According to the obtained database we constructed in a 3D plot of expression T=F(t $,\varphi$, λ), where t is time, which participates in the model as the catalog time of the given earthquake in the converted time series format (vertical axis) and (φ, λ) are geographic coordinates (Fig.1). Models built program Mathalb2015a.

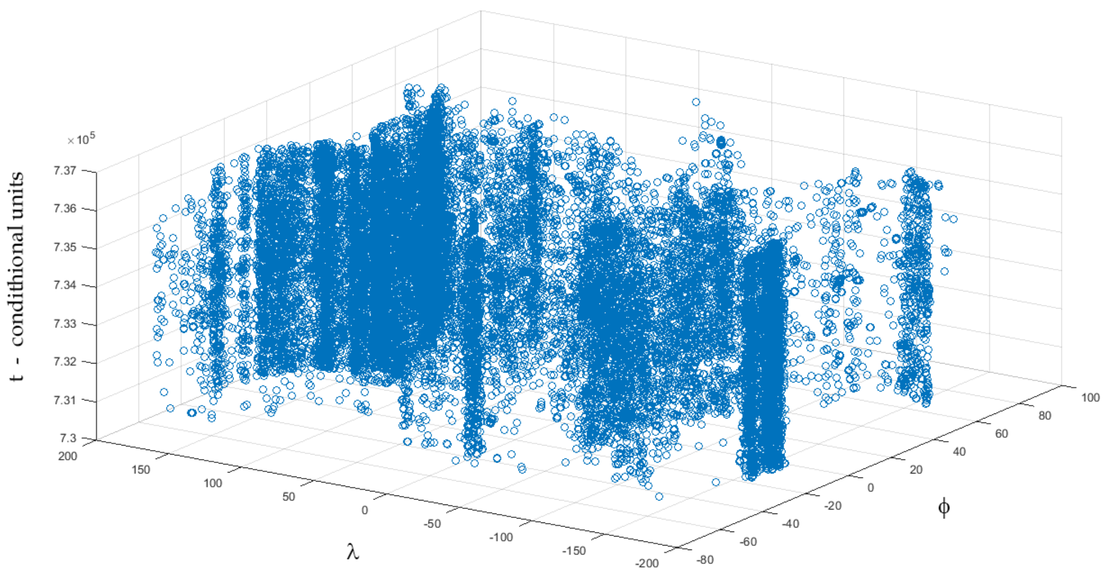

Figure. 1. 3D visualization of spatio-temporal structure of earthquakes hypocentres locations in 2000-2015 (magnitude >=5). (φ, λ) geographic coordinats (degrees), t- condithional units.

Rezults and Discussion

The developed 3D model enables assessing the confidence intervals for specific regions with certain assumptions in time. When we insert geographic parameters range diapason in the model it will return the time interval of the ?following earthquake with a specific probability for a specific region. Visualization enables distinguishing linearly arranged structures positioned vertically on the time axis in certain regions. The structures develop in time and the final pattern is shown in Fig.1.

It is interesting also to construct the graphical interpretation of simultaneous structure of spatio-temporal distribution in seismically very active regions.

Taking into account these data we observed the most active regions separately in time and space. Quite interesting statistical structures were revealed for various regions (Fig.2). The graphical image shows that for some regions during the whole time (2000-2015) the earthquakes are not distributed normally in time, except some cases. The red signs in the scheme denote the cases strongly declined from normal distribution and the vertical red dividing line in a rectangle means an median value **.**

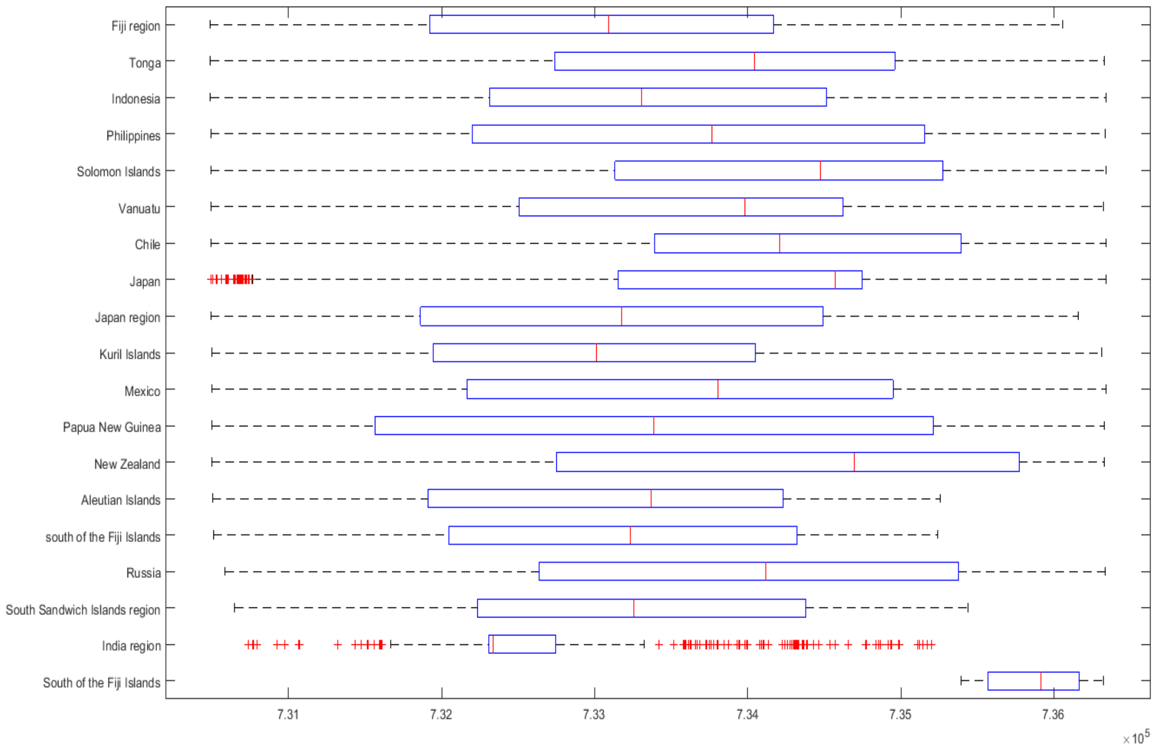

Figure 2. Comparative survey of temporal distribution of earthquakes for active seismic regions. (boxplot, Soft - Mathlab 2015a)

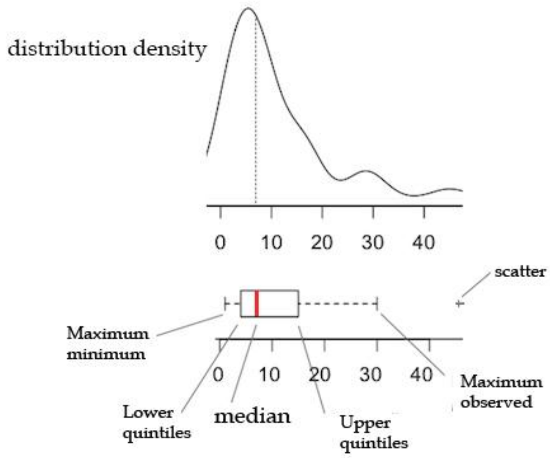

Figure 2a. Example of how to read infographic

The extreme points of the rectangles are known as quantiles and dotted lines to the left and right of the rectangle are the statistics left beyond the normal data distribution area of the specific region.

The individual percentage ratio of (temporally) normally distributed and outlying events for different regions is obvious.

This is also can be seen in the hypocentres' distribution visualization (Fig.3).

The following is the visual image of the hypocentres' values normality for the most active regions, where 3 regions are distinguished for their 80% normality with average depth 400 km (see Fiji regions).

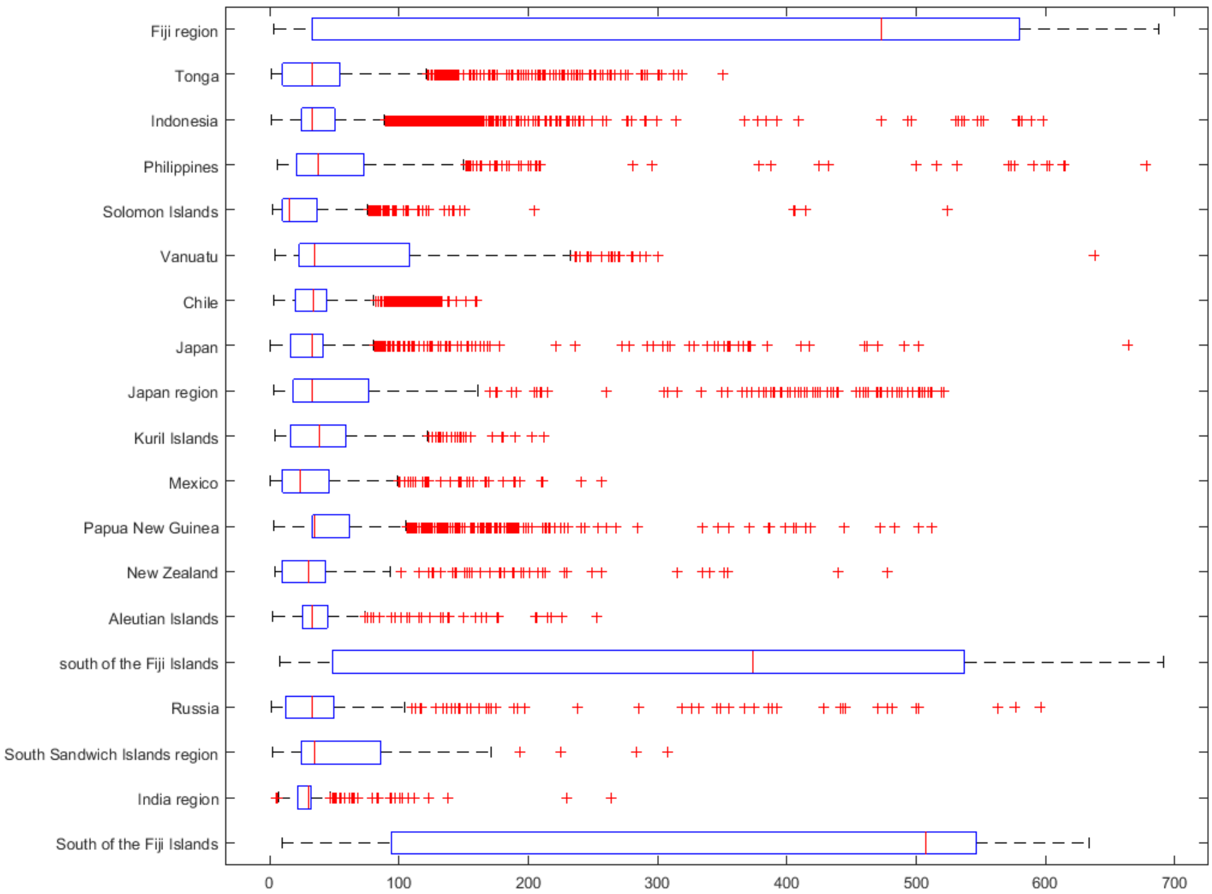

Figure 3. Comparative survey of hypocentres' distribution normality of earthquakes for most active seismic regions: hypocentres depth are shown on the x-axis.

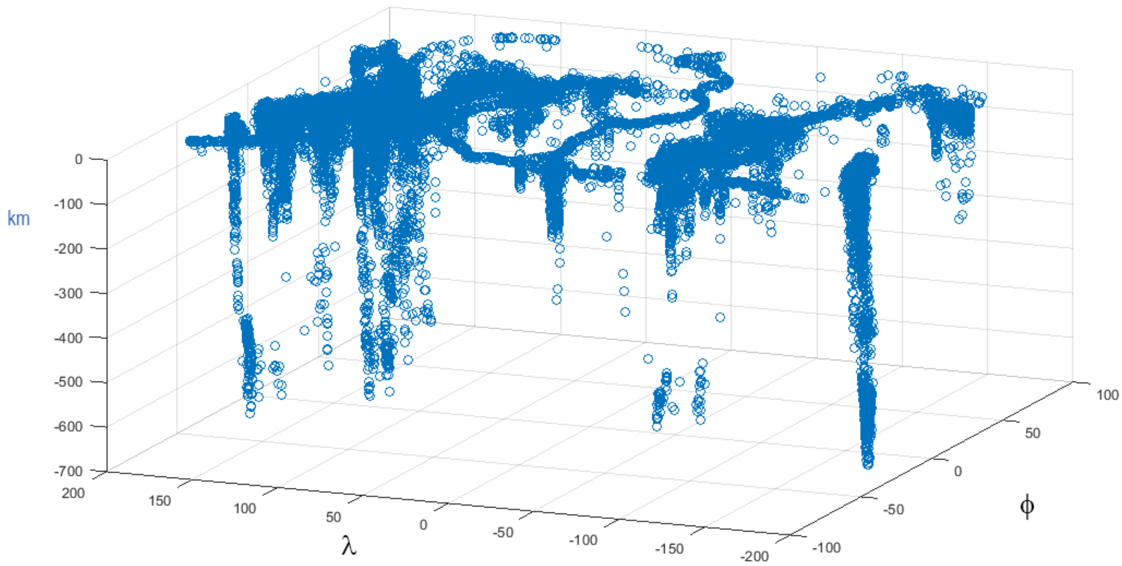

Figure 4. 3D model of hypocentres distribution of earthquakes for top seismic regions (vertically, depth in km, (φ, λ) longitude-latitude in degrees.

Figure 4 presents the 3D model of above mentioned supposition on hypocentres distribution. The highlighted vertical linear structures show certain order in depth distribution of earthquakes in relevant regions. Such regions are apparently a minority and this is a separate issue for consideration.

Finally it is to be said that according Figures 3 and 4 we may distinguish so called regional clusters with distribution visualization.

Acknowledgments

The author expresses their gratitude to Prof. T. Chelidze for useful discussions.

References:

[1] Hua-Wei Zhou, Practical Seismic Data Analysis. March 2014

[2] M. Bacon, R. Simm, T. Redshaw , 3-D Seismic Interpretation 1st Edition.

[3] Bernard Marr, Big Data: Using SMART Big Data, Analytics and Metrics To Make Better Decisions and Improve Performance Paperback – March 9, 2015.

2000-2015 წლების მსოფლიოს სეისმურად აქტიური რეგიონების მიწისძვრების განაწილება სივრცეში და დროში

თ. ქირია

რეზიუმე

ნაშრომში განხილულია სეისმური კატალოგიდან ამორჩეული ძლიერ აქტიური რეგიონების მძლავრი მიწისძვრების გარშემო ჩატარებული სტატისტიკური სტრუქტურების და კლასტერული ანალიზის საკითხები, მიწისძვრის, როგორც დროში მიმდინარე შემთხვევითი პროცესის პარამეტრების დრო-კოორდინატის და კოორდინატი-ეპიცენტრის ურთიერთკავშირების და განაწილებითი თვისებების არაერთგვაროვნების ნიშნები, რომელიც ამყარებს აქამდე არსებულ შედეგებს (იხ. Public Release of the ISC–GEM Global Instrumental Earthquake Catalogue (1900–2009) Dmitry A. Storchak, Domenico Di Giacomo, István Bondár, E. Robert Engdahl, James Harris, William H. K. Lee, Antonio Villaseñor, and Peter). მოყვანილი ვიზუალიზაციიდან იკვეთება რეგიონები, რომლებიც დროით სივრცეში უკეთ განაწილდებიან ნორმალურობის თვალსაზრისით და, ასევე, აშკარად ჩანს რეგიონები, რომელთა მიწისძვრები დროში არ განაწილდნენ ნორმალურად (მხოლოდ 10%-15% სტატისტიკით). საბოლოოდ, შეიძლება ითქვას, რომ არსებობენ ძლიერად მსგავსი, მეტნაკლებად მსგავსი და ძლიერ განსხვავებული სტატისტიკური სტრუქტურების მქონე სეისმური რეგიონები.

Information for contributors

Papers intended for the Journal should be submitted in two copies to the Editor-in-Chief. Papers from countries that have a member on the Editorial Board should normally be submitted through that member. The address will be found on the inside front cover.

1. Papers should be written in the concise form. Occasionally long papers, particularly those of a review nature (not exceeding 16 printed pages), will be accepted. Short reports should be written in the most concise form not exceeding 6 printed pages. It is desirable to submit a copy of paper on a diskette.
2. A brief, concise abstract in English is required at the beginning of all papers in Russian and in Georgian at the end of them.
3. Line drawings should include all relevant details. All lettering, graph lines and points on graphs should be sufficiently large and bold to permit reproduction when the diagram has been reduced to a size suitable for inclusion in the Journal.
4. Each figure must be provided with an adequate caption.
5. Figure Captions and table headings should be provided on a separate sheet.
6. Page should be 20 x 28 cm. Large or long tables should be typed on continuing sheets.
7. References should be given in the standard form to be found in this Journal.
8. All copy (including tables, references and figure captions) must be double spaced with wide margins, and all pages must be numbered consecutively.
9. Both System of units in GGS and SI are permitted in manuscript
10. Each manuscript should include the components, which should be presented in the order following as follows:
    Title, name, affiliation and complete postal address of each author and dateline.
    The text should be divided into sections, each with a separate heading or numbered consecutively.
    Acknowledgements. Appendix. Reference.
11. The editors will supply the date of receipt of the manuscript.

CONTENTS

სარჩევი

საქართველოს გეოფიზიკური საზოგადოების ჟურნალი

სერია ა. დედამიწის ფიზიკა

ჟურნალი იბეჭდება საქართველოს გეოფიზიკური საზოგადოების პრეზიდიუმის დადგენილების საფუძველზე

ტირაჟი 100 ცალი

ЖУРНАЛ ГРУЗИНСКОГО ГЕОФИЗИЧЕСКОГО ОБЩЕСТВА

Серия А. Физика твердой Земли

Журнал печатается по постановлению президиума Грузинского геофизического общества

Тираж 100 экз

JOURNAL OF THE GEORGIAN GEOPHYSICAL SOCIETY

Issue A. Physics of Solid Earth

Printed by the decision of the Georgian Geophysical Society Board

Circulation 100 copies